Evaluation of Enzymes in the Sulfur Metabolic Pathway of Mammals and Bacteria

by

Dianna Leah Forbes

A dissertation submitted to the Graduate Faculty of
Auburn University
in partial fulfillment of the
requirements for the Degree of
Doctor of Philosophy

Auburn, Alabama
December 15, 2018

Keywords: sulfur, enzyme, cysteine dioxygenase,
L-cysteine, desulfonation, chemistry

Approved by

Holly R. Ellis, Chair, Professor of Chemistry
Douglas C. Goodwin, Associate Professor of Chemistry
Christopher J. Easley, Professor of Chemistry
Paul A. Cobine, Associate Professor of Biological Sciences

ABSTRACT

Sulfur-containing molecules are essential for all organisms. Mammals depend on the availability of amino acid methionine and cysteine, whereas bacteria rely on sulfite and cysteine. The research presented in this dissertation focuses on enzymes found within the sulfur metabolic pathway. These enzymes play an important role in cysteine oxidation in mammals and sulfite acquisition in bacteria.

Cysteine dioxygenase (CDO) is a mononuclear non-heme iron enzyme that belongs to the cupin superfamily. CDO catalyzes the conversion of L-cysteine to cysteine sulfinic acid in the presence of dioxygen. Several cupin enzymes contain two partially conserved motifs, $GX_5\mathbf{H}X\mathbf{H}X_{3\text{-}6}\mathbf{E}X_6G$ (motif 1) and $GX_{5\text{-}7}PXGX_2\mathbf{H}X_3N$ (motif 2), that represent the 3-His/1-Glu coordination of the metal center. In mammalian CDO the traditional glutamate residue from the first motif is replaced with a cysteine (Cys93). Substitution of Cys93 with glutamate was shown to inhibit dioxygen consumption. The three dimensional structure of C93E CDO showed glutamate coordinates the iron similar to traditional 3-His/1-Glu cupins. Specifically, glutamate occupies the ligand site that is reserved for dioxygen, and therefore cysteine oxidation cannot occur. Incorporation of the cysteine residue frees the ligand site promoting bidentate coordination of the L-cysteine substrate and single site dioxygen binding.

Furthermore, replacement of glutamate with cysteine allows for the formation of a unique thioether crosslink with a nearby tyrosine residue (Tyr157). In wild-type CDO the crosslink exists as a heterogeneous mixture of non crosslinked and crosslinked isoforms. In

CDO crosslink formation is dependent on iron, dioxygen, and L-cysteine. However the Cys-Tyr crosslink in other enzymes is not dependent on the substrate. It is unusual that crosslink formation in CDO is dependent on the L-cysteine substrate.

To understand the role of L-cysteine in crosslink formation, wild-type CDO was incubated with L-cysteine analogs. In addition to L-cysteine, wild-type CDO is able to form the crosslink with D-cysteine, but is unable to form the crosslink with cysteamine and 3-mercaptopropionic acid. However, previous studies found the CDO variant R60A was able to form the crosslink with cysteamine. Through electrostatic interactions Arg60 plays an important role in substrate stabilization. Evaluation of non crosslinked R60A CDO suggests that Arg60 also plays a role in substrate specificity for crosslink formation. In addition, non crosslinked R60A was able to form the crosslink with D-cysteine. These findings suggests that crosslink formation in cysteine dioxygenase is not specific to L-cysteine, but can occur with any small molecule capable of promoting dioxygen binding. Currently all proposed mechanisms for crosslink formation are based on the formation of a hydroxyl radical from Tyr157. Three dimensional analysis of non crosslinked wild-type CDO suggests that crosslink formation could also occur via a thiol radical from Cys93.

Bacterial organisms require sulfur for survival, but sulfur is often limiting in the environment. However, bacteria possess several sets of enzymes capable of scavenging sulfite from organosulfate molecules. Two proteins expressed during sulfur limiting conditions in *E. coli* are a FMN-reductase SsuE and an alkanesulfonate monooxygenase SsuD. SsuD utilizes reduced flavin, supplied by SsuE, to cleave the carbon-sulfur bond of 1-alkanesulfonates into sulfite and the corresponding aldehyde. Flavin transfer between SsuE and SsuD occurs through a channeling mechanism involving protein-protein interactions.

The alkanesulfonate monooxygenase system is one of several identified FMN-dependent two-component systems activated during sulfur starvation. In addition to Ssu, Msu and Sfn systems have been identified in *Pseudomonas sp.*. Together these enzymes catabolize dimethyl sulfone into inorganic sulfite. A high amino acid sequence identity exists between the reductases and monooxygenases involved in sulfur acquisition, and may utilize similar mechanistic approaches for flavin transfer. Initial desulfonation assays with SsuE and SsuD from *P. putida* do not support flavin transfer by a channeling mechanism. However, further investigation into the mechanism of flavin transfer for Msu and Sfn enzymes could provide evidence to support a channeling mechanism.

ACKNOWLEDGEMENTS

During my time at Auburn University I have been influenced by so many people, both good and bad. I am truly grateful for each experience because it shaped me into the person I am today. First, I would like to thank Victoria Owens for encouraging me to come to graduate school. If it wasn't for your relentless nagging I would have never filled out the graduate school application. Secondly, I would like to thank my advisor Dr. Holly R. Ellis for providing me an opportunity to learn and grow into the scientist I am today. Furthermore, I appreciate the support, encouragement, and understanding I received from you when I wanted to pursue my teaching license. Thank you for believing that I could do both at the same time.

I would like to thank my current and former lab mates Dr. Catherine Njeri, Paritosh Dayal, Dr. Jonathan Musila, Katie Tombrello, Claire Graham, and Richard Hagen. Thank you, so much, for all of the great memories that were made in CB 151. Also a special thank you to Katie and Claire for continuously putting up with my inadequate singing and my constant need to reference Twilight and Marvel movies.

Thank you to the Auburn University and the Department of Chemistry and Biochemistry for providing financial support throughout my time here at Auburn. Thank you to Dr. John Gorden and Dr. Ash Curtiss for your mentorship and for allowing me to do my own thing with the honors labs. Thank you to Dr. Kyle Willian and Mrs. Mary "Beth" Smith for making my TA experience a positive one. Thank you to Dr. Duin, Dr. Mansoorabadi, and Dr. Cobine for allowing me to come into your lab and use your instruments to complete my

research. Thank you to my committee members Dr. Easley, Dr. Goodwin, and Dr. Cobine for your patience, understanding, and mentorship. I would also like to give a special thank you to Dr. Christine Schnittka, my university reader and my Department of Education advisor, for helping me grow, not only as an educator but as a person.

I would also like to thank my dad, Terry Forbes, for his support during my hard times and his constant reminder to proceed through life in a logical manner. I would also like to thank my mom, Lisa Crocker, for her love and support. I would like to thank my two best friends, of over twenty years, Glenda Gurley and Ava Schoen for your unconditional love and support throughout my life. I would also like to thank my extended Martin family for all the positivity and encouragement. Thank you to Dr. Rene Fuanta and Dr. Emily Hardy for your friendship along with your patient and thoughtful scientific discussions over the years. Thank you to Carly Engel for being my Tuesday night movie buddy, travel companion, and friend.

Most importantly, I would like to thank and dedicate this dissertation to my children, Dashawn and Nathaniel Martin. Thank you so much for unknowingly giving up a portion of your childhood so I could selfishly pursue this and other degrees. I promise this is the last one. I love you.

TABLE OF CONTENTS

LIST OF TABLES

LIST OF FIGURES

LIST OF SCHEMES

LIST OF ABBREVIATIONS

CD	circular dichroism
CDO	cysteine dioxygenase
CSA	cysteine sulfinic acid
DTNB	5,5’-dithiobis(2-nitrobenzoic acid)
EPR	electron paramagnetic resonance
FAD	flavin adenine dinucleotide
FMN	flavin mononucleotide
HEPES	4-(2-hydroxyethyl)-1-piperazineethanesulfonic acid
ICP-AES	inductively coupled plasma atomic emission spectroscopy
NAD(P)H	nicotinamide adenine dinucleotide (phosphate)
OCS	octanesulfonate
PDB	protein data bank
SDS-PAGE	sodium dodecyl sulfate polyacrylamide gel electrophoresis

CHAPTER ONE

LITERATURE REVIEW: PART I

1.1 Sulfur metabolism in mammals

The amino acids L-methionine and L-cysteine are the main sources of sulfur in mammals. Methionine and cysteine are crucial molecules for maintaining normal physiological functions. Three sources represent the overall contribution of sulfur in mammals: dietary sources, transsulfuration by methionine, and the breakdown of endogenous proteins. Cysteine, despite its metabolic importance, is only considered a semiessential amino acid whereas methionine is an essential amino acid [1]. Cysteine is considered semiessential because it can be synthesized from methionine via the transsulfuration pathway, and therefore is not required in the diet. It has been experimentally determined that homocysteine can serve as a replacement for methionine [2]. Both cysteine and methionine can be synthesized from homocysteine; however homocysteine is not abundant in dietary sources and therefore methionine is required. Alternatively, methionine and cysteine are found in many dietary proteins such as meat, dairy, and nuts. Normal dietary consumption of proteins satisfies the recommended daily requirement for both methionine and cysteine [1].

Ultimately the sulfur found in methionine and cysteine are incorporated into several important biomolecules such as vitamin B_1, glutathione, acetyl-CoA, and S-adenosylmethionine. For humans, the amount of sulfur intake is essentially equally to the amount of cysteine being

catabolized [1]. When there is a high influx of sulfur the liver plays a crucial role in preserving homeostasis [3]. This homeostasis is made possible due to two branch points present within sulfur metabolic pathways (**Figure 1.1**).

1.2 Conversion of methionine to homocysteine

The methionine derived molecule, homocysteine, serves as the first branch point in sulfur metabolism. Homocysteine is formed after methionine undergoes two enzymatic reactions and a transmethylation to become homocysteine. First methionine adenosyltransferase (MAT) transfers the adenosyl group of adenosyl triphosphate (ATP) to the sulfur group of methionine forming S-adenosylmethionine (AdoMet) (**Figure 1.2**). Catalysis by MAT occurs through a sequential mechanism with ATP binding prior to methionine, resulting in an ATP-MAT-Met complex [4, 5]. It is proposed that there is a simultaneous attack on the sulfur of methionine and the C5 of ATP to form AdoMet and tripolyphosphate [5]. The terminal phosphate of PPP_I is hydrolyzed into PP_I and P_I. It has also been shown that MAT exhibits optimal activity when Mg^{2+} or K^+ cations are present [5, 6].

Several isoenzymes of MAT are found in mammalian tissues. There are three hepatic MAT isoenzymes, with MAT3 being the predominate form [1, 7]. It has been shown that MAT1 is inhibited at high concentrations of AdoMet [6]. Alternatively, MAT3 is activated by excess concentrations of methionine and AdoMet. Curiously, MAT3 is only found in the liver and therefore the liver is the only organ that can respond during an increase of methionine [2]. Once produced, AdoMet becomes demethylated by a wide variety of methyltransferase. Through an S_N2 like reaction, the methyl group of AdoMet serves as a methyl donor to many important biological molecules such as biotin, epinephrine, proteins, creatine, and DNA [1, 5]. Although demethylation

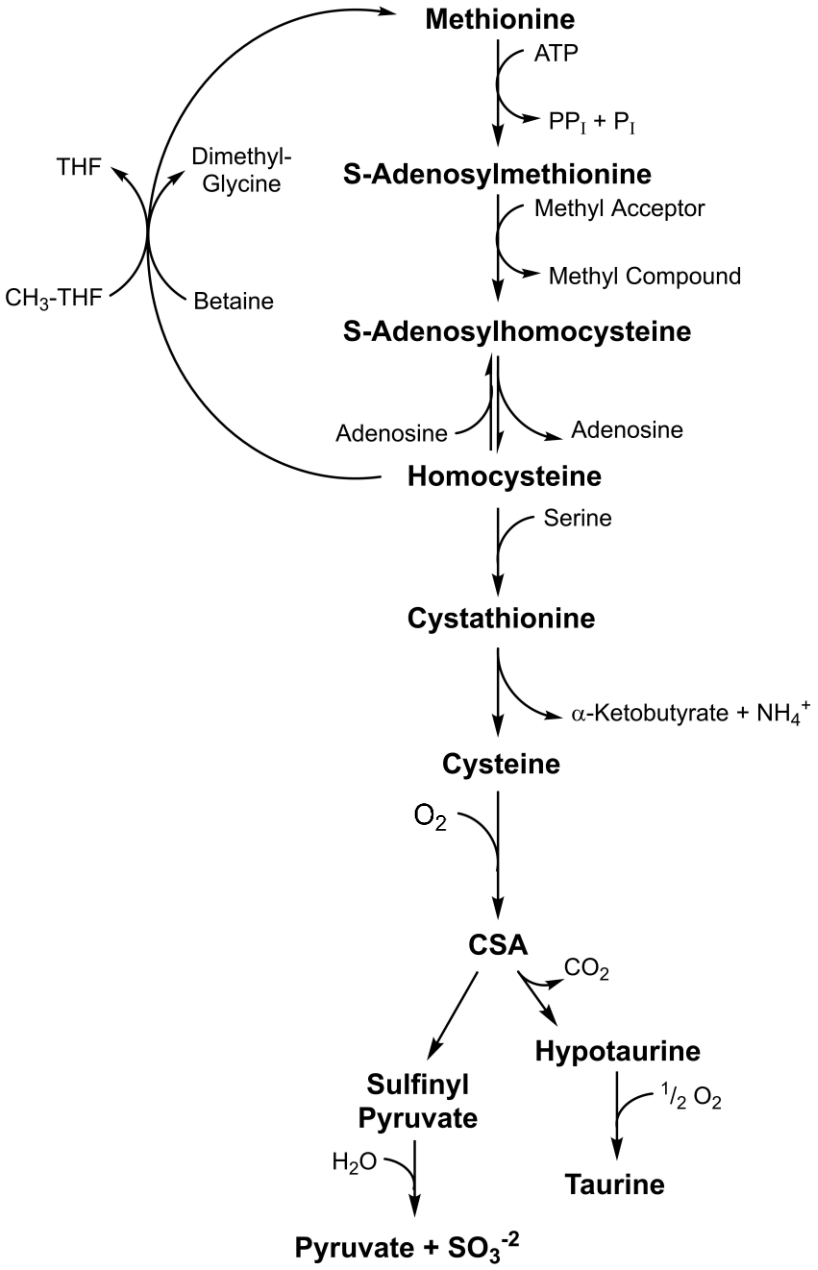

Figure 1.1. The sulfur metabolic pathway in mammals adapted from [7]. 1 - methionine adenosyltransferase (MAT); 2 – methyltransferase; 3 – adenosylhomocysteinase (SAH); 4 – methionine synthase (MS); 5 – betaine-homocysteine methyltransferase (BHMT); 6 – cystathionine β-synthase (CBS); 7 – cystathionine γ-lyase (CGL); 8 – cysteine dioxygenase (CDO); 9 – aspartate aminotransferase (AAT); 10 – cysteinesulfonate decarboxylase (CSD).

is the most common fate, it is proposed that AdoMet can donate any group surrounding the sulfur atom [5]. However in mammals, it has yet to be shown that AdoMet can donate the adenosine moiety [8].

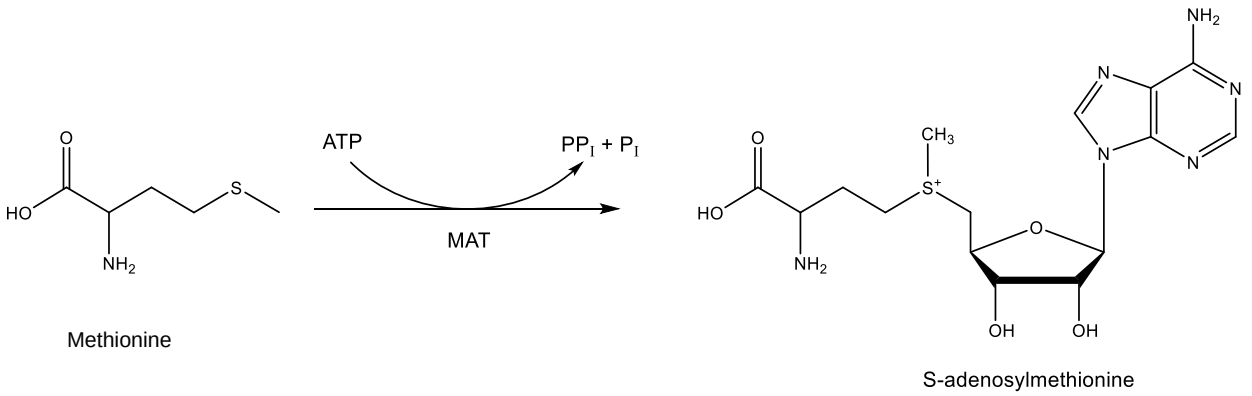

Figure 1.2. Conversion of methionine to S-adenosylmethionine (AdoMet) by methionine adenosyltransferase (MAT) [4].

Upon demethylation by a methyltransferase, AdoMet becomes S-adenosylhomocysteine (AdoHcy) (**Figure 1.3**). AdoHcy is then hydrolyzed by adenosylhomocysteinase (SAH) to form homocysteine and adenosine (**Figure 1.4**). It is proposed that SAH is the only way intracellular AdoHcy is metabolized in mammals [7]. SAH has four subunits each containing a tightly bound NAD^+ [9, 10]. Upon substrate binding, NAD^+ oxidizes the 3'-hydroxyl group of AdoHcy forming 3'-keto-S-adenosyl-L-homocysteine and NADH. Subsequently an active site base removes the C4-proton resulting in a cleaved homocysteine moiety. Addition of water to this homocysteine-free intermediate and further reduction by NADH forms adenosine [9]. This reaction is a reversible reaction in which the production of homocysteine (Hcy) and adenosine (Ado) is non-enzymatically converted back to AdoHcy.

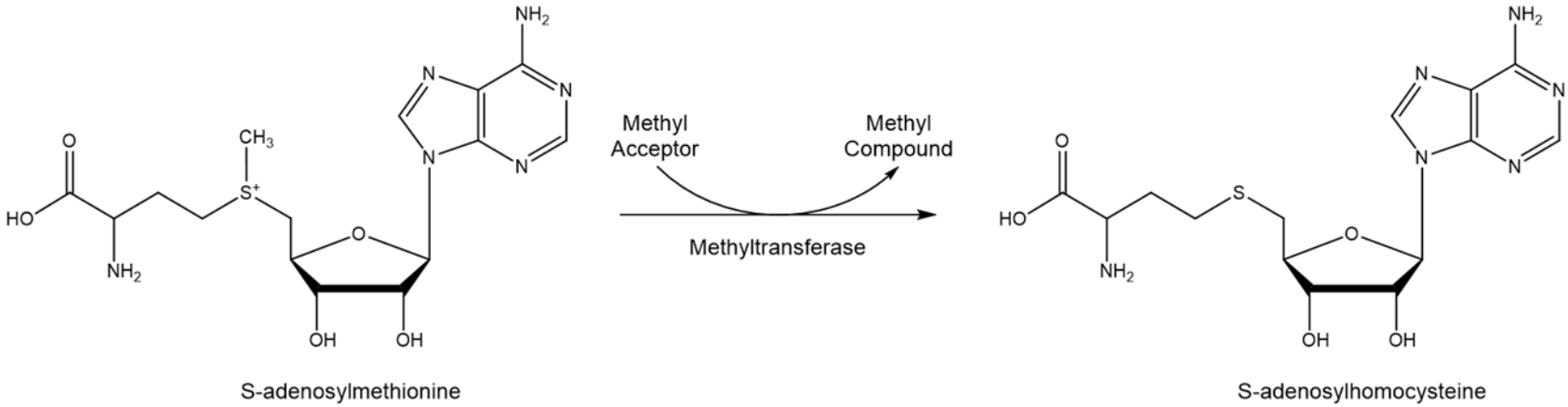

Figure 1.3. Conversion of S-adenosylmethionine (AdoMet) to S-adenosylhomocysteine (AdoHcy) by methyltransferase [4].

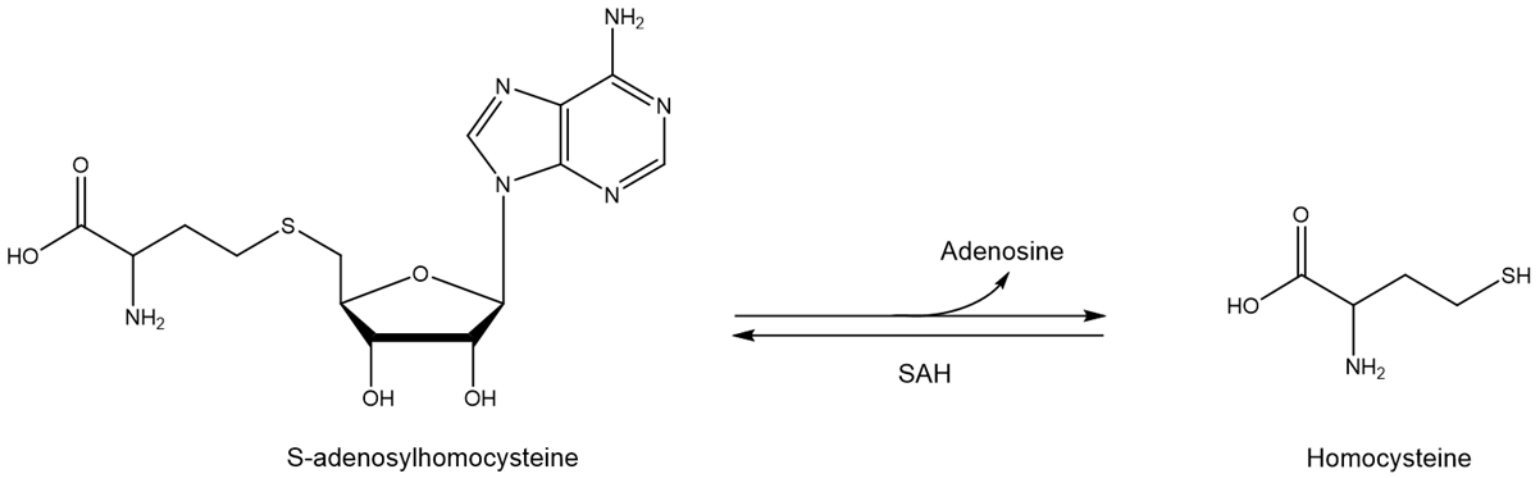

Figure 1.4. Conversion of S-adenosylhomocysteine (AdoHcy) to homocysteine by adenosylhomocysteinase (SAH) [9].

Interestingly, the reverse reaction is highly favored over the enzymatic hydrolysis of AdoHcy [1, 7, 9, 11-13]. SAH is inhibited by both Ado and Hcy. The SAH enzyme in the presence of excess Ado forms a stable, non-active complex [7, 14]. The enzymatic reaction is only favored when products Ado and Hcy are quickly metabolized [12]. Ado is removed by adenosine kinase, whereas the fate of Hcy lies in one of three metabolic reactions [1]. Two of these reactions recycle homocysteine back into methionine (transmethylation), while the third reaction converts homocysteine to cystathionine which proceeds to yield cysteine (transsulfuration). Therefore, homocysteine represents the first major branch point in cysteine metabolism: transmethylation or transsulfuration.

1.3 Homocysteine: The first branch point

Transmethylation of methionine can occur by either betaine-homocysteine methyltransferase or methionine synthase. Betaine-homocysteine methyltransferase (BHMT) demethylates betaine (trimethylglycine), forming dimethylglycine (**Figure 1.5**). Betaine, an irreversible oxidative intermediate, is a product of choline metabolism [12, 15]. Choline serves as an antecedent for the neurotransmitter acetylcholine. Currently, BHMT is the only known mechanism for betaine break down.

Similarly, methionine synthase or 5-methyltetrahydrofolate-homocysteine methyltransferase (MS) is the only know enzyme to demethylate 5-methyltetrahydrofolate (5-MTHF) to tetrahydrofolate (THF) (**Figure 1.6**) [12]. Methylcobalamin, or vitamin B_{12}, is a cofactor for methyltransferase [11]. In addition to providing the methyl group so Hcy can form Met, THF is also produced. The folate molecule THF serves as a precursor in the synthesis of nucleic acids [16]. Insufficient B_{12} or folate levels in mammals can result in megaloblastic anemia; inhibition of DNA synthesis during production of red blood cells [12, 16].

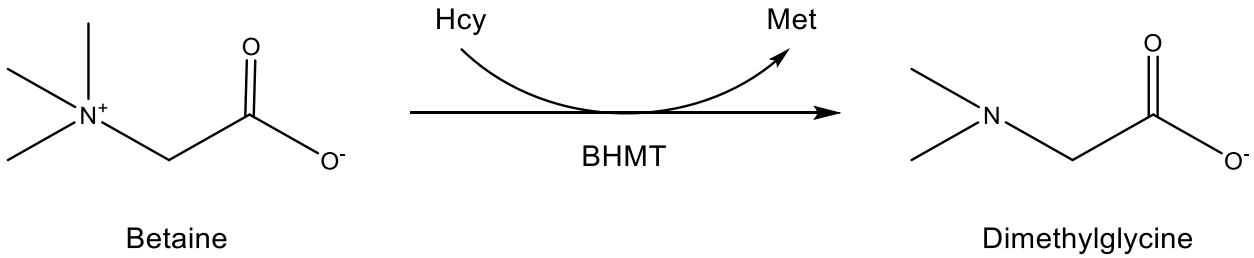

Figure 1.5. Conversion of betaine to dimethylglycine by betaine-homocysteine methyltransferase (BHMT) [12].

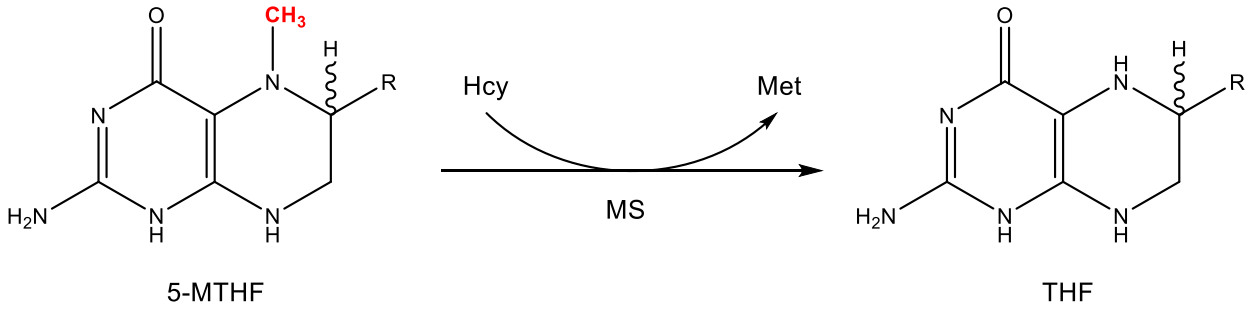

Figure 1.6. Conversion of 5-methyltetrahydrofolate-homocysteine (5-MTHF) to tetrahydrofolate (THF) by methionine synthase (MS) [12].

Alternatively, homocysteine can proceed under the transsulfuration pathway. Homocysteine to cystathionine by cystathionine β-synthase represents the first reaction in the transsulfuration pathway and is the only reaction which removes homocysteine from the methionine cycle [2, 12]. Cystathionine β-synthase (CBS) is a pyridoxal phosphate (PLP) containing enzyme consisting of a heme-bound N-terminal region and regulatory activated C-terminal region. In an irreversible reaction, CBS condenses the β-OH of serine with homocysteine to form cystathionine (**Figure 1.7**) [17]. Interestingly, the N-terminal heme-bound region is inherently absent in yeast homologs [18, 19]. The purpose of the heme has not been fully evaluated but is thought to act as a redox sensor or play a role in PLP binding [1, 20, 21]. Deletion of the N-terminal region yields a 50% decrease in activity compared to the wild-type enzyme. Conversely, mutation or deletion of the allosterically activated C-terminal domain results in a stable, highly responsive enzyme [1, 20, 22].

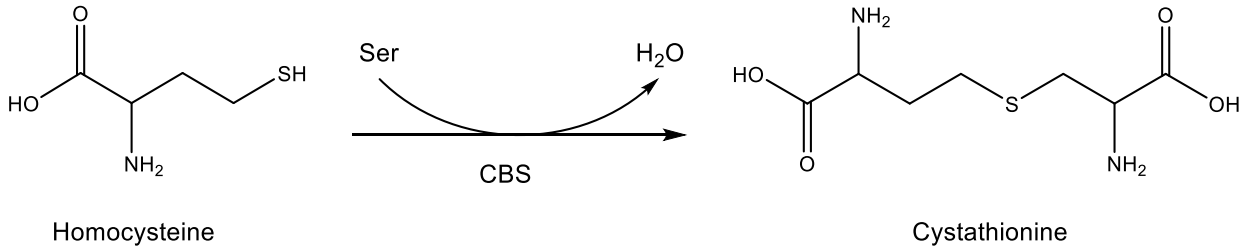

Figure 1.7. Conversion of homocysteine to cystathionine by cystathionine β-synthase (CBS) [2].

1.3.1 Regulation of homocysteine

The regulation of homocysteine to cystathionine by CBS is directly correlated to the overall regulation of the homocysteine branch point. It is proposed that the regulation between

transmethylation or transsulfuration of homocysteine is dependent on either the kinetic abilities of each enzyme or regulation due to diet, with more evidential support of the later [1, 2, 11, 12, 23-26]. CBS is allosterically regulated by AdoMet [27]. AdoMet binds to the C-terminal region of CBS activating the protein to a dimeric form. In 1990, Finkelstein compared the Michaelis constants (K_m) for enzymes in the transmethylation and transsulfuration pathways. It was shown that enzymes involved in transmethylation had a low K_m value (< 0.1 mM) and were inhibited by AdoMet. On the other hand, enzymes involved in transsulfuration had a high K_m value (1.0 mM) and were activated by AdoMet [12]. Based on these observations, it was proposed that transmethylation is favored in the presence of low concentrations of AdoMet. Additionally, when AdoMet concentrations are high, transsulfuration is favored citing this as the sole regulatory mechanism. The inherent flaw in this argument is concentrations of AdoMet are dependent on dietary intake [11]. When methionine enters the body it is either used for protein synthesis or catabolized to form AdoMet [2].

In human and rat species on a normal diet, 45-60% of homocysteine is converted to cystathionine [24, 28, 29]. Subjects fed a limited sulfur diet showed a decrease in transsulfuration, whereas an increase of sulfur in the diet favored the transsulfuration [24, 30]. Comparably, when the transmethylation substrates choline and betaine are increased, transmethylation becomes favored and when choline and betaine are restricted transsulfuration occurs [26]. Given results from both dietary and enzymatic studies, it can be concluded that the overall pathway is regulated based on substrate availability. Even the initial reaction producing AdoMet, contributes to the overall regulation between transmethylation and transsulfuration.

1.3.2 Conversion of homocysteine to cysteine sulfinic acid

Proceeding in the unidirectional transsulfuration pathway, cystathionine is converted to cysteine by cystathionine γ-lyase (**Figure 1.8**). Cystathionine γ-lyase (CGL) exists as a homotetramer with a PLP cofactor in each monomer. Cystathionine undergoes an elimination reaction cleaving the γ-carbon resulting in α-ketobutyrate and cysteine [31].

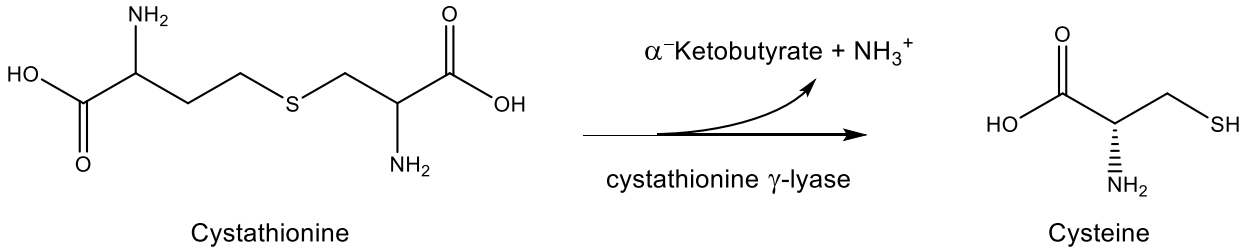

Figure 1.8. Conversion of cystathionine to cysteine by cystathionine γ-lyase (CGL) [31].

Cysteine is considered a precursor to many important biological molecules such as glutathione, taurine, and acetyl-CoA. However in transsulfuration pathway cysteine is further metabolized by cysteine dioxygenase (CDO). CDO converts L-cysteine to L-cysteine sulfinic acid (CSA) in the presence of O_2 (**Figure 1.9**) [32]. CDO contains a crosslinked adduct between a cysteine and tyrosine residue which plays a role in the catalysis of CSA [33].

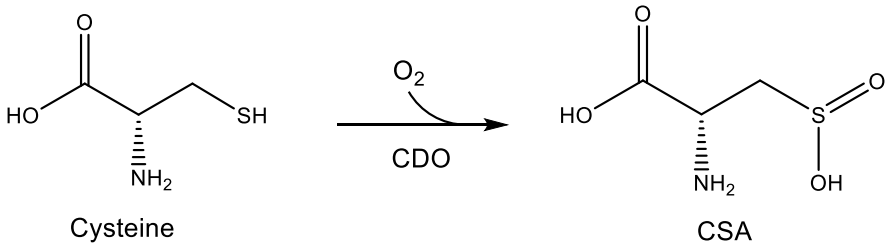

Figure 1.9. Conversion of cysteine to cysteine sulfinic acid by cysteine dioxygenase (CDO) [34].

1.4 Cysteine sulfinic acid: the second branch point

Although in its own right CSA is not metabolically significant, it serves as the second branch point in sulfur metabolism. CSA can be further metabolized to form pyruvate and inorganic sulfite or taurine. To produce pyruvate and sulfite, cysteinesulfinate must first undergo a transamination. Aspartate aminotransferase (AAT) catalyzes the transamination of CSA to sulfinylpyruvate (**Figure 1.10**) [1, 35]. Typically, AATs transfer the amino group of L-aspartate or L-glutamate to oxaloacetate or α-ketoglutarate [36]. CSA is a structural analog of L-aspartate and can be used as a substrate for AAT [35, 37]. Once sulfinylpyruvate is formed it quickly hydrolyzes to pyruvate and inorganic sulfite. It is unknown whether this hydrolysis occurs spontaneously or by an enzymatic process.

Alternatively, cysteinesulfinate can be metabolized by the PLP-dependent enzyme cysteinesulfinate decarboxylase (CSD) to form hypotaurine (**Figure 1.11**). In addition, CSD can also use cysteinesulfonate as a substrate [1, 7, 38, 39]. After the CSD catalyzed reaction, hypotaurine is converted to taurine. The illusive conversion of hypotaurine to taurine is not well understood. Many researchers think it is a simple non-enzymatic oxidation due to the presence of

taurine being found as a product in the CSD catalyzed reaction [40] . This autooxidation could also explain why hypotaurine does not accumulate in mammalian tissue [1].

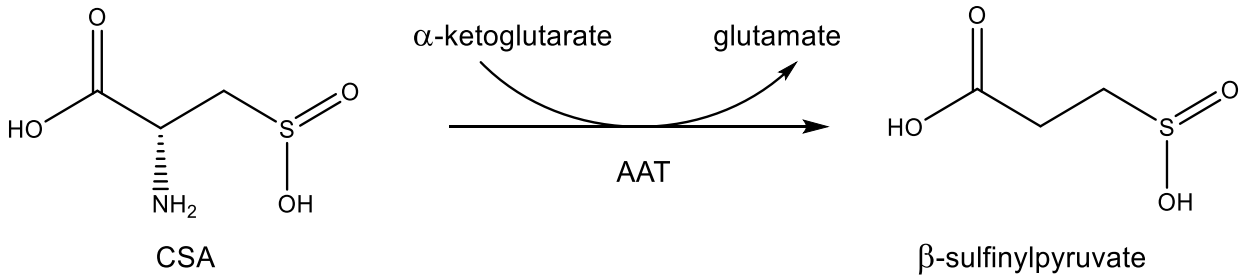

Figure 1.10. Conversion of cysteine sulfinic acid (CSA) to β-sulfinylpyruvate by aspartate aminotransferase (AAT) [35].

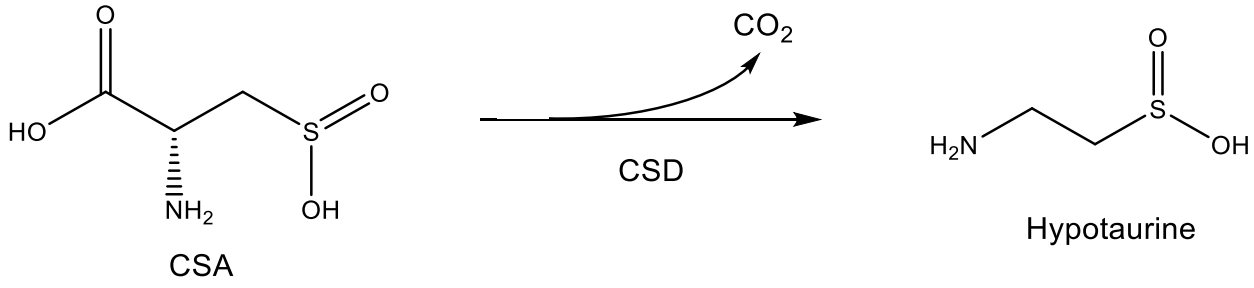

Figure 1.11. Conversion of cysteine sulfinic acid (CSA) to hypotaurine by cysteinesulfinate decarboxylase (CSD) [39].

1.4.1 Regulation of cysteine sulfinic acid

Like the homocysteine branch point, the branch point of CSA is also dietarily regulated. Several studies have shown that varying concentrations of dietary cysteine impacts cysteine regulation, enzyme activity, and pyruvate and taurine production [41-43]. Whether CSA is converted to pyruvate or taurine depends on the amount of cysteine present in hepatic tissue [3]. When cysteine is in excess of normal physiological levels, pyruvate and sulfite production (via AAT) is favored, and when cysteine is limiting, taurine production (via CSD) is favored [41, 44-46]. Looking at the kinetic properties, the K_m value for CSA with AAT (3-25 mM) is much larger than the K_m value for CSA with CSD (0.04-0.17 mM) providing evidence that AAT can endure large concentrations of CSA [35, 47-49].

1.5 Structural properties of cysteine dioxygenase

Cysteine dioxygenase (CDO) is a mononuclear non-heme iron enzyme belonging to the cupin superfamily. This superfamily, consisting of prokaryotes and eukaryotes, is considered the most diverse superfamily next to the triosephosphateisomerase (TIM) barrel superfamily [50, 51]. Cupins include a vast array of enzymatic and non-enzymatic proteins which have a higher level of thermostability and show resistance to proteases [51]. Thermostability and protease resistance are products of close, compact structural packing and short loops between secondary structural components [50]. Concerning proteases degradation, the short loops (< 50 amino acid residues) reduce the amount of sites accessible for protease cleavage [50]. The main characteristic of the cupin superfamily is represented by the double-stranded β-helix (DSBH) structural fold [50-53]. This conserved structure is typically composed of six or eight β-strands imitating a sandwich like fold (**Figure 1.12**) [52, 53].

This conserved cupin "jelly roll" fold forms a flexible, small molecule binding active site creating an environment for unique chemistry to take place [50, 53]. Members of the cupin family generally contain two conserved motifs defined as GX_5**H**X**H**X_{3-6}**E**X_6G (motif 1) and $GX_{5-7}PXGX_2$**H**X_3N (motif 2). The first motif highlights two conserved histidines and one glutamate, while motif 2 has an additional conserved histidine. Together these two motifs represent a 3-His/1-Glu ligand responsible for active site metal coordination (**Figure 1.13**).

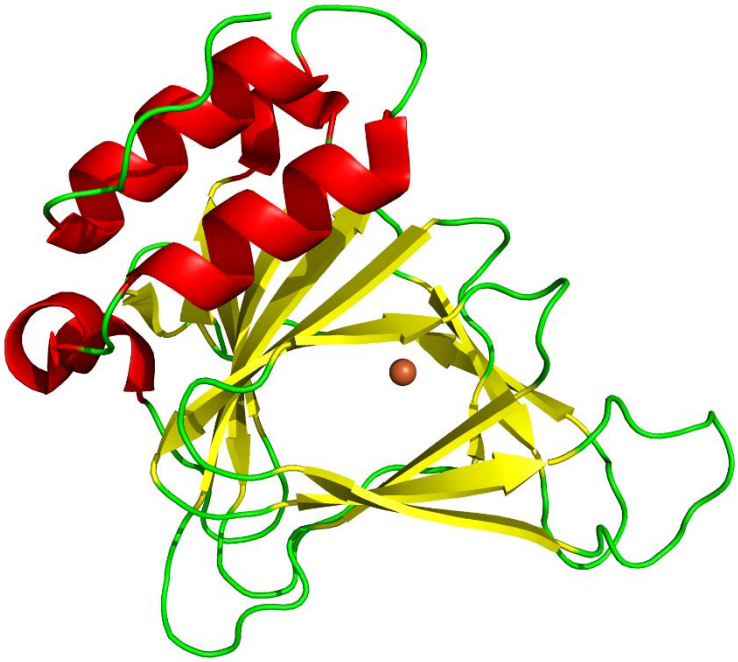

Figure 1.12. Crystal structure of CDO depicting the DSBH cupin superfamily fold; alpha helices (red), beta sheets (yellow), turns/loops (green), and iron core (bronze). PDB: 4KWJ [54].

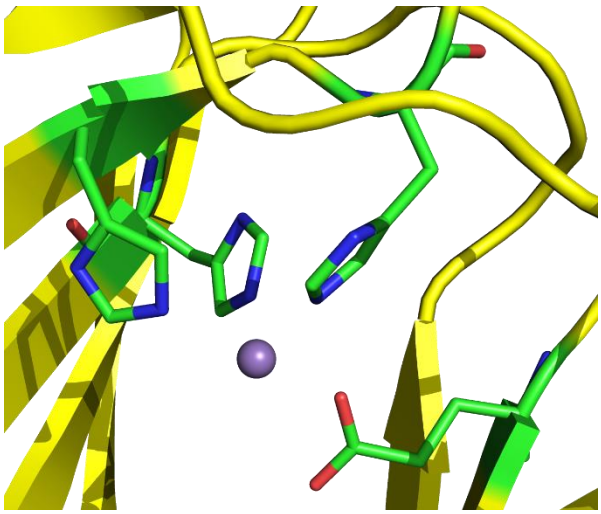

Figure 1.13. Crystal structure of cupin oxalate oxidase depicting the traditional 3-His/1-Glu coordination of a metal. Mn cation (purple). PDB: 2ET1 [55].

Advances in sequencing have shown these motifs to be less conserved than originally thought, but they are still used as a general standard for cupins [51]. In cupins, histidine and glutamate have been known to coordinate a wide variety of transition metals. The most common active site metal is iron, but other metals such as copper, nickel, and manganese have been found [51-53]. Interestingly, the very first crystal structure of CDO contained a nickel center as an artifact of purification techniques [56]. Regardless of the metal, the cation typically exhibits a six-coordinate octahedral style geometry, although alternative coordination has also been observed [53, 57-60]. The metallo-cupins frequently share a sequential substrate binding mechanism where the substrate is first to coordinate followed by dioxygen coordination to the metal cation [52].

Cysteine dioxygenase lacks the typical glutamate from the first motif leaving the six-coordinate iron center coordinated by only three histidines (**Figure 1.14a**). The imidazole ring of histidine acts as a monodentate ligand, so a 3-His facial triad presents a weak coordination environment for the iron. This weak coordination may account for the varied amounts (~10-70%) of reported iron bound in the recombinant enzyme active site of cysteine dioxygenase [32-34, 58, 61-63]. In the case of CDO, the glutamate from motif 1 is replaced with cysteine (Cys93). This non coordinating cysteine amino acid forms a covalent thioether bond with a nearby tyrosine (Tyr157) residue (**Figure 1.14b**).

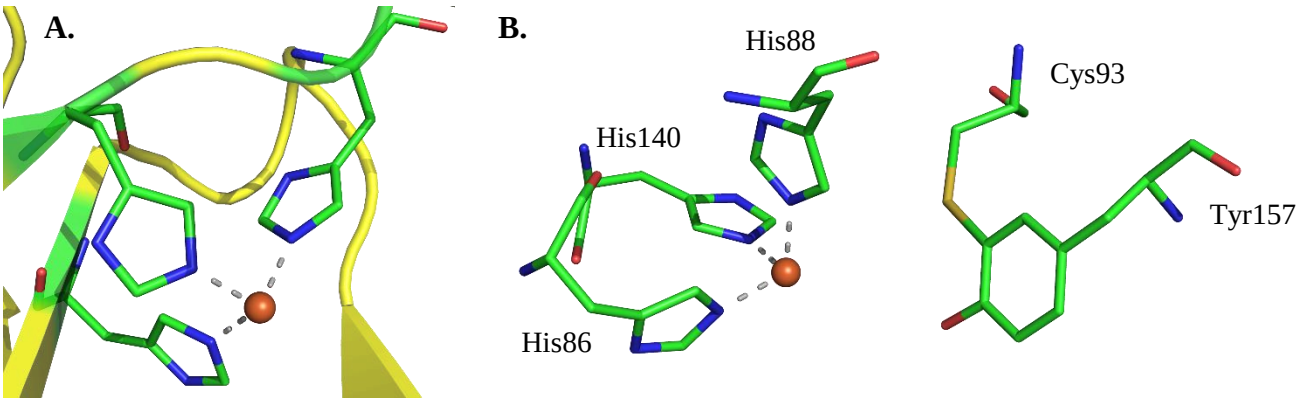

Figure 1.14. Crystal structure of the active site in cysteine dioxygenase. **A.** Iron (bronze) is weakly coordinated 3 histidine residues (His 86, 88, 140). **B.** Near the iron center lies the thioether crosslink between Cys93 and Tyr157. PDB: 4KWJ [54]

1.5.1 Crosslink formation in cysteine dioxygenase

The thioether adduct in recombinant wild-type CDO exists as a heterogeneous mixture of non crosslinked and crosslinked isoforms [64]. Overall few enzymes have been shown to have a

thioether crosslink. To date only five known enzymes contain a Cys-Tyr crosslink: galactose oxidase, glyoxal oxidase, siroheme- and [Fe4-S4]-dependent sulfite reductase (NirA), cytochrome c nitrite reductase, and cysteine dioxygenase [56, 65-69]. Cysteine dioxygenase stands-out from the other enzymes because the formation of the crosslink is not essential for activity. For instance, galactose oxidase, a copper enzyme that catalyzes the oxidation of D-galactose by the reduction of molecular oxygen and hydrogen peroxide, contains a homogeneous crosslinked thioether adduct [70]. The crosslinked-involved tyrosine in galactose oxidase actually coordinates the Cu(II) ion along with four other ligands in a square pyramidal arrangement [65]. It has been shown that no external enzymes or substrates are needed to form the Cys-Tyr cofactor in galactose oxidase.

Crosslink formation in galactose oxidase is a self-starting reaction only requiring the presence of the Cu(II) metal center and dioxygen [71]. Upon mutation of cysteine to glutamate, in galactose oxidase, the crosslink was abolished and there was no measurable activity [72]. This strongly suggested that the crosslink is needed for catalytic activity in galactose oxidase. Similar trends were seen with glyoxal oxidase and NirA. Additionally these other thioether containing enzymes exist solely as a crosslinked isoform [56, 65-69]. It is interesting that CDO is able to exist as a heterogeneous mixture of both non crosslinked and crosslinked isoforms. Even more intriguing is the crosslink in CDO is not needed for catalytic activity. When crosslinked involved Cys93 was mutated to serine, catalytic activity was still present [33]. This and other mutational studies of Cys93 suggest the Cys-Tyr crosslink is not essential for activity [73].

1.5.2 Identification of the crosslink in cysteine dioxygenase

Early analysis of CDO, purified from rat liver, revealed a single, ~22,500 kDa, molecular weight band on SDS-PAGE [74]. Later studies showed an appearance of a second, lower molecular weight band. The lower molecular weight band was identified during an investigation on the

effects of a high sulfur diet in rats [75]. Rats that were fed high concentrations of protein and/or methionine displayed an increase in the lower molecular weight band of CDO [75]. Based on these results it was suggested that the production of the lower molecular weight band was diet dependent. Further studies investigated the effects of excess sulfur amino acids on cysteine metabolism in rats. These studies showed rats, who were fed a high cysteine diet, had a prominent lower molecular weight band, which raised the question of whether the presence of the lower band was correlated with activity [44]. Studies to individually isolate the two bands by anion-exchange FPLC were unsuccessful [64]. However the two bands were successfully analyzed and sequenced through mass spectrometry which resulted in a ~ 25 kDa higher molecular weight band and a ~ 23 kDa lower molecular weight band that had identical amino acid sequences [64]. The difference between the two bands was established when the first three-dimensional crystal structure of CDO revealed a covalent bond between Cys93 and Tyr157 [56, 58]. The higher molecular weight band does not contain the crosslinked Cys-Tyr (non crosslinked), whereas the lower molecular weight band contains the covalently bonded Cys-Tyr (crosslinked) [33]. Purified recombinant rat CDO exists as a ~ 50/50 mixture of non crosslinked and crosslinked CDO.

1.5.3 Mechanism of crosslink formation in cysteine dioxygenase

Currently all proposed mechanisms of cysteine sulfinic acid assume that the fully crosslinked isoform is present before cysteine oxidation begins [33, 73]. However, no study has provided any evidence to support this. A method was developed to purify the homogenous non crosslinked isoform [33]. Results of the study found that in the presence of iron, an external reductant, and increasing concentrations of L-cysteine, the non crosslinked isoform could form the homogenous crosslinked isoform. A distinct lag phase was observed while measuring the catalytic consumption of dioxygen while CDO converts the homogenous non crosslinked enzyme to the

crosslinked isoform. These studies further revealed that the homogenous crosslinked isoform was shown to enhance catalytic activity 10-fold compared to wild-type [33, 73, 76]. So undoubtedly the presence of the Cys-Tyr crosslink plays an important role in enhancing catalysis for these enzymes.

The same study also proposed a new mechanism for crosslink (**Figure 1.15**). Briefly, the amino and thiolate group of the cysteine substrate coordinates the ferrous iron, followed by dioxygen binding oxidizing the ferrous to ferric iron. The hydroxyl group of Tyr157 stabilizes the superoxo iron species through hydrogen bonding which facilitates a proton coupled electron transfer through Tyr157. The crosslink is generated through a nucleophilic attack by the thiolate on the tyrosyl intermediate. Lastly, electron transfer and proton loss from the crosslinked intermediate reduces the ferric iron back to ferrous and the crosslinked is formed [33]. The non crosslinked wild-type CDO enzyme is in the EPR silent ferrous state, and native and fully crosslinked wild-type CDO in the high spin ferric state [33]. When cysteine is introduced aerobically with the non crosslinked isoform, the relative intensity increases and gives a high spin ferric signal. Addition of cysteine, to the crosslinked isoform gave no change in the relative intensity under aerobic conditions. Previously it was thought that the increase in signal intensity was due to the coordination of the cysteine substrate to the iron center; however, the increase in signal intensity may correlate with crosslink formation [33, 77].

1.5.4 Mechanism of product formation in cysteine dioxygenase

In addition to being a requirement for crosslink formation, iron, dioxygen, and L-cysteine are needed to form cysteine sulfinic acid. Currently proposed mechanisms suggest that the catalytic steps involved in crosslink formation are similar to those in cysteine oxidation. Previously discussed EPR studies have shown the iron in wild-type CDO exhibits a ferrous resting state,

oxidizing to the ferric form after the addition of substrates [32] . Furthermore, a six-coordinate ferrous iron ES complex was identified by X-ray absorption spectroscopy (XAS) [78]. Over the years several cysteine sulfinic acid mechanisms have been proposed [33, 56, 58, 63, 78-80]. Except for Simmons, et. al. (2006), all mechanisms agree that the cysteine substrate is first to bind bidentate followed by oxygen activate. The bidentate substrate coordination was eventually confirmed by visualization of a substrate bound crystal structure of wild-type CDO [79]. Albeit very similar to previously designed reaction mechanisms, a more recent mechanism of cysteine oxidation is shown in **Figure 1.16**.

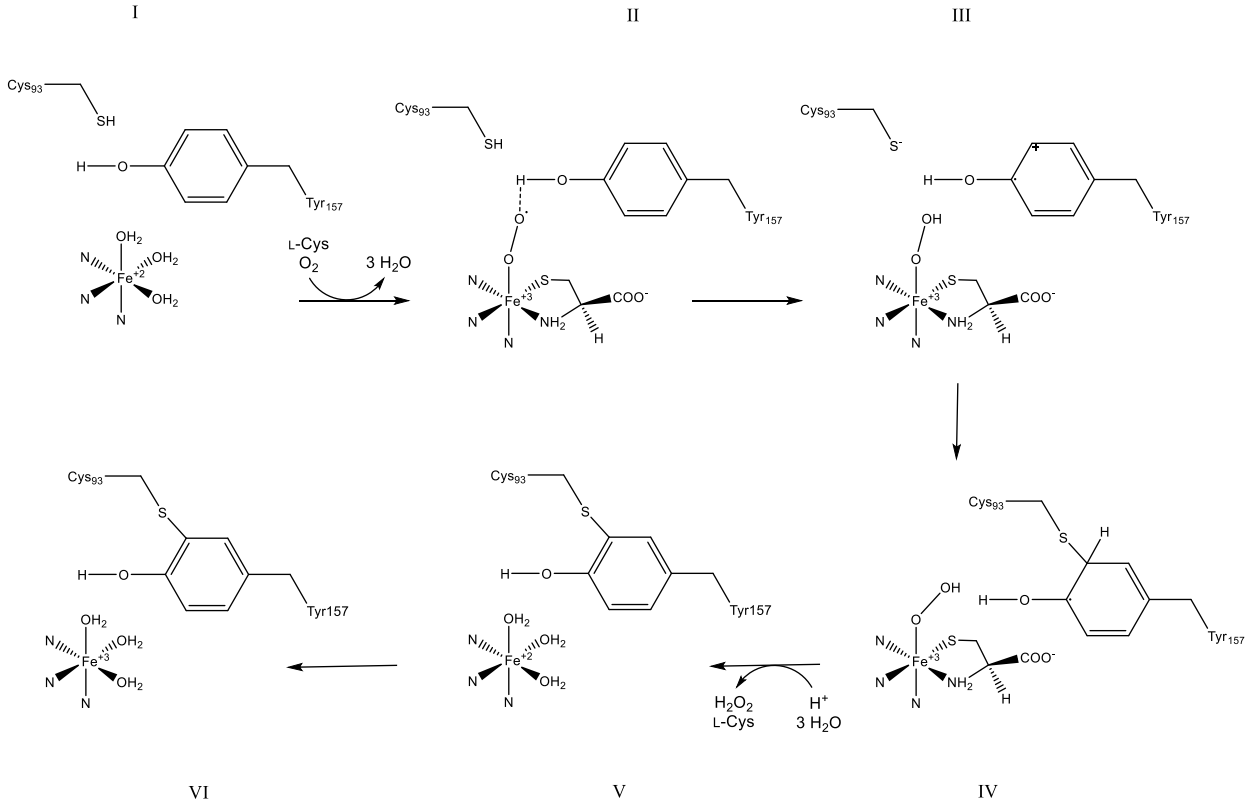

Figure 1.15. Mechanism of crosslink formation in CDO. Adapted from Njeri, et. al. [33].

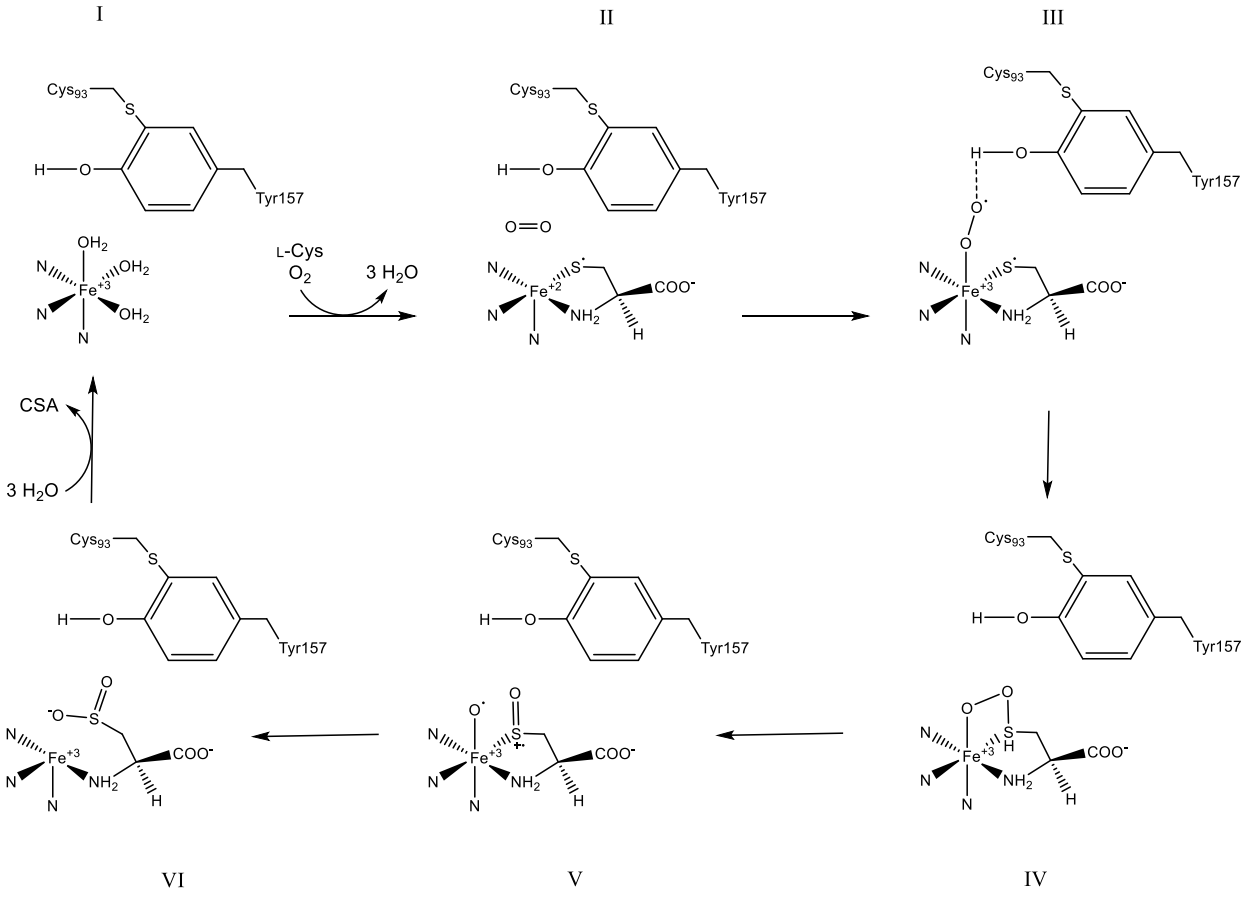

Figure 1.16. Mechanism of cysteine oxidation by cysteine dioxygenase. Adapted from [33].

1.5.5 Conserved amino acids in cysteine dioxygenase

Multiple sequence alignments of CDO homologs found nine conserved amino acid residues [56]. With the exception of Gly100, conserved residues Tyr58, Arg60, Trp77, His86, His88, His140, His155, and Tyr157 are all found within 8 Å of the active site (**Figure 1.17**). It is interesting the cysteine residue involved in the formation of the crosslink is not conserved among species. Rather, in bacteria the cysteine is replaced by a glycine residue, which is unable to form the crosslinked species. Inherently, His86, His88, and His140 make up the 3-His facial triad responsible for iron coordination. Determination of apo and substrate bound crystal structures along with site-directed mutagenesis has provided some insight into the role(s) of the remaining six residues.

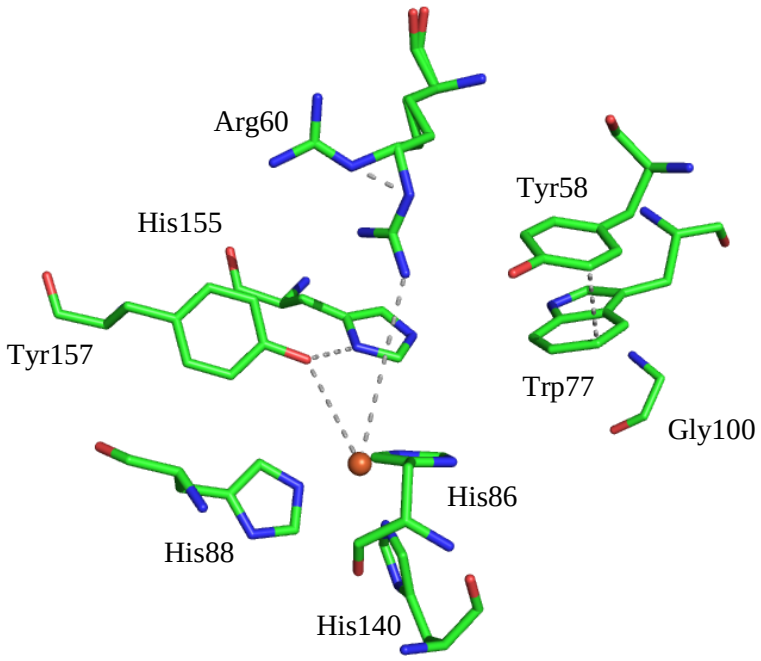

Figure 1.17. The nine conserved residues found in cysteine dioxygenase. PDB: 4KWJ [54]

The πN of His155 is located 2.8 Å from the hydroxyl group of Tyr157. The His155, Tyr157, and Ser153 (not shown) form a hydrogen bonding network [81, 82]. A H155A CDO variant showed an 80-fold decrease in CSA production compared to wild-type [83]. Furthermore, purified H155A exists as the homogeneous non crosslinked isoform, alluding that it may play an indirect role in crosslink formation.

Additionally, several mutational studies have been performed with Tyr58, Arg60 and Tyr157. Both Tyr58 and Arg60 have been proposed to play a role in L-cysteine coordination and specificity [56, 58, 79]. To further evaluate the role of Y58 and R60 in catalysis Y58A, Y58F, R60A, and R60K CDO variants were constructed [84]. Both Y58 variants had a 20-fold decrease in dioxygen consumption (k_{cat}/K_m) as compared to wild-type CDO. Variants of R60 displayed a 60-fold decrease in dioxygen consumption. This study concluded that both Tyr58 and Arg60 play a role in catalysis, with Arg60 serving as the primary amino acid involved in L-cysteine coordination [84]. Similarly, previous studies reported that variants R60A and R60Q CDO had a 70-fold decrease in cysteine sulfinic acid production [73, 79].

Interestingly, two independently determined crystal structures of apo wild-type CDO, reported Arg60 existing in two conformations, bent and extended, both sharing equal electron density (**Figure 1.17**) [54, 81]. This conformational switch takes place at the δ-carbon of Arg60. However, in the substrate bound crystal structure, Arg60 exists exclusively as the bent conformation [85]. It is currently unknown what causes this 2.0 Å switch between isoforms. However, in the bent conformation, the two nitrogens of the guanidinium group in Arg60 lie 2.9 and 3.1 Å from the carboxyl group of the cysteine substrate. Additionally, the hydroxyl group of Tyr58 lies 3.1 Å from the carboxyl group of L-cysteine (**Figure 1.18**). Therefore, Tyr58 and Arg60 stabilize L-cysteine through electrostatic and hydrogen bonding interactions. Additionally, the

aromatic ring of Trp77 provides stabilization to Tyr58 through π-π stacking interactions. Although, the exact role the π-π interactions play in catalysis is unknown.

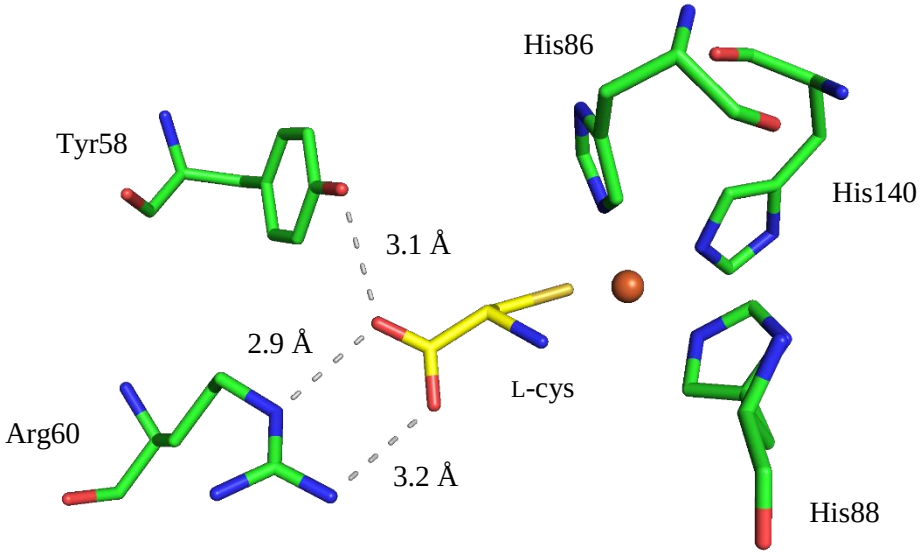

Figure 1.18. Substrate bound active site of cysteine dioxygenase, highlighting the positions of Tyr58 and Arg60 in relation to the L-cysteine substrate. PDB: 4IEV [85]

Similar to Arg60, several mutational studies have been performed to determine the role of Tyr157. In fact, there are several proposed functional roles for Tyr157. Most notably, the participation of Tyr157 in the crosslinked isoform has been shown to enhance overall catalytic efficiency by 10-fold [33, 73, 76]. Several studies have evaluated the effects of mutating Tyr157 to phenylalanine. All but one of these studies report a > 60-fold decrease in product formation [33, 73, 79, 83]. In order to further investigate the role of Tyr157, a more recently study produced twenty-one crystal structures; five being the Y157F variant [82]. These studies concluded that in

the crosslinked isoform Tyr157 enables proper cysteine coordination and dioxygen stabilization, both essential for optimal active site chemistry.

1.6 Summary

Elemental sulfur is essential for maintaining metabolic function. In mammals, the amino acids methionine and cysteine are the main dietary sources of sulfur. Generally, cysteine is found at low levels in the body to maintain a proper sulfur balance. However, when there is a high influx of sulfur, the liver plays a crucial role in preserving homeostasis. Homeostasis occurs through two regulatory branch points located within the sulfur metabolic pathway.

The first branch point occurs after methionine is catabolized to homocysteine. Homocysteine can either be converted back to methionine through the transmethylation pathway or catabolized to cysteine sulfinic acid by the transsulfuration pathway. Regulation between the two pathways is dependent on overall substrate availability, with AdoMet being the primary regulator. In general, when there is a dietary increase in sulfur, transsulfuration is favored. However, when sulfur levels are low to normal transmethylation is favored.

The second branch point in the sulfur metabolic pathway is the irreversible conversion of homocysteine to cysteine sulfinic acid. The production of cysteine sulfinic acid in mammals is an important branch point in cysteine metabolism. Key enzymes rely on the readily oxidized cysteine as a precursor for the formation of biologically relative small molecules pyruvate and taurine. Whether cysteine sulfinic acid is converted to pyruvate or taurine is dependent on the concentration of dietary cysteine present. When cysteine is in physiologically excess, pyruvate production via aspartate aminotransferase is favored. However when dietary cysteine levels are low, taurine production by cysteinesulfinate decarboxylase is favored.

In mammals, cysteine sulfinic acid is produced by cysteine dioxygenase (CDO) which catalyzes the conversion of L-cysteine to L-cysteine sulfinic acid in the presence of dioxygen. CDO is a mononuclear nonheme iron enzyme which belong to the cupin superfamily. Cupins are comprised of a series of antiparallel β-sheets which double over to make a sandwich like fold that encompasses the active site. Generally, most cupins also share two common motifs GX_5**H**X**H**X_{3-6}**E**X_6G (motif 1) and $GX_{5-7}PXGX_2$**H**X_3N (motif 2). Together the three histidines and one glutamate comprise the ligands responsible for active site metal coordination. However, CDO lacks the typical glutamate residue from the first motif, and is replaced by a non coordinating cysteine residue (Cys93). The iron center is weakly coordinated by three histidine residues.

Additionally, the non coordinating Cys93 forms a thioether crosslink with a nearby tyrosine residue (Tyr157). *In vivo*, CDO exists as a homogeneously non crosslinked isoform. However, *in vitro*, recombinant wild-type CDO exists as an equal mixture of non crosslinked and crosslinked isoforms. Unlike other enzymes that contain a thioether crosslink, the crosslink in CDO is not essential for catalysis. However, when present, the homogeneously crosslinked isoform in CDO increases catalytic efficiency 10-fold. Additionally, crosslink formation is substrate dependent, requiring L-cysteine in addition to iron and dioxygen. Several available three dimensional crystal structures of CDO are available. However, despite wild-type CDO existing in a heterogeneous mixture of non crosslinked and crosslinked isoforms, only the crosslinked species has been determined. Only recently has a method for purification of the homogeneous non crosslinked isoform developed.

The first focus of this dissertation is to investigate the evolutionary divergence of cysteine dioxygenase from the typical 3-His/1-Glu to a 3-His coordination. Studies presented in this dissertation will focus on structural, kinetic, and spectroscopical studies of the variant C93E CDO.

Secondly, resolution and investigation of the crystal structure of non crosslinked wild-type CDO has proven vital in determining a mechanism of crosslink formation. Lastly, crosslinking studies of the conserved Arg60 residue, has provided insight into the role of substrate specificity in crosslink formation.

CHAPTER TWO

Investigating the Evolutionary Advantage of a 3-His Iron Coordination in the Active Site of Cysteine Dioxygenase

2.1 INTRODUCTION

Cysteine dioxygen is a non-heme iron enzyme which catalyzes the conversion of L-cysteine to cysteine sulfinic acid [86, 87]. Cysteine sulfinic acid (CSA) serves as a major branch point in mammalian cysteine metabolism. CSA can be decarboxylated to form hypotaurine or transaminated to form a pyruvate precursor β-sulfinylpyruvate [7]. Hypotaurine and β-sulfinylpyruvate are both non-enzymatically oxidized to form taurine and pyruvate [40]. Cysteine dioxygenase belongs to the cupin superfamily which is primarily characterized by a double-stranded β-helix or DSBH [50-53]. The DSBH fold typically consists of six to eight beta sheets that fold in half creating a sandwich-like casing around the enzyme's active site (**Figure 2.1a**). Overall cupins have a low sequence identity, however many cupins share traits from two motifs. The first motif designated as $GX_5\mathbf{H}X\mathbf{H}X_{3\text{-}6}\mathbf{E}X_6G$ is comprised of two histidines and one glutamate, while the second motif $GX_{5\text{-}7}PXGX_2\mathbf{H}X_3N$ only contains one histidine. Together this 3-His/1-Glu motif serves as the metal coordinating ligand in many cupin enzymes (**Figure 2.1b**). The nitrogen of histidine's imidazole ring bonds monodentate to the metal, while glutamate coordinates the metal by the hydroxyl functional group. In cupins, the resting state of the enzyme's

metal center exhibits a wide range of geometrical configurations [52, 53, 57, 88]. Alternatively, the substrate bound metal cation usually exhibits octahedral geometry, allowing for a total of six coordination sites. Overall this 3-His/1-Glu ligand occupies four coordination sites with solvent molecules filling the remaining sites. For many cupin dioxygenases, the solvent molecules are displaced by single-site binding of the substrate followed by dioxygen [52].

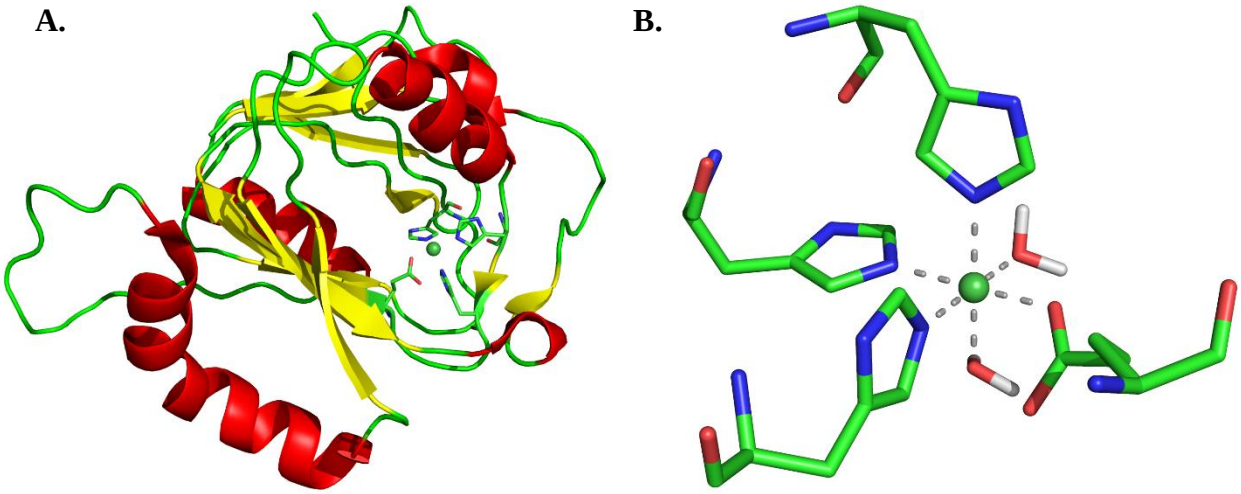

Figure 2.1. Cupin superfamily enzyme acireductone dioxygenase. **A.** Double-stranded beta-helix DSBH sandwich fold, **B.** Active site displaying the 3-His/1-Glu nickel coordination environment. PDB: 1ZRR [89].

The active site of cysteine dioxygenase lacks the typical 3-His/1-Glu cupin motif. Instead the glutamate residue in motif 1 is replaced by a noncoordinating cysteine (Cys93), leaving iron weakly coordinated by three histidine residues (His 86, 88, and 140). Interestingly, the noncoordinating cysteine residue forms a thioether bond with a nearby tyrosine (Tyr157) residue **Figure 2.2**). Recombinant wild-type CDO exists as an approximate equal mixture of non

crosslinked and crosslinked isoforms. When evaluted by SDS-PAGE these isoforms resolve as two distinct bands with the non crosslinked isoform representing the upper molecular weight band.

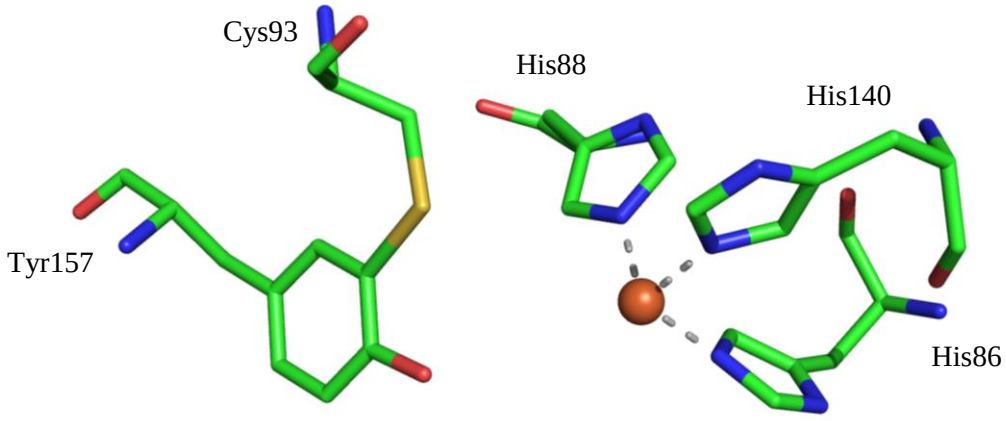

Figure 2.2. Active site of cysteine dioxygenase with the Cys-Tyr crosslink highlighted. PDB: 4KWJ [54].

Several mutational studies on Cys93 have been performed to evaluate the overall contribution of this amino acid in both crosslink formation and catalysis [73, 76, 78, 85]. Studies have shown the Cys-Tyr crosslink is not required for product formation but when present the crosslink enhances catalytic effeciency 10-fold [33]. However no study to date has investigated the evolutionary divergence of the coordinating glutamate in cysteine dioxygenase. The conserved Cys93 residue was replaced with glutamate to determine how the substitution affected the kinetic and structural properties of the enzyme.

2.2 METHODS AND MATERIALS

2.2.1 Materials

4-(2-Hydroxyethyl)piperazine-1-ethanesulfonic acid (HEPES), L-cysteine, D-cysteine, cysteamine, 3-mercaptopropionic acid, L-ascorbate, ammonium sulfate, ampicillin, streptomycin sulfate, lysozyme, and brilliant blue R were purchased from Sigma (St. Louis, MO). Isopropyl-β-D-thiogalactoside (IPTG) was purchased from Gold Biotechnology (St. Louis, MO). Glycerol and sodium chloride were purchased from Macron Fine Chemicals (Center Valley, PA). Difco-brand Luria-Bertani (LB) media was purchased from Becton Dickinson and Company (Sparks, MD). Macro-Prep® High Q Support column media was purchased from Bio-Rad Laboratories (Hercules, CA).

2.2.2 Construction and Purification of C93E CDO

The expression vector for C93E CDO was constructed through PCR amplification using 29 base oligonucleotide primers that replace the wild-type Cys codon with the Glu codon (GAA). The PCR product containing the Cys to Glu substitution was confirmed by DNA sequence analysis (Davis Sequencing, Davis, CA), and the C93E CDO vector was transformed into BL21 (DE3) competent *E. coli* cells and stored as 20% glycerol stock at -80 °C. Expression of wild-type and C93E CDO was carried out as previously described [32]. Cell pellets were resuspended with 100 mL 25 mM HEPES, pH 7.5, 10% glycerol and 0.02 mg/mL lysozyme in 10 mM Tris-Cl, pH 8.5. The resuspended cell mixture was lysed by sonication followed by centrifugation at 10 000 rpm, 4 °C for 15 min. Addition of 1.5% streptomycin sulfate (w/v) was added to the supernatant, and the solution was slowly stirred at 4 °C for 1 hour. The solution containing precipitated nucleic acids was centrifuged at 10 000 rpm at 4 °C for 20 min. An additional 100 mL 25 mM HEPES,

pH 7.5, 10% glycerol was added to the supernatant before loading onto the Macro-Prep® High Q Support (Bio-Rad Laboratories, Hercules, CA). Protein was eluted from the column using a linear gradient from 0 - 150 mM sodium chloride in 25 mM HEPES, pH 7.5, 10% glycerol. Fraction purity was determined by SDS-PAGE (5% stacking with 12% resolving), and fractions determined to be of the highest purity were pooled and concentrated with 70% ammonium sulfate (w/v) and stirred at 4 °C for 1 hour. The enzyme solution was centrifuged at 10 000 rpm, 4 °C for 20 minutes, and the pellet resuspended in 10 - 15 mL of 25 mM HEPES, pH 7.5, 10% glycerol, 100 mM sodium chloride. The protein concentration was determined by UV-visible absorption spectroscopy at 280 nm using a molar extinction coefficient of 25 440 M^{-1} cm^{-1}. A 1:1.2 protein to ferrous ammonium sulfate molar ratio was added to the protein solution, and the protein was dialyzed twice against one liter 25 mM HEPES, pH 7.5, 10% glycerol, 100 mM sodium chloride to remove any unbound iron. After dialysis, the protein was centrifuged at 10 000 rpm, 4 °C for 15 minutes to remove any precipitated protein, and the total iron content was quantified as previously described [33]. Aliquots of the protein were flash frozen with liquid nitrogen, and stored at -80 °C.

2.2.3 Circular Dichroism

Protein samples were buffer exchanged with 10 mM potassium phosphate, pH 7.5 using a 10 000 kDa MWCO Amicon Ultra Centrifugal Filters (Millipore) at 5000 RPM, 4°C. Far-UV circular dichroism spectra were recorded on a JASCO J-810 spectropolarimeter. Spectra of wild-type and C93E CDO (10 μM) were taken in 0.1 nm increments in continuous scanning mode from 300 to 185 nm in a 0.1 cm cuvette with a bandwidth of 1 nm and scanning speed of 20 nm/min. Each spectra is an average of six scans. Background subtraction and smoothing of the data were performed using the software provided. Final data was plotted using KaleidaGraph™ software (Synergy Software, Reading, PA).

2.2.4 Wild-type and C93E CDO Activity and Product Analysis

Steady-state kinetic parameters were determined using a Clark-type oxygen electrode to monitor the rate of dioxygen consumption. Each assay contained a final concentration of 2 μM protein and 1 mM ascorbate in 25 mM HEPES, pH 7.5, at 37 °C. The assays were initiated by the addition of L-cysteine substrate (50 μM to 5 mM), and the initial linear velocities were recorded 5-10 seconds after initiation of the reaction and then plotted against the substrate concentration. Steady-state kinetic parameters were corrected based on the amount of iron bound. Data calculated was an average of at least four individual experiments and was plotted and evaluated using the Michaelis-Menten equation in KaleidaGraph™ software (Synergy Software, Reading, PA).

Cysteine sulfinic acid (CSA) formation was quantified using mass spectrometry (MS) and then correlated with the rate of dioxygen consumption. Assays conditions were similar to steady-state kinetic experiments, and reactions were initiated with the addition of 1 mM L-cysteine. After one minute the reaction was quenched with 1 μL formic acid (90% v/v). Acetonitrile was added to the quenched reaction in a 1:1 ratio (v/v). Mass analysis was performed on an Ultra Performance LC System (ACQUITY, Waters Corp., Milford, MA, USA) in conjunction with a quadrupole time-of-flight mass spectrometer (Q-Tof Premier, Waters) with electrospray ionization (ESI-MS) in negative mode. Cysteine sulfinic acid concentrations were evaluated against a CSA standard curve which ranged from 50 - 200 μM. Substrate analogs D-cysteine, cysteamine (2-aminoethanethiol), and 3-mercaptoproprionic acid (3-MPA) were also tested for dioxygen consumption and product formation using the same parameters described.

2.2.5 EPR Spectroscopy

Electron paramagnetic resonance (EPR) studies were performed on a Bruker EMX spectrometer at X-band frequency (Bruker Biospin Corporation, Billerica, MA). Cooling to 9.8 K was performed using an Oxford Instruments ESR 900 flow cryostat and an ITC4 temperature controller. All samples prepared for EPR analysis had a final concentration of 100 μM enzyme in 25 mM HEPES, 10% glycerol, pH 7.5, with 0.1 M NaCl. Samples containing L-cysteine, or L-cysteine analogs, were incubated in a final concentration of 10 mM L-cysteine on ice for 1 min and then flash frozen in EPR tubes with liquid nitrogen. All spectra were recorded using the following settings: 9.39 GHz microwave frequency, 1.99 mW microwave power, 2 x 10^4 or 4 x 10^4 receiver gain, 100 kHz modulation frequency, 6 G modulation amplitude, with a time constant of 163.84 ms, and a sweep time of 167.77 s. Percent iron bound was calculated by spin quantification using 1 mM copper (II) sulfate in 10 mM EDTA (pH 8.0) as the standard.

2.2.6 Crystallization and Diffraction Data Collection

Recombinant wild-type and C93E CDO enzymes were purified as described above for crystallization trials. After dialysis, CDO was concentrated using 10 000 kDa MWCO Amicon Ultra Centrifugal Filters (Millipore) at 5 000 RPM, 4°C. Concentrated enzyme was flash frozen with liquid nitrogen and stored at - 80°C. Final concentration of enzyme ranged from 15 – 20 mg/mL. Crystals were grown at 24°C using the hanging drop method. Each drop contained 1.5 μL of protein mixed with an equal volume of reservoir solution. The reservoir buffer for wild-type CDO contained 1 M lithium chloride, 22.5% (w/v) poly(ethylene glycol) (PEG) 10,000 in 0.1 M MES, pH 5.5, and the reservoir buffer of C93E CDO contained 1 M lithium chloride, 30% PEG 6,000 in 0.1 M sodium acetate. Crystals were formed after one day and grew to full size within four days. For data collection, crystals were serially washed in 1 M lithium chloride, 30% PEG

600 in 0.1 M sodium acetate supplemented with 20% (w/v) sucrose as a cryoprotectant and flash frozen to - 160°C.

Wild-type CDO diffraction data (0.15° oscillation images for a total of 83°) was collected at the Stanford Synchrotron Radiation Laboratory (Stanford, CA) on beamline 12-2 at a wavelength of 0.9795 Å at 100 K. The exposure time per frame was 0.5 s with 79.5% attenuation and a crystal to detector distance of 344.6 mm. The data was indexed and scaled with XDS to 2.49 Å. The crystals were assigned to the space group $P4_12_12$ with unit cell dimensions a = b = 57.45 Å and c = 122.26 Å. C93E CDO diffraction data (0.4° oscillation images for a total of 360°) was collected on beamline 7-1 at a wavelength of 1.1271 Å at 100 K. The exposure time per frame was 5.71 s with 0% attenuation and a crystal to detector distance of 243.6 mm. The data was indexed and scaled with XDS to 1.91 Å. The crystals were assigned to the space group $P4_12_12$ with unit cell dimensions a = b = 57.69 Å and c = 122.21 Å (**Table 2.1**). Molecular replacement calculations were performed using Phaser in the PHENIX program suite, using PDB: 2B5H as the search model with iron and waters removed yielding a clear solution with each structure. Log likelihood gains ranged from 2282.3 – 9483.4 with TFZ scores of 48.1 – 94.0. Model building and refinement were performed using Coot and Phenix Refine [90].

Table 2.1: Data collection and refinement statistics for wild-type and C93E CDO

	Wild-Type CDO PDB: 6DL5	C93E CDO PDB: 6DL3
Data collection[a]		
Beamline	12-2	7-1
Wavelength (Å)	0.9795	1.1271
Space group	$P4_12_12$	$P4_12_12$
Cell dimensions; *a*, *b*, *c* (Å), β (°)	57.45, 57.45, 122.26	57.69, 57.69, 122.21
Resolution (Å)	38.55 – 2.49 (2.59 – 2.49)	38.69 – 1.91 (1.96 – 1.91)
R_{merge}[b]	0.082 (0.452)	0.085 (0.417)
Total observations	43530 (4665)	451694 (18259)
Total unique observations	7638 (809)	16741 (1068)
Mean ((*I* / sd(*I*))	13.5 (3.1)	33.4 (7.4)
Completeness (%)	99.2 (96.7)	99.9 (98.2)
Redundancy	5.7 (5.8)	27.0 (17.1)
Refinement		
Resolution (Å)	38.553 – 2.490 (2.683 – 2.490)	38.691 – 1.911 (1.967 – 1.911)
R_{cryst}[c]	0.1781 (0.2304)	0.1735 (0.1755)
R_{free}	0.2605 (0.3268)	0.2154 (0.2390)
Total unique observations	7599 (1307)	16517 (1154)
No. of non-hydrogen atoms		
Protein	1502	1481
Iron	1	1
Ligand	0	4
Water	5	84
rms deviation bonds (Å)	0.015	0.01
rms deviation angles (°)	1.283	1.037
Overall mean B-factor (Å^2)	36.94	18.42
Ramachandran plot analysis[d]		
Favored region	97.81	99.44
Allowed region	2.19	0.56
Outlier region	0.00	0.00

[a]data indexed and scaled with XDS

[b]$R_{merge} = \Sigma_h|I_h - \langle I \rangle|/\Sigma_h I_h$, where I_h is the intensity of reflection *h*, and $\langle I \rangle$ is the mean intensity of all symmetry-related

[c]$R_{cryst} = \Sigma||F_o| - |F_c||/\Sigma|F_o|$, F_o and F_c are observed and calculated structure factor amplitudes. Five percent of the relections were reserved for the calculation of R_{free}.

[d]Calculated with Molprobity

2.3 RESULTS

2.3.1 Characterization and Steady-state Kinetics of Wild-type and C93E CDO

Purification of wild-type and C93E CDO yielded pink and blue isoforms. However, it has been found that very few catalytic differences exist between the two isoforms (unpublished data). For this study, all results reported are from the blue isoform. Following purification, wild-type and C93E CDO enzymes were evaluated for crosslink formation by SDS-PAGE (**Figure 2.3**). Wild-type existed as a heterogenous mixture of both non crosslinked and crosslinked isoforms. Since C93E CDO lacks the crosslinked-involved cysteine, the mutated enzyme existed solely as the non crosslinked isoform. Additionally, far-UV circular dichroism spectra of wild-type and C93E CDO were recorded to determine the overall gross secondary structure (**Figure 2.4**). C93E CDO variant had a similar CD spectrum as wild-type CDO.

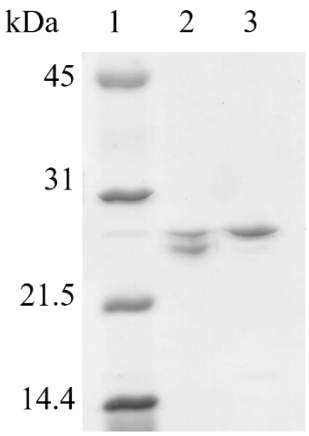

Figure 2.3. Analysis of wild-type CDO and C93E CDO by SDS-PAGE. (1) Molecular weight marker, (2) purified wild-type CDO containing a heterogeneous mixture of non crosslinked and crosslinked isoforms, and (3) purified C93E CDO existing only as the non crosslinked isoform.

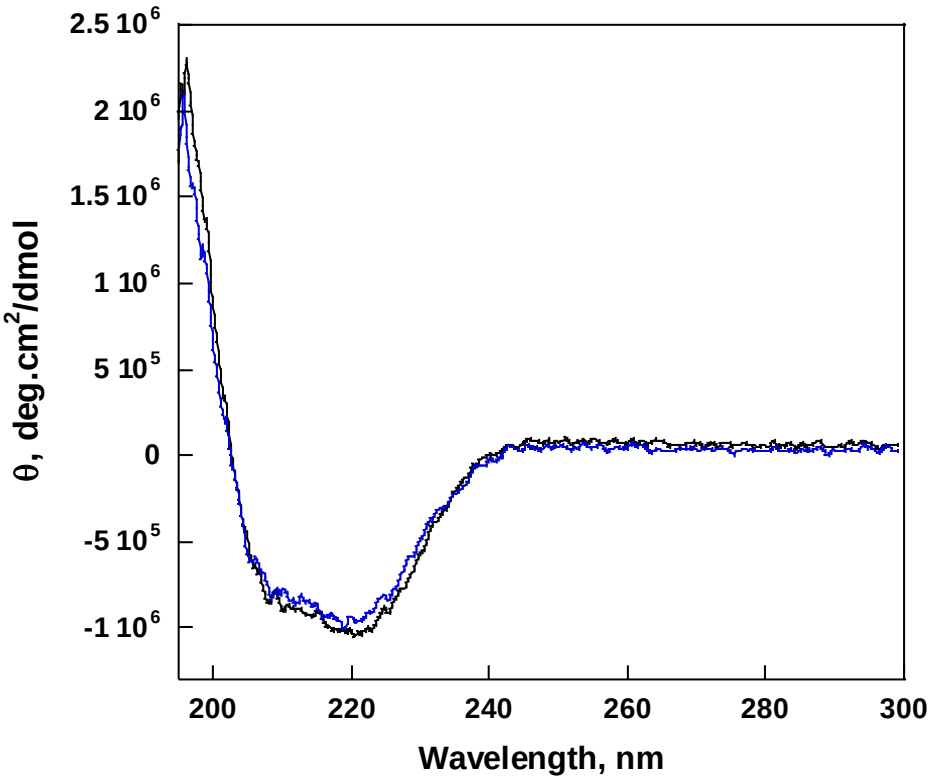

Figure 2.4. Circular dichroism spectra of wild-type and C93E CDO. Wild-type CDO (black line) and C93E CDO (blue line) spectra were taken with 10 μM protein in 10 mM potassium phosphate, pH 7.5.

Wild-type CDO had an iron content of ~50%, while C93E CDO had ~100% iron. Kinetic properties of the enzymes were determined by measuring the rate of dioxygen consumption using a Clark-type oxygen electrode. The k_{cat}/K_m value for C93E CDO resulted in a ~75-fold decrease in oxygen consumption compared to wild-type (**Table 2.2**). To evaluate substrate coordination of the active site, three analogs of L-cysteine were used (**Figure 2.5**). For C93E CDO, substrate analogs D-cysteine and cysteamine showed comparable k_{cat}/K_m values as L-cysteine, whereas 3-mercaptoproionic acid had no measurable activity with C93E or wild-type CDO (**Table 2.3**).

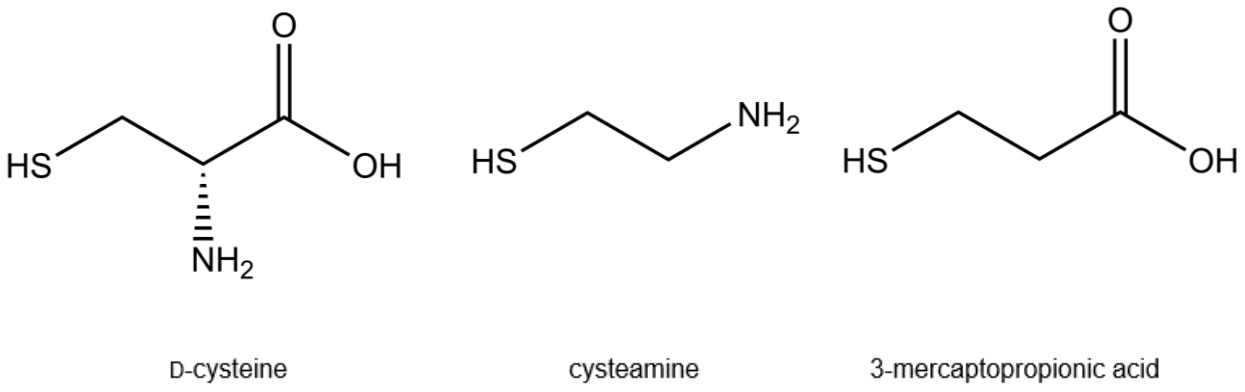

Figure 2.5. Structural analogs of L-cysteine: D-cysteine, cysteamine, and 3-mercaptopropionic acid (3-MPA).

Table 2.2: Steady-state kinetic parameters of wild-type and C93E CDO with L-cysteine.[a]

	k_{cat} (min^{-1})	K_m (mM)	k_{cat}/K_m ($mM^{-1}min^{-1}$)	% Iron Bound
wild-type CDO[b]	128 ± 6	0.06 ± 0.01	2133 ± 362	50%
C93E CDO	8 ± 1	0.29 ± 0.14	29 ± 15	35%

[a] Kinetic parameters adjusted for iron content
[b] Previously reported [33]

Table 2.3: Steady-state kinetic parameters of C93E CDO with cysteine analogs.[a]

	k_{cat} (min^{-1})	K_m (mM)	k_{cat}/K_m ($mM^{-1}min^{-1}$)
D-cysteine	12 ± 2	0.65 ± 0.35	19 ± 11
cysteamine	73 ± 11	1.6 ± 0.6	45 ± 18
3-mercaptopropionic acid	---	---	---

[a] Kinetic parameters adjusted for iron content

2.3.2 Analysis of Cysteine Sulfinic Acid Product

Mass spectrometric analyses were performed to correlate product formation with dioxygen utilization. Wild-type CDO formed 4001 ± 218 nmol of CSA per $min^{-1}mg^{-1}$ of enzyme which correlated with 4320 ± 244 nmol of O_2 consumed per $min^{-1}mg^{-1}$ of enzyme. Despite minimal oxygen consumption, C93E CDO was unable to form the CSA product. When cysteamine was used as a substrate, both wild-type and C93E CDO exhibited comparable dioxygen utilization. However, neither wild-type or C93E CDO were able to form hypotaurine in the presence of cysteamine (**Table 2.4**).

Table 2.4: Dioxygen utilization and cysteine sulfinic acid production of wild-type and C93E CDO with L-cysteine and cysteamine substrates.

	L-cysteine		cysteamine	
	wild-type CDO	C93E CDO	wild-type CDO	C93E CDO
Dioxygen utilization (nmol/min/mg)	4320 ± 244	265 ± 23	950 ± 16	1282 ± 13
Cysteine sulfinic acid production (nmol/min/mg)	4001 ± 218	---	---	---

2.3.3 EPR Analyses of Wild-type and C93E CDO

EPR analyses were performed to determine the oxidation state of the iron in the resting and substrate bound state of wild-type and C93E CDO. Previous EPR studies showed wild-type CDO to have a high spin iron (III) oxidation state with a g = 4.3 [32, 77]. Furthermore, the addition of L-cysteine gives rise to an increase in relative signal intensity [33, 63]. The increase in signal

intensity is attributed to L-cysteine coordination of the active site. Comparable to previous reported results, wild-type and C93E CDO existed in the high spin iron (III) oxidation state with an EPR signal of g = 4.3 (**Figure 2.6**). Spin quantification determined that 100% of the 50% iron present in wild-type was bound to the enzyme. However, despite being oxidized with 5 – 10 mM ferricyanide, only 35% of the reported 100% iron content was bound in C93E CDO.

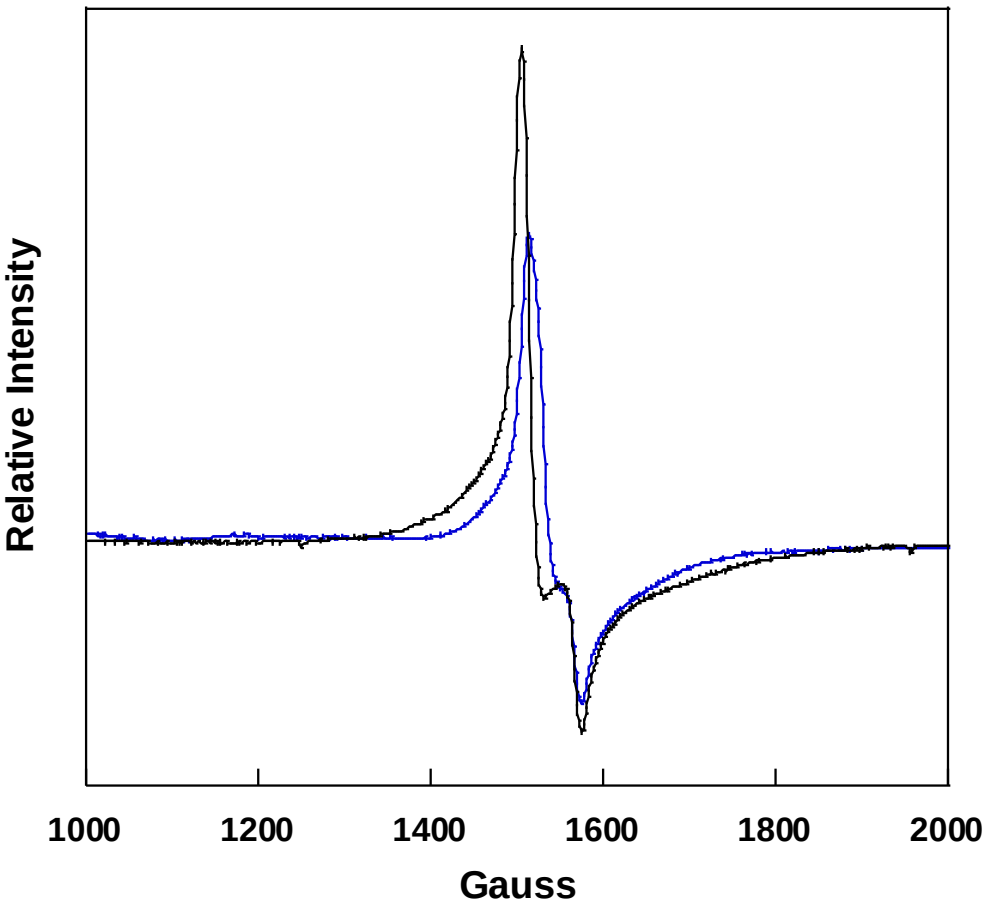

Figure 2.6. EPR spectra of wild-type (black trace) and C93E (blue trace) CDO. Spectra were taken with 100 μM protein in 25 mM HEPES buffer, pH 7.5, 10% glycerol, 100 mM sodium chloride.

To determine the effects of substrate in the active site, C93E CDO was incubated in the presence of L-cysteine, cysteamine, or 3-MPA. Compared to resting state C93E CDO, addition of substrates L-cysteine and 3-MPA resulted in an increase in the relative signal intensity whereas there was no observable increase in the presence of cysteamine (**Figure 2.7**).

2.3.4 Determination of Three-dimensional Crystal Structures of Wild-type and C93E CDO

The crystal structures of wild-type and C93E CDO were refined to 2.49 Å and 1.91 Å resolution, respectively. Overall the monomeric tertiary structure is comparable to previously solved CDO crystal structures [56, 58, 79, 85]. The monomer is composed of 11 antiparallel β-sheets, three α-helices, and one partial α-helix located between β7 and β8 (**Figure 2.8**). The N-terminus region begins with three α-helices followed by eleven β-sheets which fold to form the sandwich-like casing around the active site. The upper β-fold contains β3, β5, β6, β8, β10, and β11 while the lower (N-terminus) fold is composed of β1, β2, β4, β7, and β9. Together they encompass a mononuclear non-heme iron molecule. Previously solved crystal structures report two additional β-sheets (β12 and β13) located near the C-terminus in addition to a 3_{10} α-helix located between β1 and β2 (**Figure 2.9**) [56, 58, 79]. The absence of the two β-sheets is most likely due to the lower resolution or solvation interference in the secondary structure due to crystallization techniques.

In wild-type CDO the iron is coordinated by three histidine residues and one water molecule giving rise to a distorted tetrahedral coordination. The three coordinating histidines (His86, 88, and 140) and water molecule all lie within 2.2 Å from the iron. Despite being a heterogenous mixture of non crosslinked and crosslink isoforms, wild-type CDO resolved as the crosslinked isoform as previously observed. The hydroxyl group of the Cys93-Tyr157 adduct is located 4.2 Å away from the iron (**Figure 2.10**).

Alternatively, the iron in C93E CDO exhibits an octahedral coordination environment. Three of the six sites are coordinated by the nitrogen on the imidazole ring of histidine, two sites are coordinated monodentate by a water and acetate molecule, and the last site is occupied by the hydroxyl group of glutamate (**Figure 2.11**). Since glutamate is coordinating the iron, C93E CDO exists as the homogeneous non crosslinked isoform. Consequently, Tyr157 now lies 5.1 Å from the iron and 2.9 Å away from the carboxyl functional group of C93E.

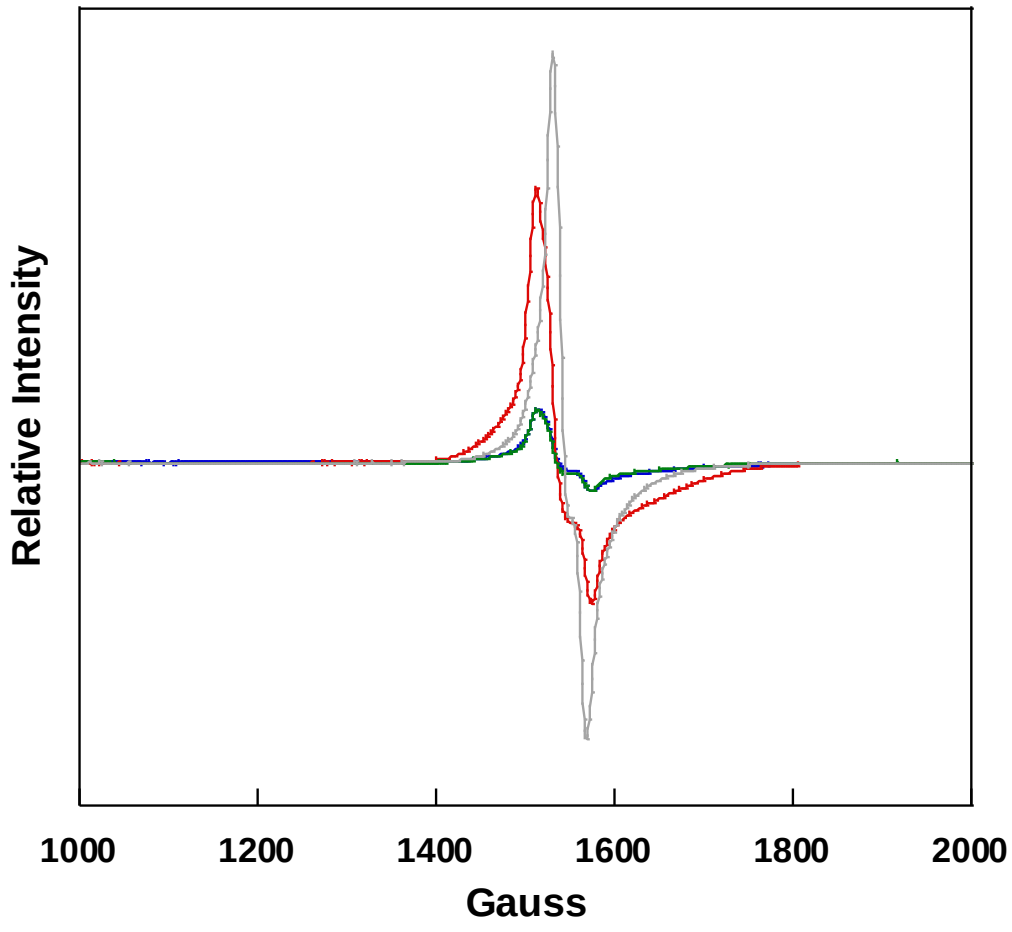

Figure 2.7. EPR spectra of C93E CDO (blue) with L-cysteine (red), cysteamine (green), and 3-MPA (gray).

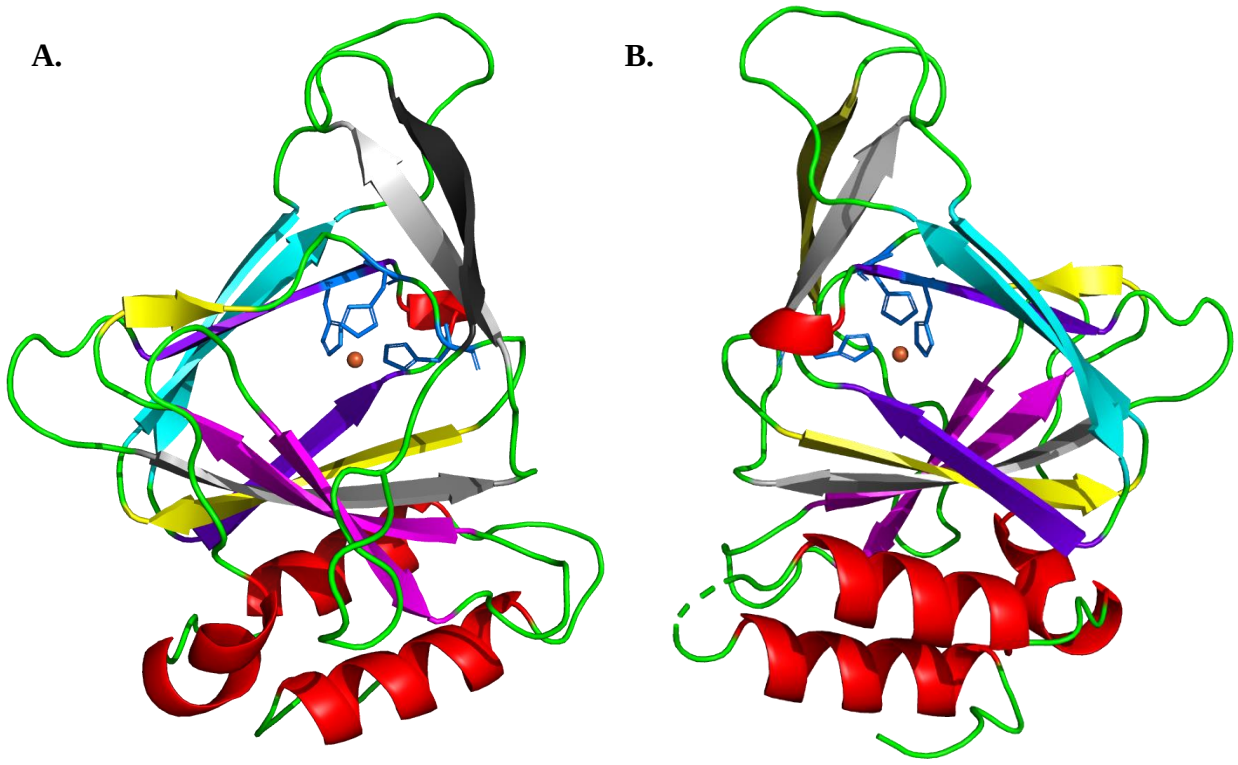

Figure 2.8. Tertiary structures of **A.** wild-type CDO (left) and **B.** C93E CDO (right). Color scheme corresponds to Figure 2.9: loops green), α-helices (red), β1/β2 (magenta), β3/β4 (yellow), β5/β6 (cyan), β7/β8 (purple), β9/β10 (gray), and β11 (black).

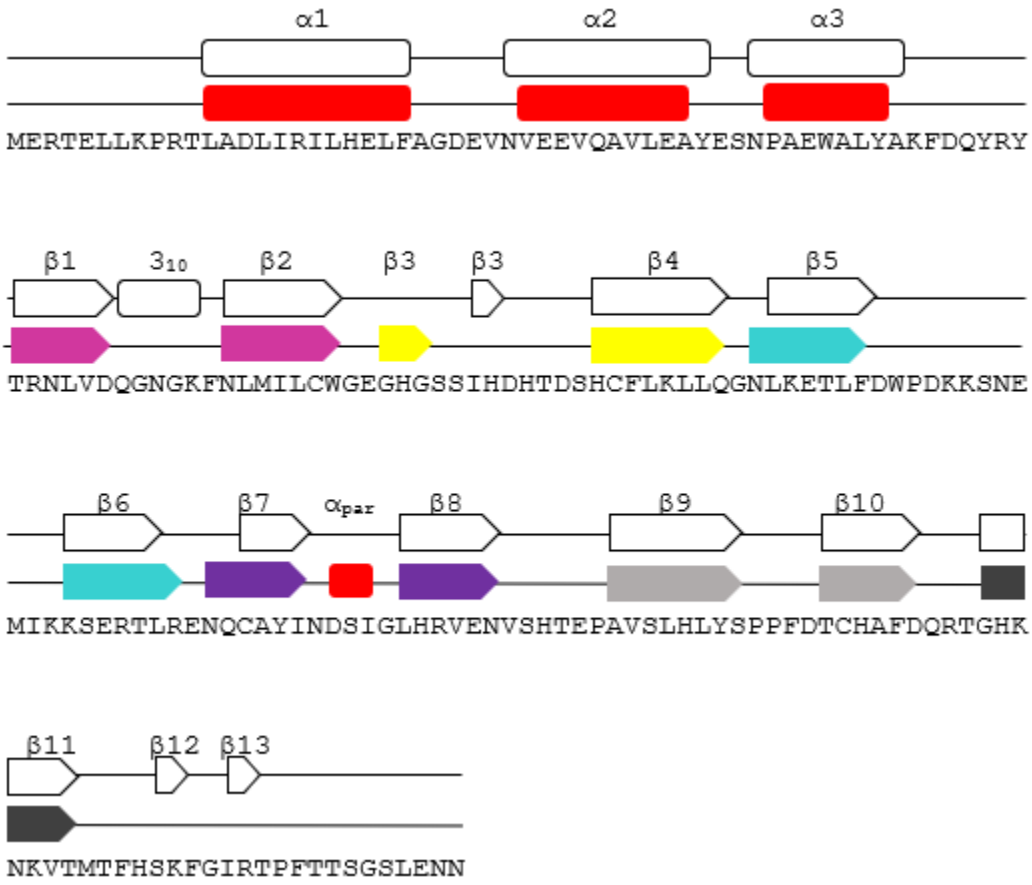

Figure 2.9. Secondary structure alignment for CDO. Top (unshaded) shapes are what is seen in previous CDO crystal structures. Bottom (colored) shapes represent the secondary structure of the reported crystal structure.

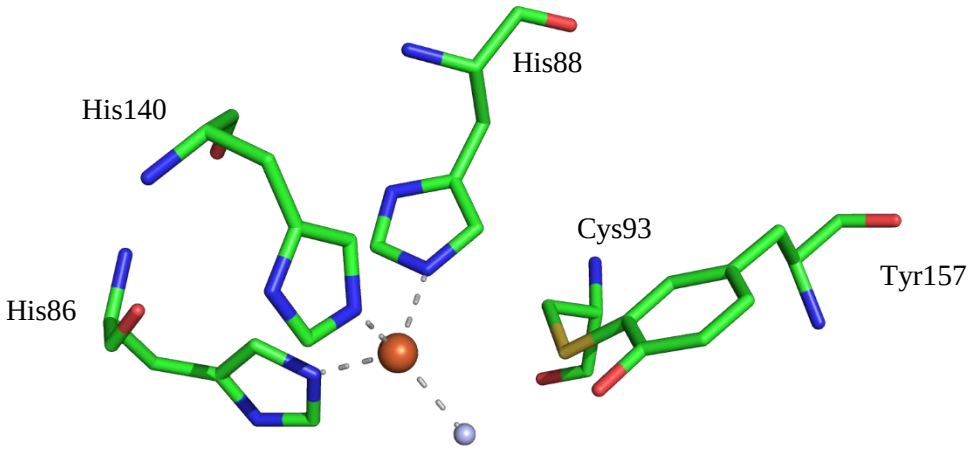

Figure 2.10. Active site of wild-type CDO with nearby Cys-Tyr crosslink. PDB: 6DL5

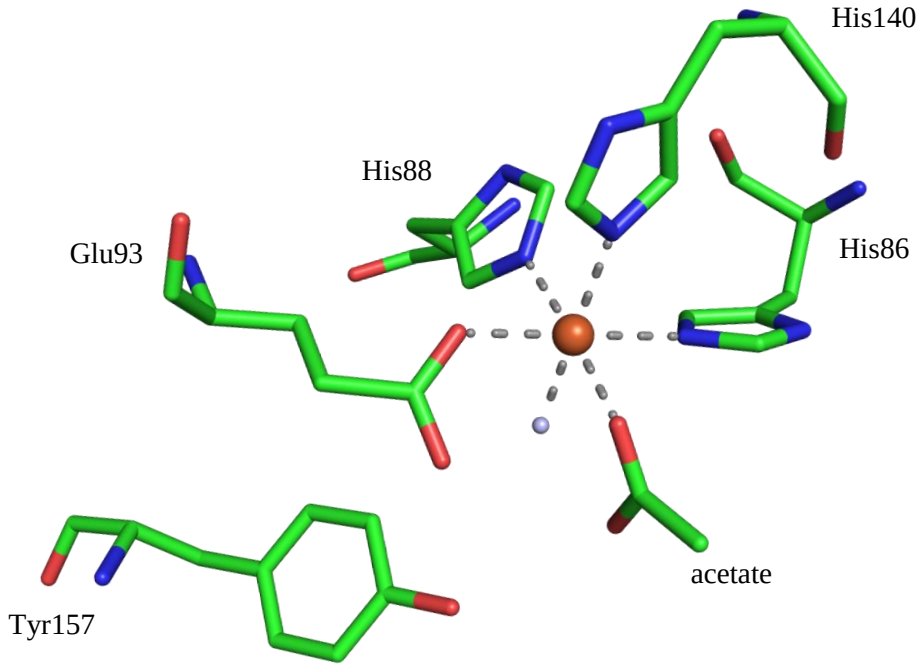

Figure 2.11. Active site of C93E CDO with mutated glutamate reside. PDB: 6DL3

2.4 DISCUSSION

Over four decades of research have gone into investigating the structural, functional, and dietary regulatory implications of cysteine dioxygenase. Although these studies have provided valuable insight into CDO, no study has sought to understand the evolutionary divergence of cysteine dioxygenase from the 3-His/1-Glu coordination exhibited by a vast number of proteins in the cupin superfamily. However, like other cupin dioxygenases, basic mechanistic properties remain constant. The oxidative catabolism of L-cysteine to cysteine sulfinic acid follows an ordered sequential mechanism in which CDO binds L-cysteine first followed by dioxygen [52, 53, 63, 91]. Three dimensional structures of wild-type CDO show that L-cysteine binds bidentate to the iron by the amino and thiol groups, and the carboxylic group is stabilized by a nearby arginine residue [79, 85, 92]. After L-cysteine coordinates, dioxygen binds monodentate filling the remaining site of iron. Although it is known that both molecules of dioxygen are incoorporated in the final cysteine sulfinic acid product, it is still unclear whether the proximal or distal oxygen binds to the sulfur first [93, 94]. Mechanisms for both proximal and distal dioxygen incoorporation have been proposed, with more experimental evidence for the later. Regardless of the mechanism of dioxygen incoorporation, three sites on the iron cation must be available in order for cysteine oxidation to occur.

In an effort to roll back evolution, generation of the C93E CDO variant provided an opportunity to study the effects of a 3-His/1-Glu active site environment. The replacement of Cys93 to a glutamate residue yielded the 3-His/1-Glu coordination environment exhibited by many cupins. Steady-state kinetics showed a ~ 75-fold decrease in activity compared to the wild-type enzyme (**Table 2.2**). Since several studies have shown L-cysteine to coordinate the iron bidentate,

it is most likely that the addition of L-cysteine occupies the remaining two iron coordination sites leaving no room for dioxygen binding (**Scheme 2.1**).

Additionally, substrate analogs D-cysteine and cysteamine displayed similar catalytic efficiency compared to L-cysteine with C93E CDO, whereas 3-MPA had no measurable activity (**Table 2.3**). However it is notable that the k_{cat} of cysteamine is 9-fold higher than L-cysteine, suggesting the mutated enzyme is able to consume dioxygen at a faster rate with cysteamine, albeit no product was formed with either substrate (**Table 2.4**). A previous study found there was a 20-fold increase in cysteine sulfinic acid production in wild-type CDO when cysteamine was added to a reaction containing L-cysteine [61]. Although when L-cysteine was removed product formation ceased, indicating that cysteamine was not a viable substrate for CDO. It was concluded that cysteamine may be a redox activator for the oxidation of L-cysteine [61]. However in C93E CDO, the increase in dioxygen consuption with cysteamine is most likely due to the monodentate coordination of the iron, leaving an open coordination site for dioxygen binding. Whereas L-cysteine, D-cysteine, and 3-MPA coordinate bidentate leaving no site open for dioxygen binding (**Scheme 2.1**).

Attempts to co-crystalize C93E CDO in the presence of L-cysteine and substrate analogs have been unsuccesful. However, further justification for monodentate coordination of cysteamine can be demostrated through EPR studies. Resting wild-type CDO has an iron (III) EPR signal, but in the prescene of L-cysteine the relative signal intensity increases. This signal increase is attributed to substrate binding and possible persulfinate formation [63]. EPR spectra of resting wild-type and C93E CDO showed comparable iron (III) signals (**Figure 2.6**). C93E CDO incubated in the presence of L-cysteine and 3-MPA showed an increase in the relative signal intensity compared to the resting state, suggesting bidentate substrate coordination. Alternatively, when incubated with

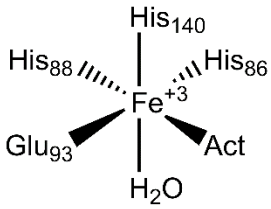

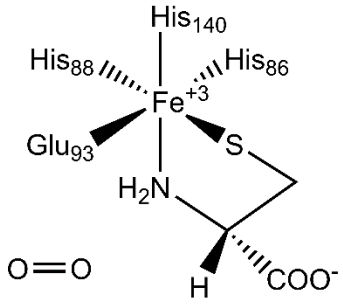

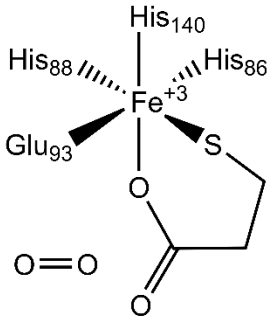

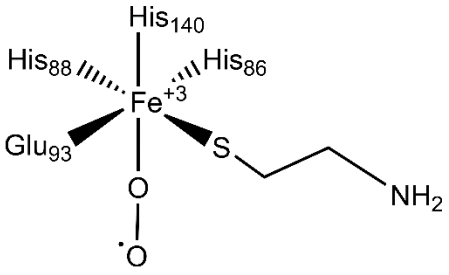

IV a

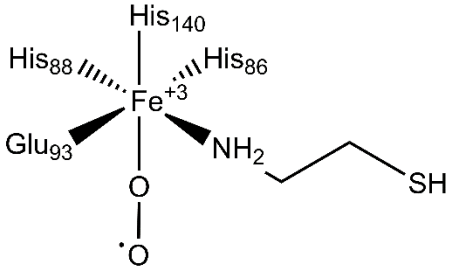

IV b

Scheme 2.1. Coordination environment of C93E CDO. **I.** Resting state of C93E CDO; **II.** Coordination by L-cysteine; **III.** Coordination by 3-MPA; **IV.** Two possible coordinations by cysteamine and dioxygen.

cysteamine the signal intensity of C93E is comparable to the resting state indicating a weak, monodentate coordination (**Figure 2.7**).

Single-site substrate coordination in 3-His/1-Glu cupin dioxygenases is not uncommon. Quercetin dioxygenase, an enzyme that catabolizes quercetin to 2-protocatechuoylphloroglucinolcarboxylic acid and carbon monoxide, adopts the moderately conserved 3-His/1-Glu cupin motif [57, 88]. Both quercetin and dioxygen bind monodentate to the metal cation in a sequential ordered mechanism. It is important that quercetin only occupies one coordination site for two reasons: i. bidentate binding of quercetin would occupy all metal sites leaving no room for dioxygen binding, and ii. monodentate binding of the bulky substrate allows it to remain flexible so unique distortion can occur. Distortion of the quercetin ring is essential for product formation [88]. Other 3-His cupin enzymes also require bidentate substrate coordination with a single site dioxygen binding for product formation [57, 80, 88, 95]. Overall the evolutionary divergence of the 3-His/1-Glu to a 3-His coordination environment in cysteine dioxygenase allows for multi-site occupancy of L-cysteine. Additionally the replacement of glutamate to cysteine allows the unique thioether crosslink to be formed. In particular the homogeneous crosslinked enzyme increases enzymatic efficiency 10-fold [33].

CHAPTER THREE

Investigation of Distinct Structural Features in the Non crosslinked Isoform of Cysteine Dioxygenase.

3.1 INTRODUCTION

Cysteine dioxygenase catalyzes the conversion of L-cysteine to cysteine sulfinic acid in mammals (**Figure 3.1**). Unlike L-cysteine, cysteine sulfinic acid (CSA) is not metabolically significant. However, CSA can be metabolized further to pyruvate and taurine [7, 40]. Cysteine dioxygenase (CDO) is a non-heme iron enzyme belonging to the cupin superfamily. Many cupin proteins contain two motifs, represented by GX_5**H**X**H**X_{3-6}**E**X_6G (motif 1) and $GX_{5-7}PXGX_2$**H**X_3N (motif 2), which are involved in metal coordination [53].

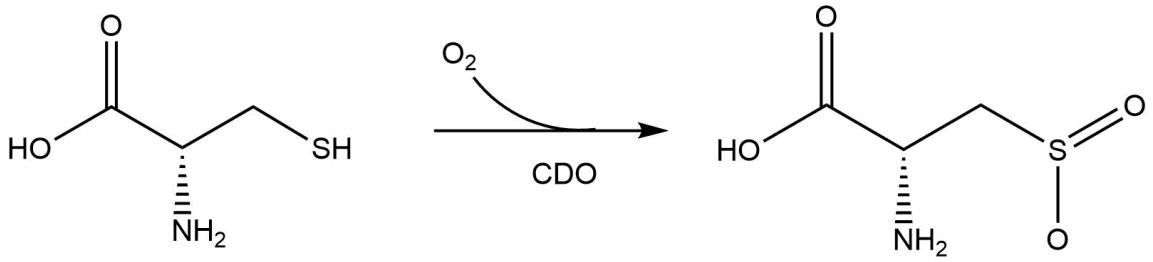

Figure 3.1. Oxidation of L-cysteine to cysteine sulfinic acid by cysteine dioxygenase (CDO).

Instead, the iron in CDO is weakly coordinated by 3-His residues (His86, 88, and 140). The glutamate, found in the first motif, is replaced by a non-coordinating cysteine residue (Cys93). This cysteine is able to form a thioether bond with a nearby tyrosine residue (Tyr157) (**Figure 3.2**). In hepatic tissue, CDO exists as the homogeneous non crosslinked isoform. However, studies showed that when rats were fed a moderate to high sulfur diet, CDO formed the crosslinked isoform [64, 75]. Purified recombinant wild-type CDO exists as a heterogeneous mixture of non crosslinked and crosslinked isoforms, but CDO forms the fully crosslinked isoform in the presence of L-cysteine [33, 73, 76, 83, 96]. It has been reported that the homogenously crosslinked isoform enhances catalytic efficiency up to 10-fold compared to wild-type CDO [33, 73, 76].

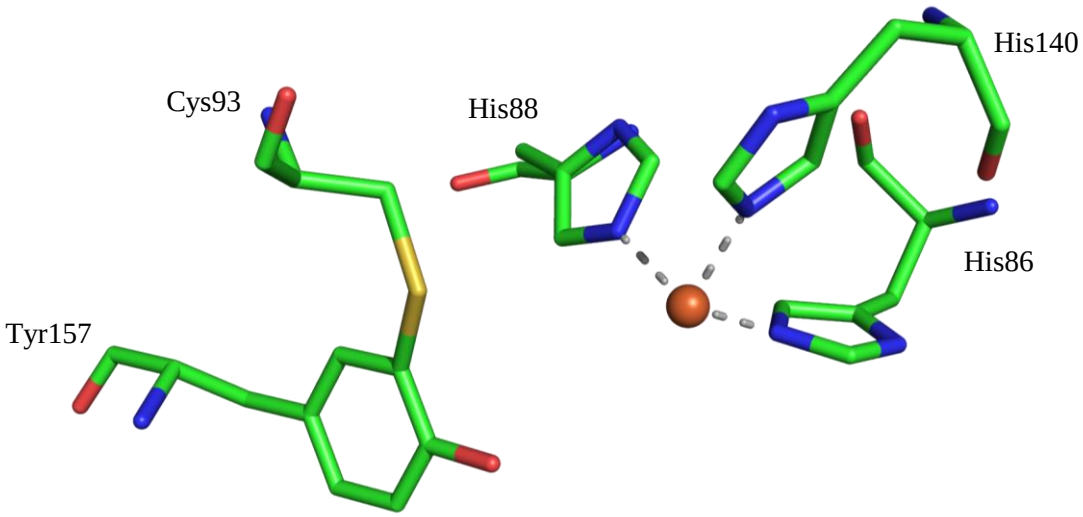

Figure 3.2. Active site of cysteine dioxygenase with the Cys-Tyr crosslink. PDB: 6DL5

Over the last decade a great deal of research has gone into investigating this impalpable thioether adduct. More specifically, the main topics of investigation have been to obtain the homogeneously non crosslinked isoform, determine the requirements for crosslink formation, evaluate the spatial separation between crosslink formation in relation to cysteine oxidation, and finally arbitrate the role of Arg60 in substrate specificity. Until recently, attempts to purify or isolate the homogeneously non crosslinked isoform have been marginally unsuccessful [73, 97]. In 2014, Njeri, et. al, found crosslink formation was inhibited when recombinant wild-type CDO was expressed in the presence of the iron chelator 1,10-phenanthroline, yielding only the non crosslinked isoform [33]. Also, obtaining a crystal structure for the homogeneously non crosslinked species has proven difficult. Despite reports of up to 70% non crosslinked wild-type CDO, only the crosslinked species crystallizes. Unable to obtain a crystal structure for non crosslinked CDO, one study compared the crystal structures of C93A and Y157F CDO variants to crosslinked wild-type CDO [82]. Despite stating that C93A and Y157F CDO variants may not be a comparable substitute for the non crosslinked isoform, many conclusions about the structural differences between the pseudo non crosslinked variants and crosslinked wild-type CDO were hypothesized.

Conversely, progress has been made in determining the requirements for crosslink formation. Studies have shown that in addition to L-cysteine, dioxygen and iron are required for crosslink formation [33, 58, 61, 73, 97]. However, the requirement of the substrate, L-cysteine, is in direct opposition to other enzymes containing amino acid derived cofactors [98]. Thioether crosslinks found in galactose oxidase and glyoxal oxidase form in the absence of their substrates [67, 71]. Therefore, it is interesting that cysteine dioxygenase requires L-cysteine for crosslink formation. Additionally, crosslink formation is required for catalysis in galactose oxidase, glyoxal

oxidase, NirA, and cytochrome c nitrite reductase [67-69, 71]. However, in CDO, site-directed mutagenesis studies show that the crosslink is not required for CSA production [33, 73, 79, 83].

Additionally, another source of debate is when the crosslink is formed. It has yet to be determined whether crosslink formation takes place prior, concurrently, or after the formation of cysteine sulfinic acid. Only two studies have attempted to correlate crosslink formation to CSA production. In 2008, Dominy Jr. et. al, reported *in vitro* wild-type CDO can form the homogeneously crosslinked isoform in 10 minutes when incubated with L-cysteine, dioxygen, and ferrous iron. Alternatively, *in vivo*, the crosslink is formed when rats are fed moderate to high concentrations of L-cysteine (0.2 mM) for an extended time (12-144 hours). The requirement for high concentrations of L-cysteine could indicate that formation of the crosslink serves more as a regulatory response than a requirement for catalysis. Unfortunately this study never directly correlated the timing of crosslink formation with cysteine oxidation in wild-type CDO. Rather, the study compared the time of crosslink formation and CSA production between wild-type CDO and C93S CDO, a variant unable to form the crosslink. Naming C93S CDO as a non crosslinked isoform mimic, and therefore a kinetic substitute for non crosslinked CDO, it was concluded that CDO takes ~ 800 catalytic cycles to form 50% of the crosslink. It was further stated that crosslink formation and CSA production occur in an undetermined split-path, citing crosslink formation as the inefficient route. Based on evidence from this study, the first mechanism of crosslink formation was proposed [73].

Additional studies directly compared crosslink formation to CSA production in recombinant wild-type CDO. However, like Dominy Jr., Siakkou, et. al, was unable to produce a homogeneously non crosslinked enzyme. Instead anaerobic purification yielded a 70% non crosslinked isoform [97]. Moreover, to form the homogeneous crosslinked isoform, an extensive

incubation time of three hours was required. This incubation time is at least ten times greater than any other reported method for wild-type CDO [33, 73]. Nevertheless, the study reported low product formation during the initial incubation (0-40 minutes) period, and then a linear dependence for the remainder of the reaction. Based on representation of a slow phase, it was concluded that crosslink formation occurs prior to cysteine oxidation [97]. In a separate study, a slow phase was also observed during the consumption of dioxygen in the homogeneous non crosslinked wild-type CDO [33]. However, previously reported data suggests cysteine oxidation is independent of crosslink formation, which is in direct opposition with the observance of a slow phase [73].

With the exception of one, the studies mentioned above were conducted prior to obtention of the homogeneously non crosslinked isoform. Using the non crosslinked purification method developed by our group, we report the first non crosslinked wild-type crystal structure and an updated crosslink mechanism. Furthermore, we provide evidence that crosslink formation is not solely dependent on L-cysteine. Rather, the crosslink can form with any small molecule capable of activating the iron for dioxygen binding.

3.2 METHODS AND MATERIALS

3.2.1 Materials

4-(2-Hydroxyethyl)piperazine-1-ethanesulfonic acid (HEPES) and all buffers, L-cysteine, D-cysteine, cysteamine, 3-mercaptopropionic acid, L-ascorbate, ampicillin, streptomycin sulfate, lysozyme, 1,10-phenanthroline, formic acid (90% v/v), ICP-grade iron standard, and brilliant blue R were purchased from Sigma (St. Louis, MO). Isopropyl-β-D-thiogalactoside (IPTG) was purchased from Gold Biotechnology (St. Louis, MO). Glycerol and sodium chloride were purchased from Macron Fine Chemicals (Center Valley, PA). Difco-brand Luria-Bertani (LB) media was purchased from Becton, Dickinson and Company (Sparks, MD). Macro-Prep® High Q Support column media, SDS-PAGE resolving and stacking buffers, 30% acrylamide, and Blue Laemmli was purchased from Bio-Rad Laboratories (Hercules, CA).

3.2.2 Purification of Non crosslinked Wild-type and Non crosslinked R60A CDO

Expression of non crosslinked wild-type and non crosslinked R60A was carried out in the presence of 1,10-phenanthroline as previously described [33]. Cell pellets were resuspended with 100 mL 25 mM HEPES, pH 7.5, 10% glycerol and 0.02 mg/mL lysozyme in 10 mM Tris-Cl, pH 8.5. The resuspended cell mixture was lysed by sonication followed by centrifugation at 10 000 rpm, 4 °C for 15 min. Addition of 1.5% streptomycin sulfate (w/v) was added to the supernatant, and the solution was slowly stirred at 4 °C for 1 hour. The solution containing precipitated nucleic acids was centrifuged at 10 000 rpm at 4 °C for 20 min. An additional 100 mL 25 mM HEPES, pH 7.5, 10% glycerol was added to the supernatant before loading onto the Macro-Prep® High Q Support (Bio-Rad Laboratories, Hercules, CA). Protein was eluted from the column using a linear gradient from 0 - 150 mM sodium chloride in 25 mM HEPES, pH 7.5, 10% glycerol. Fraction

purity was determined by SDS-PAGE (5% stacking with 12% resolving), and fractions determined to be of the highest purity were pooled and dialyzed twice against two liters of 25 mM HEPES, pH 7.5, 10% glycerol, 100 mM sodium chloride to remove any remaining 1,10-phenanthroline. After dialysis the protein concentration was determined by UV-visible absorption spectroscopy at 280 nm using a molar extinction coefficient of 25 440 M^{-1} cm^{-1}. Enzyme was reconstituted with iron at a 1:1.2 protein to ferrous ammonium sulfate molar ratio. The enzyme was dialyzed two more times against one liter 25 mM HEPES, pH 7.5, 10% glycerol, 100 mM sodium chloride to remove any unbound iron. After dialysis, the protein was centrifuged at 10 000 rpm, 4 °C for 15 minutes to remove any precipitated protein, and the total iron content was quantified by ICP-AES as previously described [33]. Aliquots of the protein were flash frozen with liquid nitrogen, and stored at -80 °C.

3.2.3 Activity of Non crosslinked R60A CDO

Steady-state kinetic parameters were determined using a Clark-type oxygen electrode to monitor the rate of dioxygen consumption. Each assay contained a final concentration of 2 μM protein in the presence of 1 mM ascorbate in 25 mM HEPES, pH 7.5 buffer at 37 °C. The assays were initiated by the addition of L-cysteine substrate (200 μM to 5 mM), and linear velocities were recorded 5-10 seconds after the lag phase in the reaction and then plotted against the substrate concentration. Steady-state kinetic parameters were corrected based on the percentage of iron. For time course experiments with non crosslinked R60A CDO, the reaction was initiated by the addition of L-cysteine (1 – 100 mM) at t = 60 seconds and was terminated by the addition of 1 μL formic acid (90% v/v) at t = ~ 950 seconds. Data calculated was an average of two experiments and was plotted and evaluated using the Michaelis-Menten equation in KaleidaGraph™ software (Synergy Software, Reading, PA).

3.2.4 EPR Analysis of Wild-type and Non crosslinked R60A CDO

Electron paramagnetic resonance (EPR) studies were performed on a Bruker EMX spectrometer at X-band frequency (Bruker Biospin Corporation, Billerica, MA). Cooling to 7 K was performed using an Oxford Instruments ESR 900 flow cryostat and an ITC4 temperature controller. All samples prepared for EPR had a final concentration of 100 μM enzyme in 25 mM HEPES pH 7.5, 10% glycerol, with 0.1 M NaCl. All spectra were recorded using the following settings: 9.39 GHz microwave frequency, 0.199 mW microwave power, 2 x 10^4 receiver gain, 100 kHz modulation frequency, 6 G modulation amplitude, with a time constant of 163.84 ms, and a sweep time of 167.77 seconds.

3.2.5 Generation of the Crosslinked Isoform with L-cysteine and Substrate Analogs

The crosslink in wild-type and non crosslinked R60A CDO was generated by combining 5 μM CDO with 100 mM L-cysteine, D-cysteine, cysteamine, or 3-mercaptoproprionic acid, with 1 mM ascorbate in 25 mM HEPES, pH 7.5 for a final volume of 200 μL. Reactions were initiated by the addition of enzyme and were incubated at 37 °C for 1 hour. After incubation, 10 μL of the reaction was quenched with 5 μL sample buffer (Blue Laemmli with 20% (v/v) 2-mercaptoethanol) and heat shocked at 90 – 100 °C for two minutes. Samples were analyzed immediately for crosslink formation by SDS-PAGE (5% stacking, 12% resolving) stained with Brilliant Blue.

3.2.6 Crystallization and Diffraction Data Collection for Non crosslinked Wild-type CDO

Recombinant non crosslinked wild-type CDO was purified as described above. After dialysis, CDO was concentrated using A 10 000 kDa MWCO Amicon Ultra Centrifugal Filter (Millipore) at 5 000 RPM, 4°C. Concentrated enzyme was flash frozen with liquid nitrogen and stored at - 80°C. Final concentration of enzyme was ~ 18 mg/mL. Crystals were grown at 24°C

using the hanging drop method. Each drop contained 1.5 μL of protein mixed with an equal volume of reservoir solution. The reservoir solution for non crosslinked wild-type CDO contained 1 M lithium chloride, 24% (w/v) poly(ethylene glycol) (PEG) 20,000 in 0.1 M MES at pH 6.5. Crystals formed after one day and grew to full size within four days. For data collection, crystals were serially washed in 1 M lithium chloride, 30% PEG 600 in 0.1 M sodium acetate supplemented with 20% (w/v) sucrose as a cryoprotectant and flash frozen to - 160°C.

Diffraction data (0.15° oscillation images for a total of 114°) was collected at the Stanford Synchrotron Radiation Laboratory (Stanford, CA) on beamline 12-2 at a wavelength of 0.9795 Å at 100 K. The exposure time per frame was 0.4 s with 73.5% attenuation and a crystal to detector distance of 359.1 mm. The data was indexed and scaled with XDS to 2.30 Å. The crystals were assigned to the space group $P4_12_12$ with unit cell dimensions a = b = 57.59 Å and c = 122.47 Å (**Table 3.1**). Molecular replacement calculations were performed using Phaser in the PHENIX program suite, using PDB: 2B5H as the search model with iron and waters removed yielding a clear solution with each structure. Log likelihood gains ranged from 2282.3 – 9483.4 with TFZ scores of 48.1 – 94.0. Model building and refinement were performed using Coot and Phenix Refine [90].

Table 3.1: Data collection and refinement statistics for non crosslinked wild-type CDO

	Non crosslinked wild-type CDO
Data collection[a]	
Beamline	12-2
Wavelength (Å)	0.9795
Space group	$P4_12_12$
Cell dimensions; *a*, *b*, *c* (Å), β (°)	57.59, 57.59, 122.47
Resolution (Å)	38.64 – 2.30 (2.38 – 2.30)
R_{merge}[b]	0.116 (0.459)
Total observations	75791 (6100)
Total unique observations	9683 (857)
Mean ((I / sd(I))	13.0 (4.2)
Completeness (%)	99.4 (94.2)
Redundancy	7.8 (7.1)
Refinement	
Resolution (Å)	38.645 – 2.303 (2.424 – 2.303)
R_{cryst}[c]	0.1748 (0.1935)
R_{free}	0.2333 (0.3150)
Total unique observations	9435 (1098)
No. of non-hydrogen atoms	
Protein	1502
Iron	1
Ligand	0
Water	19
rms deviation bonds (Å)	0.013
rms deviation angles (°)	1.138
Overall mean B-factor (Å^2)	20.48
Ramachandran plot analysis[d]	
Favored region	99.45
Allowed region	0.55
Outlier region	0.00

[a]data indexed and scaled with XDS

[b]$R_{merge} = \Sigma_h|I_h - \langle I\rangle|/\Sigma_h I_h$, where I_h is the intensity of reflection h, and $\langle I\rangle$ is the mean intensity of all symmetry-related

[c]$R_{cryst} = \Sigma||F_o| - |F_c||/\Sigma|F_o|$, F_o and F_c are observed and calculated structure factor amplitudes. Five percent of the relections were reserved for the calculation of R_{free}.

[d]Calculated with Molprobity

3.2.7 Effects of pH on Crosslink Formation in Non crosslinked Wild-type CDO

The dependence of crosslink formation on pH in non crosslinked wild-type CDO was determined through SDS-PAGE and densitometry analysis by ImageJ software. The buffers used in these studies were Bis-Tris (pH range of 5.8 – 7.2), Tris-HCl (pH range of 7.0 – 9.0), HEPES (pH range of 7.2 – 7.6), and CHES (pH range of 8.6 – 10.0) with all buffers made to a final concentration of 50 mM. Each reaction contained 5 μM non crosslinked CDO with 1 mM ascorbate and varying concentrations of L-cysteine (1 – 100 mM) for a total volume of 200 μL. Reactions were initiated by the addition of enzyme and were incubated at 37 °C for 30 minutes. After incubation, 10 μL of the reaction was quenched with 5 μL sample buffer (Blue Laemmli with 20% (v/v) 2-mercaptoethanol) and heat shocked at 90 – 100 °C for two minutes. Samples were analyzed immediately for crosslink formation by SDS-PAGE (5% stacking, 12% resolving) stained with Brilliant Blue.

3.3 RESULTS

3.3.1 Evaluation of Crosslink Formation of Wild-type CDO with Substrate Analogs

To evaluate crosslink formation, wild-type CDO was incubated in the presence of L-cysteine or substrate analogs. Subsequent reactions were qualitatively analyzed for crosslink formation on SDS-PAGE. Wild-type CDO was able to form the homogeneously crosslinked isoform in the presence of L-cysteine and D-cysteine. However, the crosslink was unable to form in the presence of cysteamine and 3-mercaptoproprionic acid (**Figure 3.3**).

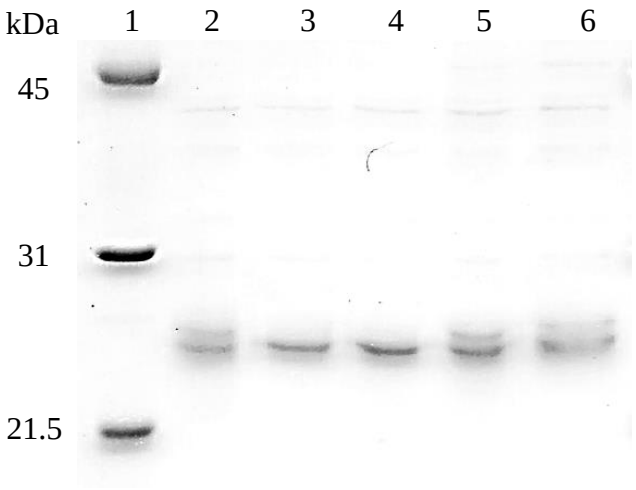

Figure 3.3. SDS-PAGE analysis of crosslink formation in wild-type CDO. (1) Molecular weight marker, (2) purified wild-type CDO, (3) wild-type CDO with L-cysteine, (4) wild-type CDO with D-cysteine, (5) wild-type CDO with cysteamine, and (6) wild-type CDO with 3-MPA.

3.3.2 Determination of Three-dimensional Crystal Structure of Non crosslinked Wild-type CDO

The crystal structure of non crosslinked wild-type CDO was refined to 2.30 Å resolution. Overall, the monomeric tertiary structure was comparable to previously solved CDO crystal structures, including our groups previously solved wild-type CDO [56, 58, 79, 85]. Non crosslinked wild-type CDO existed as a monomer, composed of 10 antiparallel β-sheets and three α-helices located at the N-terminus. The ten β-sheets fold to form the sandwich-like casing around the active site (**Figure 3.4**). The upper β-fold contains β4, β5, β7, β9, and β10, while the lower (N-terminus) fold is composed of β1, β2, β3, β6, and β8. Together they encompass a mononuclear non-heme iron molecule.

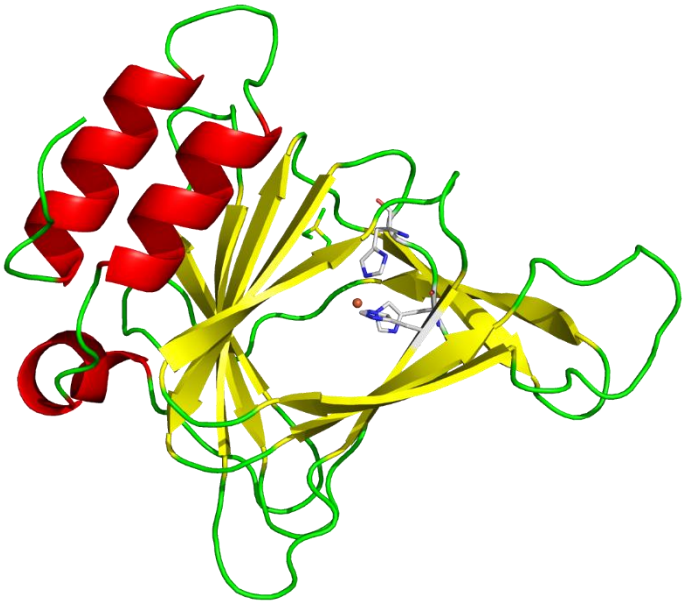

Figure 3.4. Tertiary structure of non crosslinked wild-type CDO exhibiting the traditional DSBH cupin fold.

The iron in the non crosslinked isoform is coordinated by three histidine residues and one water molecule giving rise to a distorted tetrahedral coordination. The three coordinating histidines (His86, 88, and 140) and water molecule all lie within 2.1 Å from the iron (**Figure 3.5**). The thiol of Cys93 is located 4.2 Å away from the iron and 3.8 Å away from the Cε position of Tyr157, whereas the hydroxyl group of Tyr157 is located 4.9 Å away from the iron. The non coordinating thiol group of Cys93 is located trans to His86 (**Figure 3.6 A**), and an obtuse angle of 116.5° exists between the hydroxyl group of Tyr157, the coordinating water, and the iron (**Figure 3.6 B**).

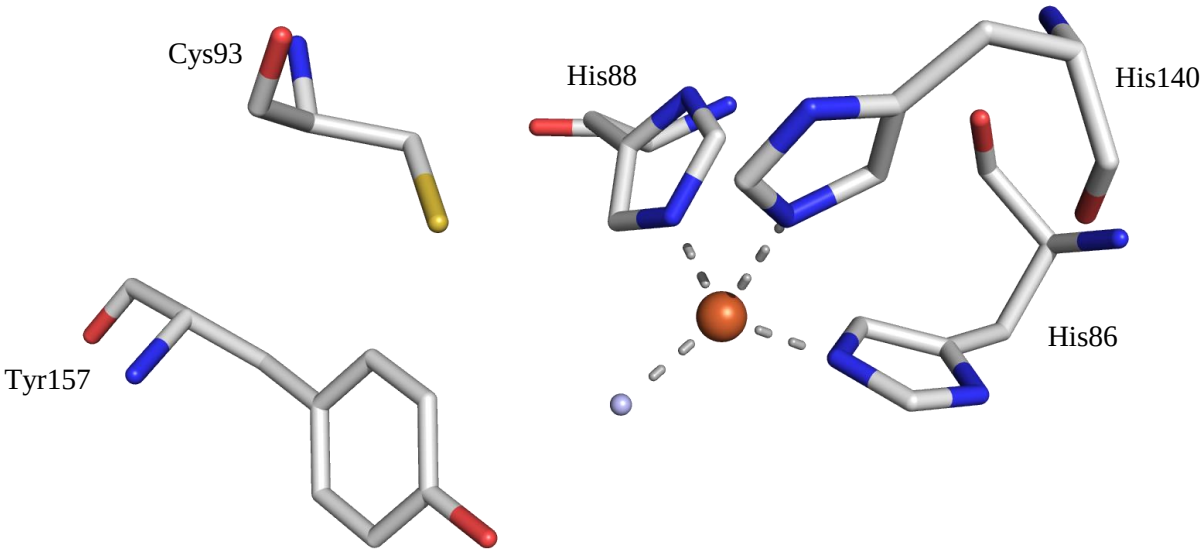

Figure 3.5. Active site of non crosslinked wild-type CDO with nearby uncoupled Cys-Tyr crosslink.

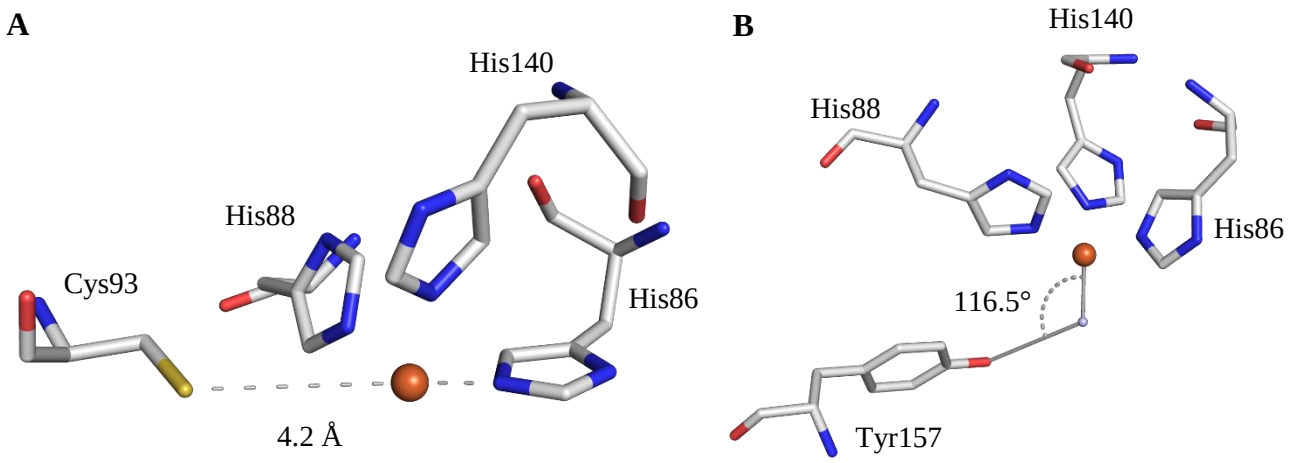

Figure 3.6 Crystal structure of non crosslinked wild-type CDO showing, **A.** The non crosslinked Cys93 lies 4.2 Å away from the iron center, trans to His86. **B.** The non crosslinked Tyr157 is located 4.9 Å away from the iron at a 116.5° angle.

Alignment of the three dimensional crystal structure of non crosslinked to crosslinked wild-type CDO revealed four primary structural differences within the active site. The first two differences are the 1.2 Å shifts between the uncoupled thiol of Cys93 and the hydroxyl of Tyr157 (**Figure 3.7 A**). The last two differences are the positions of Arg60 and Met179. In wild-type CDO, the conversed Arg60 residue existed in the predominately bent conformation, whereas in the non crosslinked structure Arg60 is predominately found in the extended conformation. Overall, there is a 5.3 Å shift between guanidium groups of Arg60. Similarly Met179 is rotated 180° from the position of Met179 in crosslinked wild-type CDO with a 3.1 Å difference between the sulfur atoms (**Figure 3.7 B**).

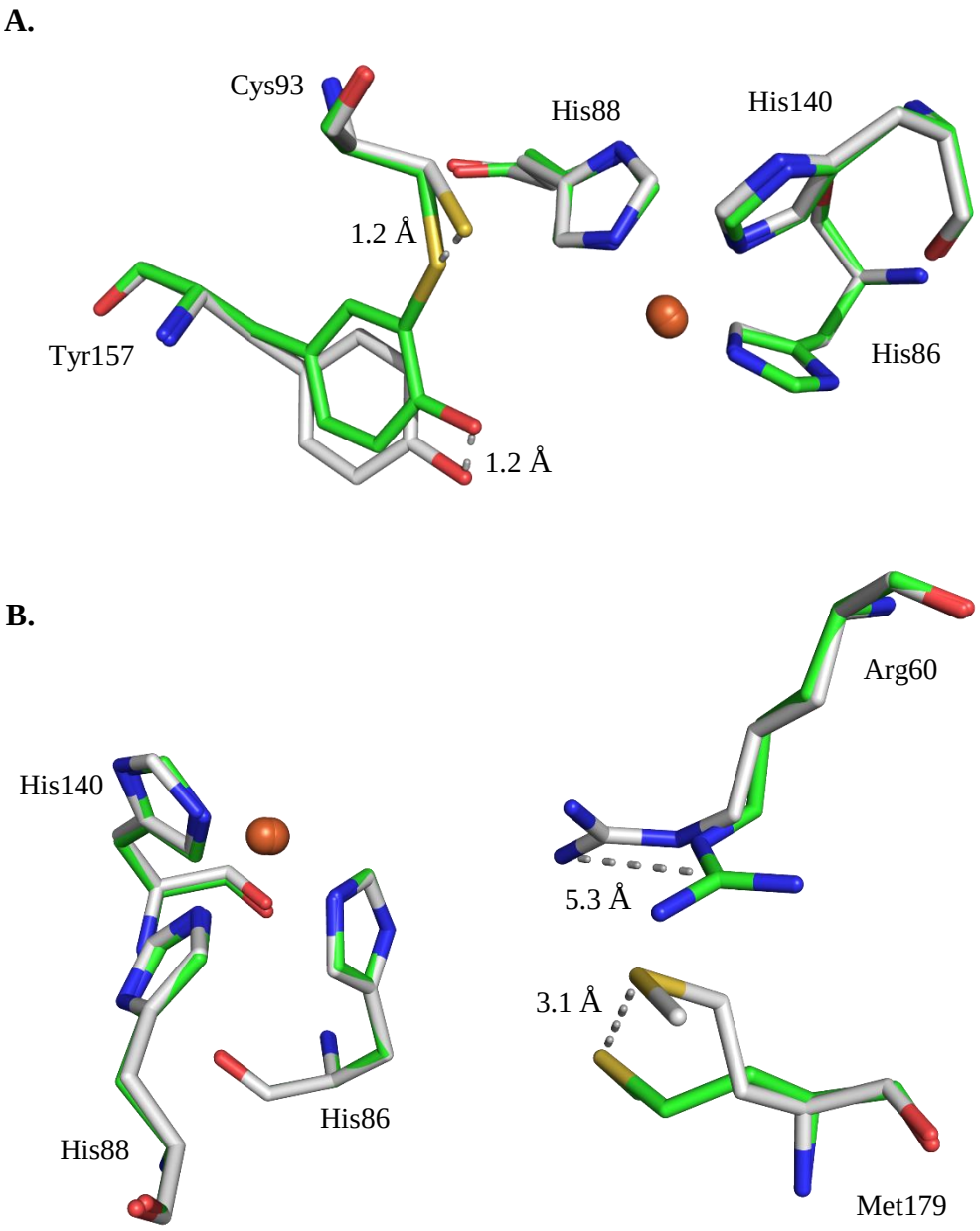

Figure 3.7. Overlay of non crosslinked wild-type CDO (gray) with crosslinked wild-type CDO (green; PDB: 6DL5) **A.** 1.2 Å difference in the position of Cys93 and Tyr157 in the non crosslinked and crosslinked crystal structure. B. Shifted positions of Arg60 and Met179 in the non crosslinked and crosslinked crystal structures.

3.3.3 Characterization of Non crosslinked R60A CDO

Previous studies showed that R60A CDO is able to form the crosslinked isoform in the presence of cysteamine. The R60A CDO variant was constructed to further understand substrate dependence in crosslink formation. To obtain the non crosslinked isoform, R60A CDO was expressed and purified in the presence of the iron chelator 1,10-phenanthroline. Purified R60A CDO existed as a homogenously non crosslinked species (**Figure 3.8**). Iron content was measured by ICP-AES, and non crosslinked R60A CDO was found to have an iron content of ~ 60%. The iron in non crosslinked R60A existed as ferrous iron (Fe^{2+}) as determined by EPR (**Figure 3.9**).

Kinetic properties of non crosslinked R60A were determined by measuring oxygen consumption using a Clark-type oxygen electrode. Non crosslinked R60A and wild-type CDO have comparable k_{cat} values of 128 ± 6 min^{-1} and 138 ± 1 min^{-1}, respectively. However, the 116-fold increase in the K_m value of non crosslinked R60A leads to a decrease in catalytic efficiency with k_{cat}/K_m values of 19 ± 12 $mM^{-1}min^{-1}$ for non crosslinked R60A compared to 2133 ± 362 $mM^{-1}min^{-1}$ for wild-type CDO (**Table 3.2**). Furthermore, after the addition of L-cysteine, a distinct lag phase in oxygen consumption was observed with non crosslinked R60A CDO (**Figure 3.10**). This lag phase is consistent with what was previously seen with non crosslinked wild-type CDO [33].

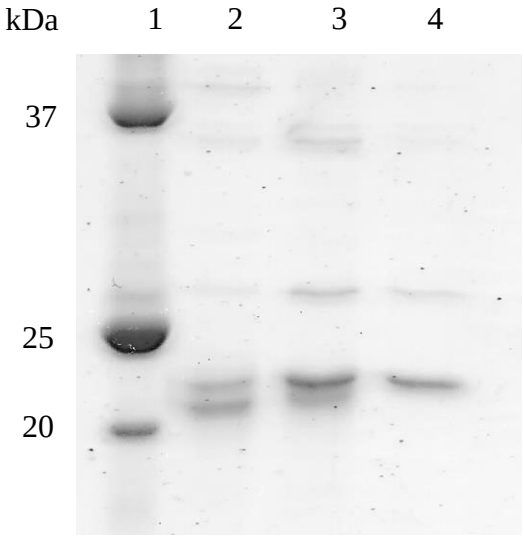

Figure 3.8. SDS-PAGE analysis of purified non crosslinked R60A CDO. (1) Molecular weight marker, (2) heterogenous wild-type CDO, (3) heterogeneous R60A CDO, and (3) homogenous non crosslinked R60A.

Table 3.2: Steady-state kinetic parameters of wild-type and non crosslinked R60A CDO with L-cysteine.[a]

	k_{cat} (min^{-1})	K_m (mM)	k_{cat}/K_m ($mM^{-1}min^{-1}$)	% Iron
wild-type CDO[b]	128 ± 6	0.06 ± 0.01	2133 ± 362	50%
non crosslinked R60A	138 ± 1	7 ± 4	19 ± 12	60%

[a] Kinetic parameters adjusted for iron content
[b] Previously reported [33]

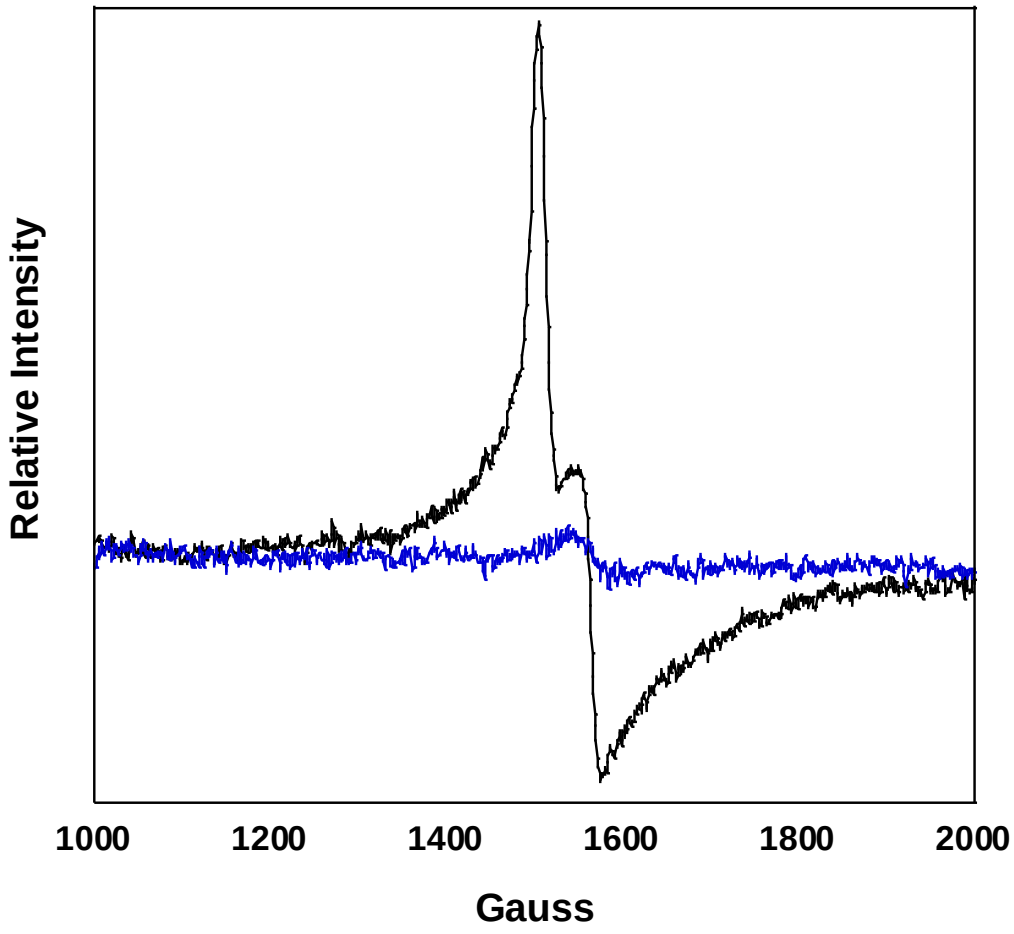

Figure 3.9. EPR spectra of wild-type CDO (black trace) and non crosslinked R60A (blue trace). Spectra were taken with 100 μM protein in 25 mM HEPES buffer, pH 7.5, 10% glycerol, 100 mM sodium chloride.

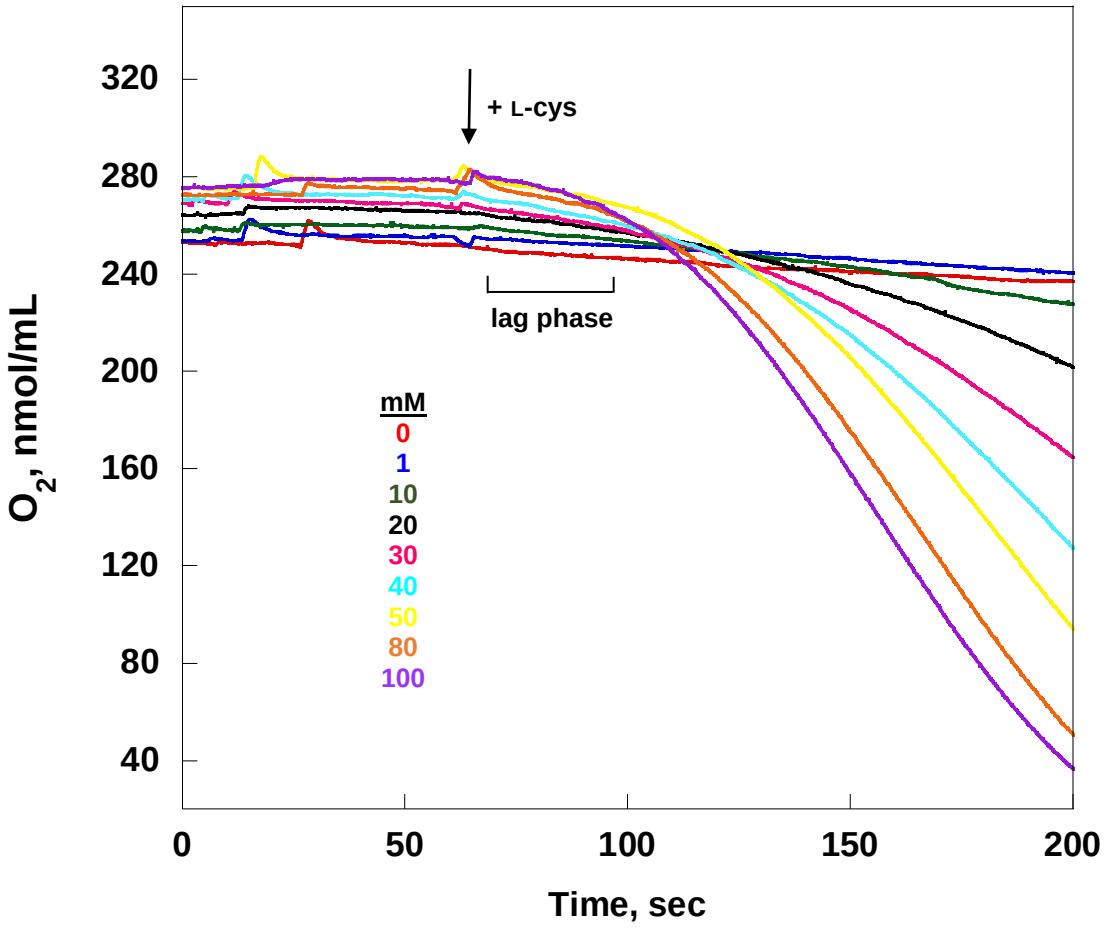

Figure 3.10. Oxygen consumption of non crosslinked R60A CDO with 0 – 100 mM L-cysteine, highlighting the lag phase, found where t = 60 – 90 seconds, after the addition of L-cysteine.

3.3.4 Evaluation of Crosslink Formation of Non crosslinked R60A CDO with Substrate Analogs

The ability of R60A CDO to form the crosslink was evaluated with L-cysteine and substrate analogs. Subsequent reactions were qualitatively analyzed for crosslink formation on SDS-PAGE. Non crosslinked R60A CDO is able to form the homogeneously crosslinked isoform in the presence of L-cysteine and D-cysteine. Non crosslinked R60A CDO is able to form a heterogeneous mixture of the crosslinked isoform in the presence of cysteamine. The crosslink is unable to form in the presence 3-mercaptoproprionic acid (**Figure 3.11**).

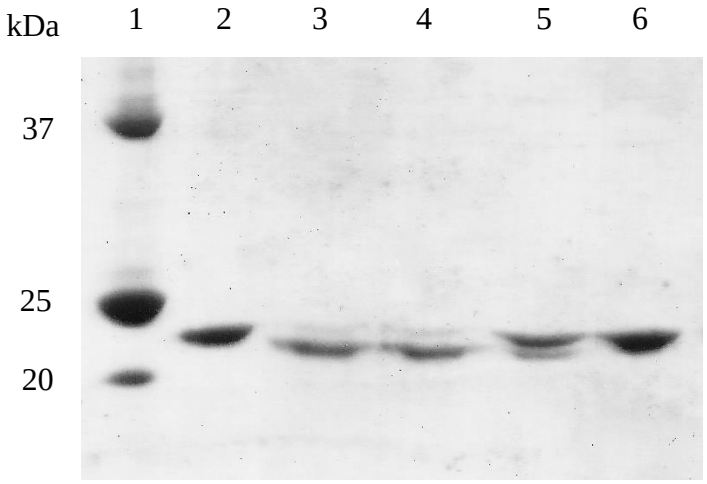

Figure 3.11. SDS-PAGE analysis of purified non crosslinked R60A CDO with L-cysteine and substrate analogs. (1) Molecular weight marker, (2) non crosslinked R60A CDO, (3) non crosslinked R60A CDO with L-cysteine, (4) non crosslinked R60A CDO with D-cysteine, (5) non crosslinked R60A CDO with cysteamine, and (6) non crosslinked R60A CDO with 3-MPA.

3.3.5 Effects of pH on Crosslink Formation in Non crosslinked Wild-type CDO

In order to determine the effects of pH on crosslink formation and how it may relate to the overall crosslink mechanism, non crosslinked wild-type CDO was incubated with varying concentrations of L-cysteine (0 – 100 mM) at pH range of 5.8 – 10.0. Each sample was resolved by SDS-PAGE, and the percent of crosslink formation was quantitatively determined through pixel densitometry analysis by ImageJ software. The formation of the crosslink is optimal around pH = 8.6, where 75 - 100% of CDO is found in the crosslinked isoform. There was a decrease in crosslink formation at pH values $\leq$ 7.0, with only 11 - 52% of CDO in the crosslinked isoform. Another decrease in crosslink formation was observed at pH values $\geq$ 9.0, with 52 – 100% in the crosslinked isoform (**Table 3.3** and **Figure 3.12**).

Table 3.3: Effects of pH on crosslink formation in non crosslinked wild-type CDO from 0 – 100 mM L-cysteine.

	% crosslinked						
pH	0 mM	1 mM	10 mM	20 mM	40 mM	80 mM	100 mM
5.8	0	0	0	0	0	18	24
6.2	0	0	0	0	29	31	41
6.8	0	0	27	37	47	67	68
7.0*	0	11	23	37	46	49	52
7.2*	0	36	40	60	68	80	87
7.6*	0	53	42	69	72	65	71
8.4	0	63	73	85	87	89	90
8.6	0	76	77	75	80	91	100
9.0*	0	73	74	71	75	61	83
9.2	0	69	71	74	65	70	88
9.6	0	73	52	63	67	76	88
10.0	0	78	75	75	83	76	100

*Averages of multiple buffers.

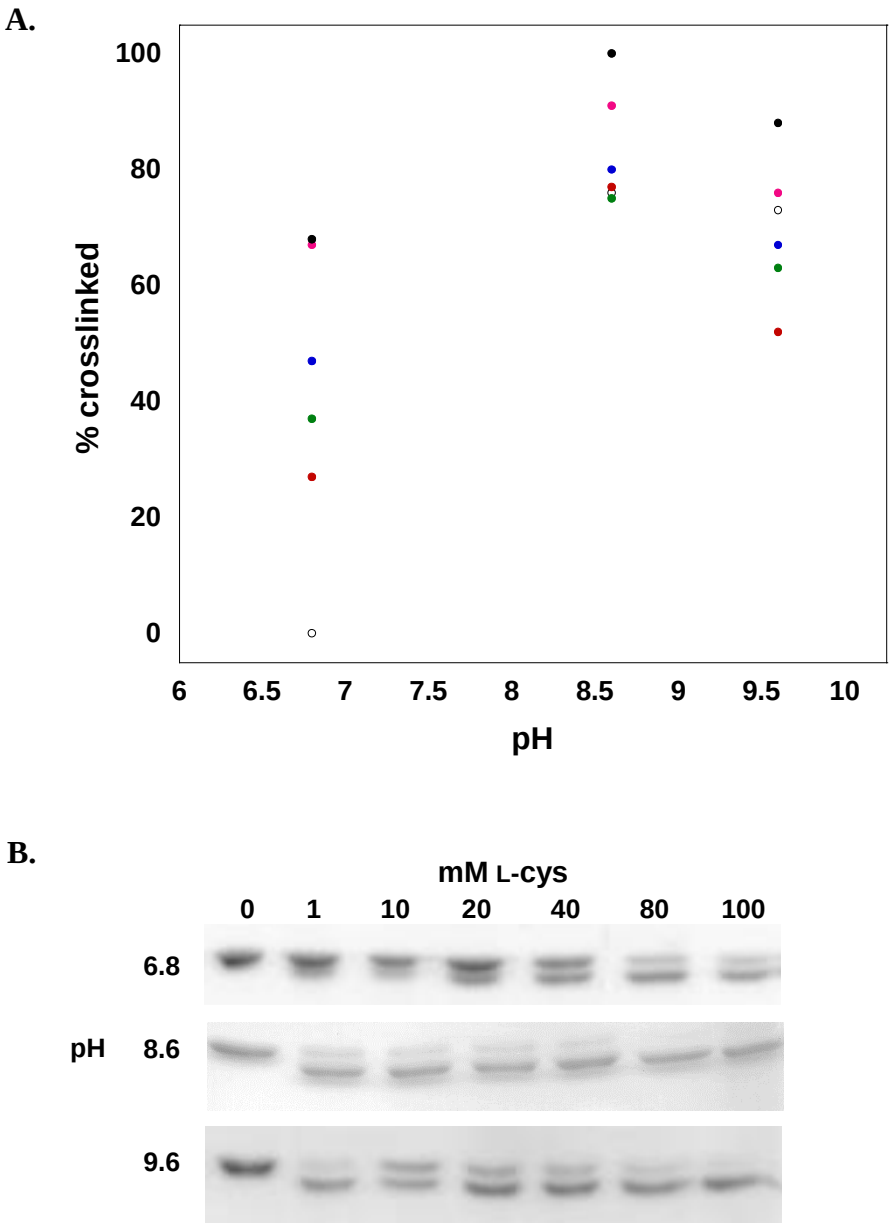

Figure 3.12. Effects of pH values 6.8, 8.6, and 9.6 on crosslink formation in non crosslinked wild-type CDO incubated with varying concentrations of L-cysteine **A.** 1 mM (black, open circles), 10 mM (red), 20 mM (green), 40 mM (blue), 80 mM (pink), and 100 mM (black, closed circles). **B.** SDS-PAGE of non crosslinked wild-type with varying concentrations of L-cysteine at pH values 6.8, 8.6, and 9.6.

3.4 DISCUSSION

In vivo, CDO exists as the homogeneous non crosslinked isoform. However in response to an increased sulfur diet the crosslinked species is formed [64, 75]. Purified recombinant wild-type CDO exists as a heterogeneous mixture of the non crosslinked and crosslinked isoforms [33, 73, 83, 97]. Several studies have found that crosslink formation requires L-cysteine, dioxygen, and iron, but the exact mechanism in which CDO utilizes L-cysteine in crosslink formation is unknown.

To date only three mechanisms for crosslink formation have been proposed [33, 58, 73]. Despite noting L-cysteine as a requirement, previous mechanisms proposed provided no role for the L-cysteine substrate in crosslink formation [58, 73]. In 2014, Njeri, et. al. was the first to propose the role of L-cysteine in crosslink formation was merely to change the redox potential, allowing for dioxygen binding [33, 83]. This idea is homologous with previous reports of ordered sequential binding of L-cysteine followed by dioxygen [94]. However, unlike the substrate-dependent crosslink in CDO, galactose oxidase, as well as other enzymes containing the Cys-Tyr crosslink, do not require the addition of substrates for crosslink formation [99].

In order to evaluate the role of L-cysteine in crosslink formation, substrate analogs D-cysteine, cysteamine, and 3-MPA were used. Wild-type CDO was able to form the crosslink in the presence of D-cysteine, but was unable to form the crosslink with cysteamine or 3-MPA (**Figure 3.3**). Previous studies have reported similar results when wild-type CDO was incubated in the presence of cysteamine and 3-mercaptoethanol [73]. Furthermore, previous EPR studies found an increase in relative signal intensity when wild-type CDO was incubated with D-cysteine [84]. The large relative signal increase can be attributed to the coordination of D-cysteine to the iron. The same signal increase was also seen with CDO in the presence of L-cysteine [33].

Additionally, bidentate coordination of D-cysteine can be supported by a recently determined crystal structure of C93A CDO co-crystallized with D-cysteine [82]. The study was unable to resolve wild-type CDO soaked with D-cysteine, however they were able to determine the structure of variant C93A CDO with D-cysteine as well as L-cysteine. The active site of C93A CDO with L-cysteine depicts identical coordination with previously solved crystal structures of wild-type CDO with L-cysteine, where the thiol group of L-cysteine is trans to His88, and the amino group is trans to His140. However comparison of C93A CDO with L-cysteine to D-cysteine shows a distorted coordination of the thiol and amino groups of D-cysteine (**Figure 3.13**). The electron density of the thiol group of D-cysteine is found with two occupancies. The dominant thiol occupancy resides 1.7 Å from the thiol of L-cysteine with the amino group of D-cysteine lying 1.5 Å away from the amino of L-cysteine. Additionally the carboxyl group is displaced by 2.0 Å. This distorted binding of the thiol group would most likely prevent cysteine oxidation. A previous study used D-cysteine to evaluate substrate specificity in cysteine oxidation, but did not evaluate the effect of D-cysteine on crosslink formation. Overall, this study concluded that CSA formation in CDO is stereospecific, and is therefore inhibited by D-cysteine [94].

Since D-cysteine is able to form the crosslink, it seems the only role L-cysteine plays in crosslink formation is to lower the redox potential of iron, priming it for dioxygen binding. This theory is supported through a previous study where CDO was anaerobically incubated with L-cysteine and the O_2 surrogate, nitrous oxide (NO) to determine substrate binding order [63]. Spectroscopic analyses determined that NO was unable to freely bind to the iron, but in the presence of L-cysteine the [ES-Fe-NO] complex could form. Similar NO activation was found when CDO was anaerobically incubated with NO and D-cysteine [63]. Therefore, based on data from crosslink formation, spectroscopical, and three-dimensional studies, we suggest that

crosslink formation in CDO is not specific to L-cysteine coordination but rather can occur with any small molecule capable of binding bidentate and lowering the redox potential of iron providing a favorable environment for dioxygen activation.

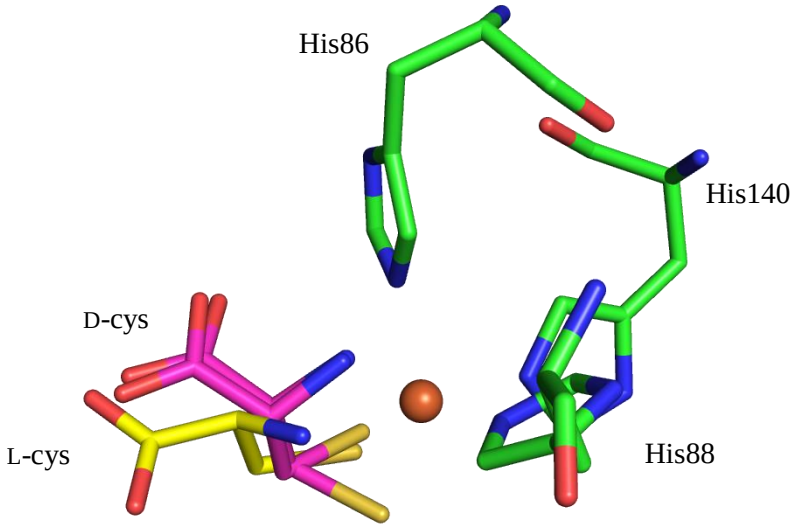

Figure 3.13. Overlay of the active site of C93A CDO with L-cysteine (yellow) and D-cysteine (magenta). PDB: 4XF0 and 5I0R [82].

It is also reasonable to assume cysteamine and 3-MPA did not form the crosslink because these substrate analogs only bind monodentate to the iron center. This theory can be supported by EPR studies that saw a small increase in relative signal intensity with cysteamine and 3-MPA, compared to wild-type CDO with L-cysteine and D-cysteine [84]. Anaerobic incubation of wild-type CDO in the presence of cysteamine or 3-MPA was unable to promote NO binding, again, suggesting monodentate coordination [63]. However, despite wild-type CDO not being able to form the crosslink in the presence of cysteamine, one study found that the R60A CDO variant was

able to form the crosslink in the presence of cysteamine [73]. It is interesting that wild-type CDO is unable to form the crosslink with cysteamine but R60A CDO can. It has been long proposed that Arg60 plays a role in substrate specificity, however new data suggest that it may also play a role in crosslink formation.

Previously solved crystal structures of wild-type CDO report Arg60 as a flexible residue, existing in a bent or extended conformation [58, 82, 85]. In non crosslinked wild-type CDO, Arg60 exists predominately in the extended position, with the guanidium group pointed toward the active site. Alternatively, in the wild-type CDO crystal structure crystalized with L-cysteine, Arg60 exists homogeneously in the bent conformation [82, 85]. The arginine switches positions at the δ-carbon, resulting in a 4.3 Å difference between the η2 nitrogen (**Figure 3.14**). The guanidium group of the bent conformation is 9.3 Å from the iron. However, in the extended conformation, the guanidium group is only 5.9 Å away from the iron.

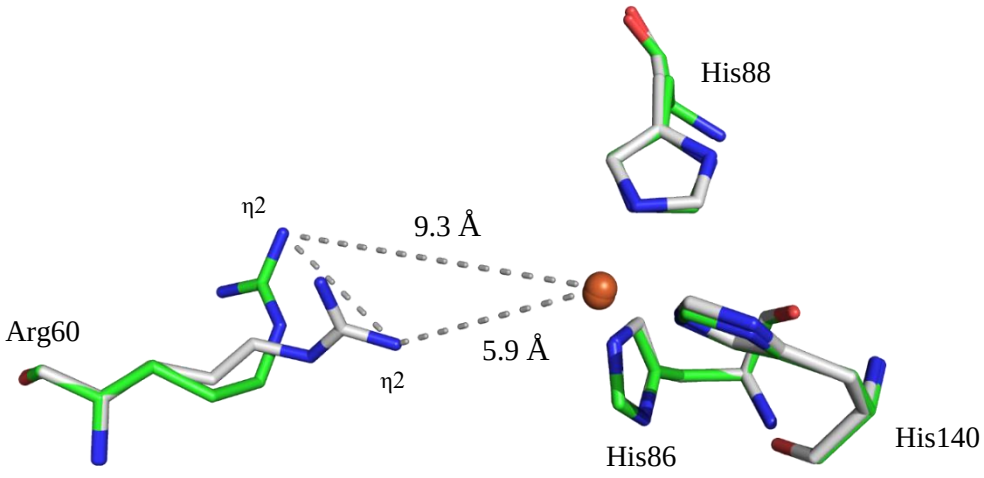

Figure 3.14. Overlay of the crystal structure of non crosslinked CDO (gray) showing the extended position of Arg60 overlay with crosslinked wild-type CDO (green, PDB: 6DL5).

The conformational switch in Arg60 could be a result of electrostatic interactions between the positive guanidium group of Arg60 and the positive amino group of L-cysteine. When L-cysteine enters the active site, it comes into contact with the positively charged guanidium group of Arg60 (**Figure 3.15**). Interactions between the amine group of L-cysteine and the guanidium group of Arg60 will cause the conformational switch in Arg60, while simultaneously repelling the amino group of L-cysteine toward the iron. The L-cysteine substrate can then coordinate the iron via the thiol and amino group, while the carboxyl group is stabilized by the positively charged Arg60 residue (**Figure 3.16**). Furthermore, the newly bent Arg60 creates additional space in the active site for cysteine oxidation to occur. To further evaluate the role of Arg60 in crosslink formation, a constructed variant of R60A CDO was used [84].

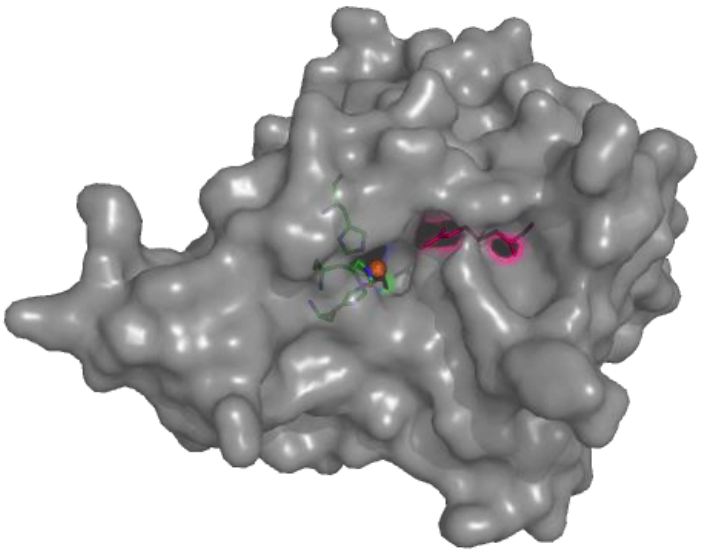

Figure 3.15. Surface model of the active site opening in non crosslinked wild-type CDO highlighting the extended position of Arg60 (pink).

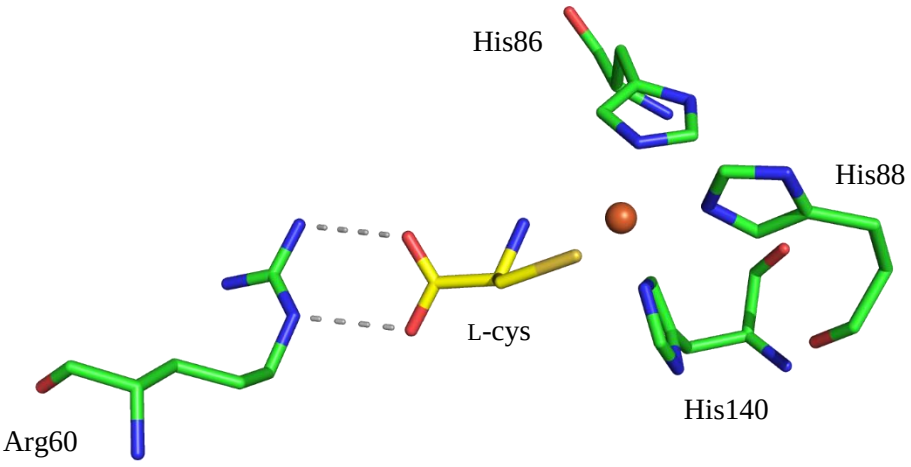

Figure 3.16. Coordination of Arg60 to L-cysteine in crosslinked wild-type CDO. PDB: 4IEV [85].

An alanine variant of Arg60 CDO contained an equal mixture of non crosslinked and crosslinked isoforms [84]. A previous study showed that when R60A CDO is incubated in the presence of L-cysteine or cysteamine, crosslink formation occurs [73]. In order to more effectively evaluate the role of Arg60 in crosslink formation, R60A CDO was expressed in the presence of the 1,10-phenanthroline. This iron chelator was found to prevent crosslink formation during expression and purification [33]. This purification yielded a homogenously non crosslinked form of R60A CDO, now referred to as non crosslinked R60A CDO. Similar to non crosslinked wild-type CDO, non crosslinked R60A CDO exists as the EPR silent iron (II) and displays a distinct lag phase while monitoring oxygen consumption. The non crosslinked R60A CDO forms the crosslink in the presence of L-cysteine and cysteamine similar to the heterogeneous R60A CDO species [73]. However, our non crosslinked R60A CDO does not form the fully crosslinked isoform. Similar to

wild-type CDO, non crosslinked R60A CDO was able to form the homogeneous crosslinked isoform with D-cysteine. With the abolishment of the positively charged arginine, cysteamine is now free to bind bidentate, lowering the redox potential of iron, creating a favorable environment for crosslink formation to occur.

The conversion of non crosslinked to the crosslinked isoform has been a topic of investigation for almost two decades. Only recently has the first homogeneous non crosslinked isoform been obtained *in vitro* [33]. Until this point, the evaluation of crosslink formation was investigated with mostly non crosslinked CDO or mutated Cys93/Tyr157 CDO variants that were thought to mimic non crosslinked CDO [82, 97]. A second hindrance in the investigation of crosslink formation was the inability to obtain the non crosslinked crystal structure. Despite wild-type CDO existing as an equal mixture of both isoforms, only the crosslinked isoform crystalized. Comparison of the non crosslinked and crosslinked wild-type CDO crystal structures has provided valuable insights into the mechanism of crosslink formation.

In the crystal structure of non crosslinked wild-type CDO, it is important to note the position of Cys93 and Tyr157 in relation to the iron. Cys93 is located trans to His86, 4.2 Å away from the iron, and the hydroxyl group of Tyr157 is tilted 26.5° below the coordinating water and 4.9 Å from the iron. In the crosslinked wild-type CDO crystal structure the hydroxyl group of Tyr157 lies closer to the iron at 4.5 Å, whereas the thiol of Cys93 slightly father away from the iron at 4.5 Å. The closer position of Tyr157 in the active site would potentially allow for a more stable coordination of the activated oxygen substrate. The slight shift of thiol group in Cys93 appears to be negligible however this minor shift creates more room in the active site. In non crosslinked wild-type CDO the angle between the Cys93, iron, and His86 there is 157°. However in crosslinked wild-type CDO, the shift of the thiol in Cys93, reduces this angle to 145° (**Figure**

3.17). The twelve degree angle decrease most likely allows more freedom for cysteine oxidation to occur.

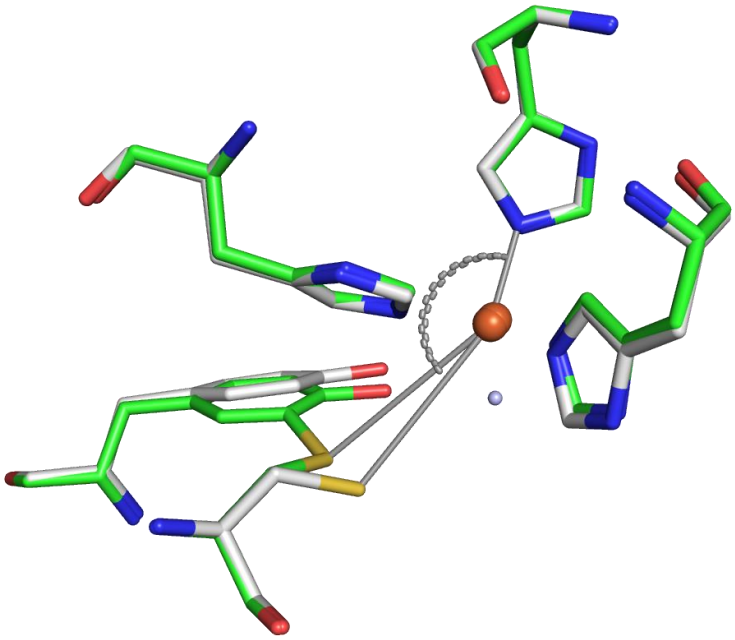

Figure 3.17. Overlay of non crosslinked (gray) and crosslinked (green) wild-type CDO showing the twelve angle decrease between Cys93-iron-His86 which is created by the shift in the thiol group of Cys93. PDB: 6DL5

In order to form the crosslinked isoform a bond distance of 2.9 Å between the thiol group of Cys93 and the hydrogen of the Cε carbon of Tyr157 must be overcome. Once the crosslinked is formed, the shift between the non crosslinked and crosslinked thiol group in Cys93 is 1.2 Å, and the shift between hydroxyl groups of Tyr157 is 1.2 Å (**Figure 3.18**). All currently proposed mechanisms for crosslink formation have been proposed to occur through a Tyr157-hydroxyl radical, however solid-state data suggests that crosslink formation via a thiyl radical would also be

favorable [33, 58, 73]. The L-cysteine substrate binds bidentate to iron, with the thiol group trans to His88 and the amino group trans to His140 [56, 79]. Binding of L-cysteine shifts the active site geometry from distorted tetrahedral to distorted octahedral, leaving iron with one unoccupied site for dioxygen binding. Dioxygen binds in an end on fashion, trans to His86. The thiol of Cys93, found directly trans to His86, would be in a direct line with the bound dioxygen. Compared to the location of Tyr157, it is reasonable to argue that the physical location of Cys93 may provide an easier pathway for the radical chemistry necessary for crosslink formation to occur. However, it is also reasonable to argue that despite the location, the hydroxyl group of Tyr157 is a better radical acceptor than the thiol of Cys93.

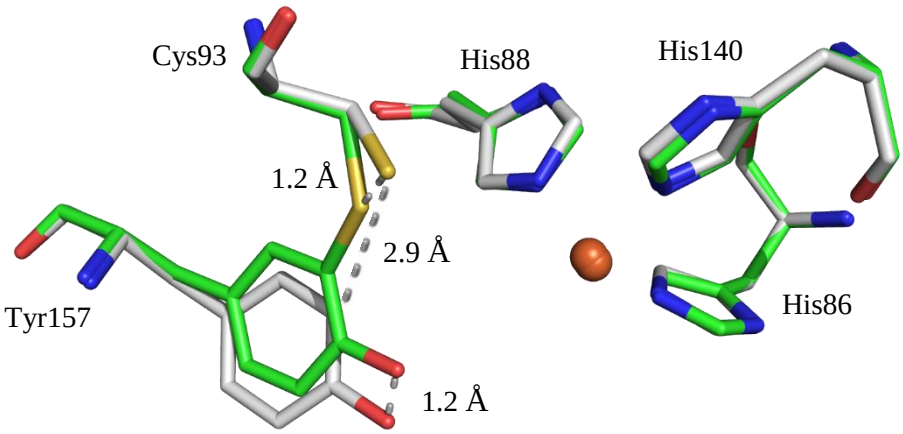

Figure 3.18. Crystal structure overlay of the active site and Cys-Tyr crosslink of non crosslinked (gray) and crosslinked wild-type CDO (green; PDB: 6DL5).

Combining new structural information with previous studies, we proposed that crosslink formation in CDO can occur via a thiyl or hydroxy radical (**Scheme 3.1**). Crosslink formation via

a thiyl or hydroxyl radical is initiated by the coordination of L-cysteine followed by dioxygen to ferrous iron (Fe^{2+}) (**Scheme 3.1, I** and **II**). Coordination of dioxygen promotes the formation of a Fe^{3+}-superoxide intermediate (**Scheme 3.1, III**). Proceeding in the direction of a thiyl radical, proton-coupled electron transfer takes place between the superoxo species and the thiol of Cys93, yielding a thiyl radical and an Fe^{3+}-peroxide complex (**Scheme 3.1, IV**). In the direction of a tyrosyl radical, the hydroxyl group of Tyr157 would provide stabilization through hydrogen bonding interactions to the Fe^{3+}-superoxide intermediate (**Scheme 3.1, III A)**. Proton-coupled electron transfer between the hydroxyl of Tyr157 and superoxide would yield Fe^{3+}-peroxide and a hydroxyl radical (**Scheme 3.1, III B**). Subsequent proton-coupled electron transfer between the hydroxyl radical and thiol of Cys93 would produce a protonated tyrosine and a thiyl radical (**Scheme 3.1, IV**). Nucleophilic attack via the thiyl radical on a π-electron contained within the double bond of Tyr157 produces the crosslinked tyrosyl radical intermediate (**Scheme 3.1, V**). Rearomatization of the crosslinked tyrosyl radical results in the loss of a proton which is combined with the peroxide complex producing one molar equivalent of hydrogen peroxide (H_2O_2). Once crosslink formation is complete, L-cysteine remains coordinated to the iron, awaiting cysteine oxidation. Cysteine oxidation begins when the second molecule of dioxygen binds, yielding another ferric superoxo radical (**Scheme 3.1, VI**).

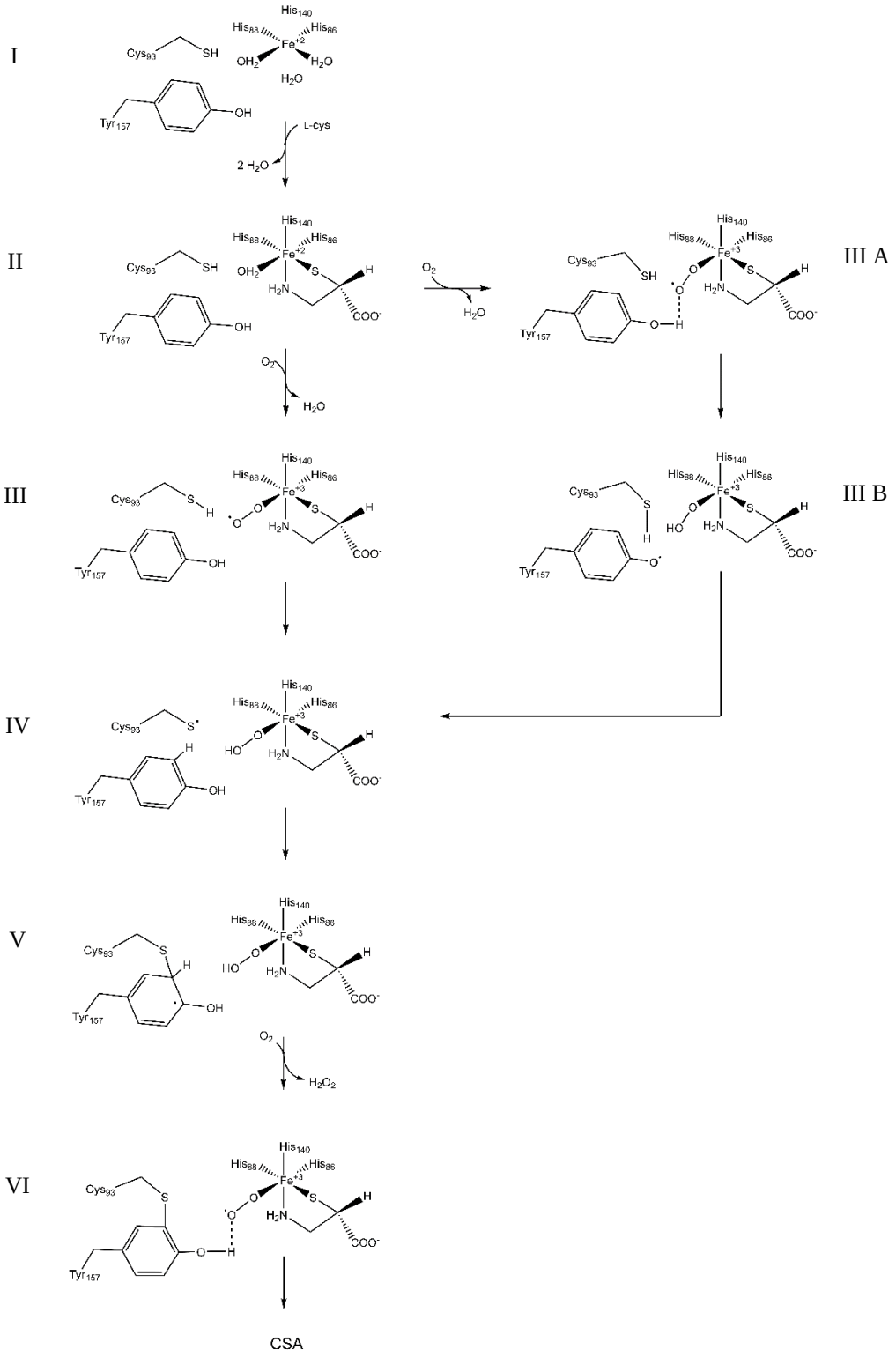

Scheme 3.1. Modified CDO crosslink mechanism. Crosslink formation via thiyl radical (**I-VI**) or a hydroxyl radical (**I-II-IIIA-IIIB-IV-V-VI**).

Monitoring the effects of pH on crosslink formation provided further insight into the mechanism of crosslink formation. It was determined that crosslink formation is optimal around a pH of 8.6, with 75 - 100% of CDO in the crosslinked isoform at L-cysteine concentration of 1 – 100 mM. There was a notable decrease in crosslink formation below pH < 7.0 and above pH > 9.0, with only 11 – 52% and 52 – 100% in the crosslinked isoform, respectively. An increase in crosslink formation as pH increases could be the result of the deprotonation of Cys93 (cysteine pKa ~ 8). The effects of pH on Cys93 is outlined in **Scheme 3.2**. At pH values below 8.0, the thiol of Cys93 would most likely exist as the protonated species. In order to form the crosslink, the superoxide radical and the protonated thiol of Cys93 would participate in proton-coupled electron transfer (PCET). However when pH increases above 8.0, the thiol would be deprotonated, and the more energetically favorable electron transfer (ET) would take place. While this theory may explain the increase in crosslink formation above a pH of 8.0, it does not account for the subsequent decrease in crosslink formation when pH > 9.0. However, deprotonation of the hydroxyl group of Tyr157 (pKa ~ 10) could account for the decrease in crosslink formation at pH values above 9.0. At a pH below 8, the protonated hydroxyl group of Tyr157 helps to stabilize the Fe^{3+}-superoxide radical. Then the iron superoxide radical and the hydrogen of the hydroxyl group of Tyr157 undergoes PCET, followed by another round of PCET between the hydroxy radical of Tyr157 and the thiol of Cys93 (**Scheme 3.3**). However if the hydroxyl group of Tyr157 is deprotonated at pH greater than 9.0, it would be unable to stabilize the superoxide iron radical, delaying proton-coupled electron transfer between the two intermediates. At an optimal pH of 8.6, Tyr157 would remain protonated and allow for favorable PCET. Then a more energetically favorable ET would occur between the hydroxyl radical of Tyr157 and deprotonated thiol of Cys93.

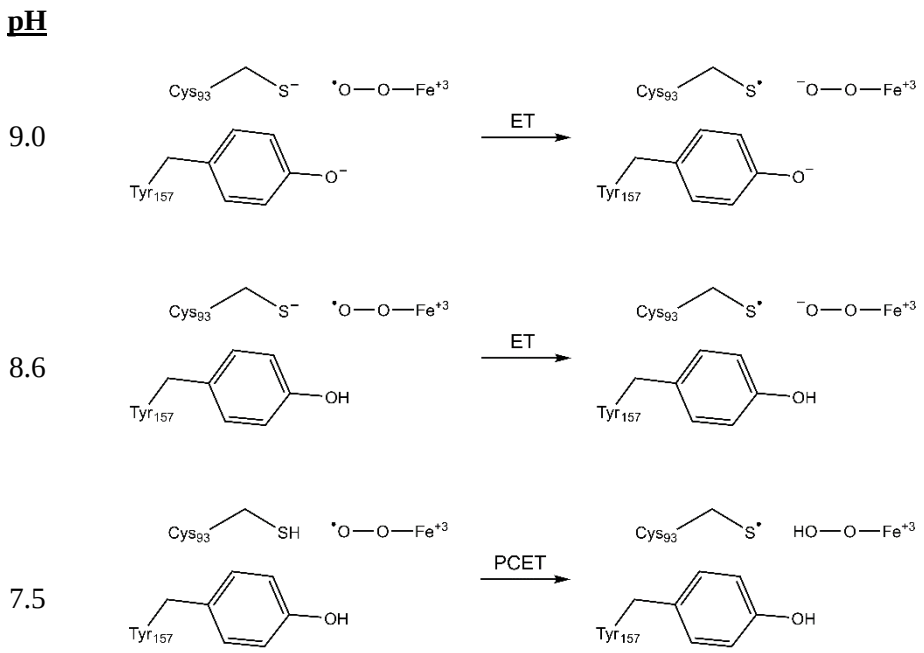

Scheme 3.2. The effect of pH on Cys93 in crosslink formation.

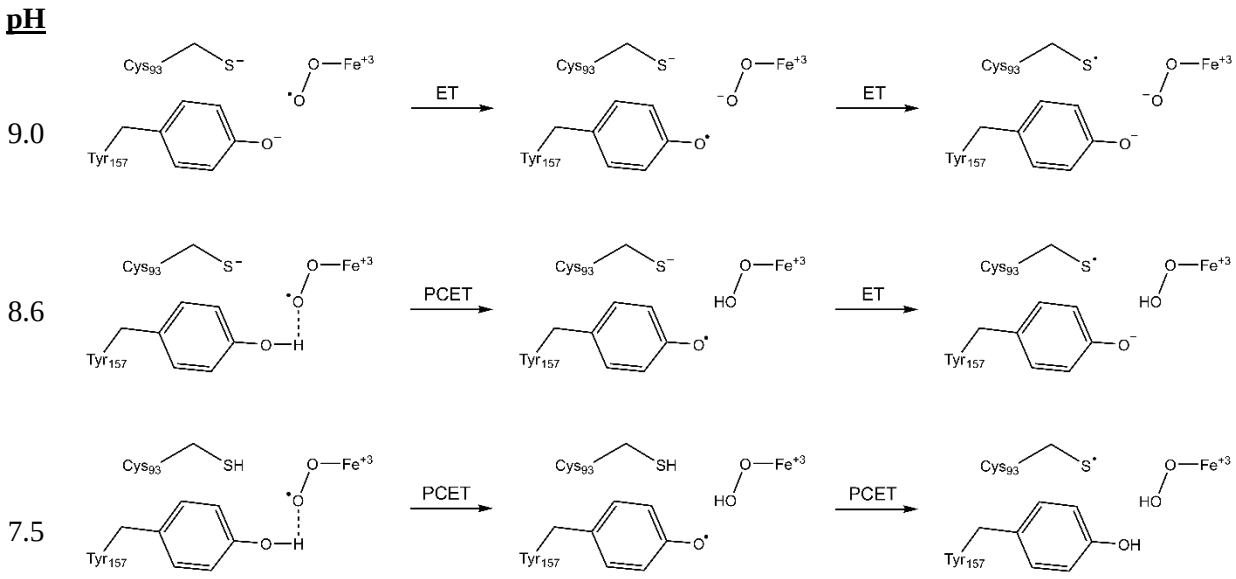

Scheme 3.3. The effect of pH on Tyr157 in crosslink formation.

Results obtained from studying the effects of pH on crosslink formation are more in line with the Tyr157 hydroxyl radical pathway of crosslink formation. However, it must be noted that PCET, or even ET, between the hydroxy radical of Tyr157 and the thiol of Cys93 would need to occur over a distance of 5.0 Å. Additionally, there is no spectroscopic evidence for a hydroxyl radical [63]. Conversely, if crosslink formation proceeded via a Cys93 thiyl radical, the crosslink should be able to form in the Y157F CDO variant. Although, it has been long established that crosslink formation does not occur in Y157F CDO. However, crosslink formation via a thiyl radical should not be discounted solely based on the inability of Y157F CDO to form the crosslink. Failure of Y157F CDO to form the crosslink could be due to the 133° rotation of the β-carbon in Cys93, as shown in the overlay of non crosslinked wild-type and Y157F CDO crystal structures (**Figure 3.19**). Furthermore, DFT calculations place the occupancy of bound O_2 within 2.2 Å of Cys93, citing the thiyl radical as a more favorable mechanism [63].

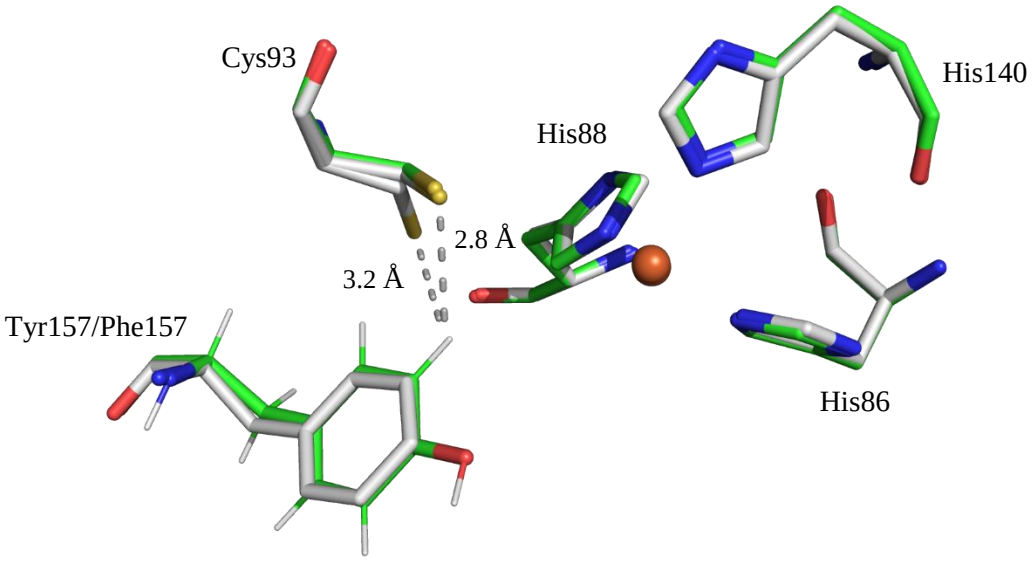

Figure 3.19. Overlay of non crosslinked wild-type CDO (green) and Y157F CDO (gray; PDB: 4XET).

This newly proposed mechanism is also consistent with previous EPR studies that determined non crosslinked CDO exists in the ferrous form, and crosslinked CDO exists in the ferric form. This mechanism can also account for why a decrease in O_2 consumption is observed when the homogeneous crosslinked isoform is incubated in the presence of an external reductant [33]. The addition of an external reductant to homogeneously crosslinked CDO could prevent the ferric species from forming, or inhibit electron coupling between Fe^{3+}-superoxide and the L-cysteine substrate, ultimately preventing or inhibiting cysteine oxidation.

Obtaining the non crosslinked wild-type CDO crystal structure has provided valuable information in the search of a crosslink mechanism. However, it is very clear that there is much work left to do in order to fully determine the mechanism of crosslink formation in cysteine dioxygenase. Ultimately, until more evidence is provided to the contrary, we propose both mechanisms are equally as likely.

REFERENCES: CHAPTERS 1 – 3

[1] Stipanuk, M. H. (2004) Sulfur amino acid metabolism: pathways for production and removal of homocysteine and cysteine, *Annu Rev Nutr 24*, 539-577.

[2] Finkelstein, J. D. (1998) The metabolism of homocysteine: pathways and regulation, *Eur J Pediatr 157 Suppl 2*, S40-44.

[3] Stipanuk, M. H. (2004) Role of the liver in regulation of body cysteine and taurine levels: a brief review, *Neurochem Res 29*, 105-110.

[4] Lombardini, J. B., and Talalay, P. (1970) Formation, functions and regulatory importance of S-adenosyl-L-methionine, *Adv Enzyme Regul 9*, 349-384.

[5] Markham, G. D., and Pajares, M. A. (2009) Structure-function relationships in methionine adenosyltransferases, *Cell Mol Life Sci 66*, 636-648.

[6] Kotb, M., and Geller, A. M. (1993) Methionine adenosyltransferase: structure and function, *Pharmacol Ther 59*, 125-143.

[7] Stipanuk, M. H. (1986) Metabolism of sulfur-containing amino acids, *Annu Rev Nutr 6*, 179-209.

[8] Finkelstein, J. D. (2000) Homocysteine: a history in progress, *Nutr Rev 58*, 193-204.

[9] Palmer, J. L., and Abeles, R. H. (1979) The mechanism of action of S-adenosylhomocysteinase, *J Biol Chem 254*, 1217-1226.

[10] Yang, X., Hu, Y., Yin, D. H., Turner, M. A., Wang, M., Borchardt, R. T., Howell, P. L., Kuczera, K., and Schowen, R. L. (2003) Catalytic strategy of S-adenosyl-L-homocysteine hydrolase: transition-state stabilization and the avoidance of abortive reactions, *Biochemistry 42*, 1900-1909.

[11] Selhub, J. (1999) Homocysteine metabolism, *Annu Rev Nutr 19*, 217-246.

[12] Finkelstein, J. D. (1990) Methionine metabolism in mammals, *J Nutr Biochem 1*, 228-237.

[13] De La Haba, G., and Cantoni, G. L. (1959) The enzymatic synthesis of S-adenosyl-L-homocysteine from adenosine and homocysteine, *J Biol Chem 234*, 603-608.

[14] Ueland, P. M., and Helland, S. (1983) Binding of adenosine to intracellular S-adenosylhomocysteine hydrolase in isolated rat hepatocytes, *J Biol Chem 258*, 747-752.

[15] Garrow, T. A. (1996) Purification, kinetic properties, and cDNA cloning of mammalian betaine-homocysteine methyltransferase, *J Biol Chem 271*, 22831-22838.

[16] Shane, B., and Stokstad, E. L. (1985) Vitamin B12-folate interrelationships, *Annu Rev Nutr 5*, 115-141.

[17] Finkelstein, J. D. (2000) Pathways and regulation of homocysteine metabolism in mammals, *Semin Thromb Hemost 26*, 219-225.

[18] Meier, M., Janosik, M., Kery, V., Kraus, J. P., and Burkhard, P. (2001) Structure of human cystathionine beta-synthase: a unique pyridoxal 5'-phosphate-dependent heme protein, *EMBO J 20*, 3910-3916.

[19] Ojha, S., Wu, J., LoBrutto, R., and Banerjee, R. (2002) Effects of heme ligand mutations including a pathogenic variant, H65R, on the properties of human cystathionine beta-synthase, *Biochemistry 41*, 4649-4654.

[20] Oliveriusova, J., Kery, V., Maclean, K. N., and Kraus, J. P. (2002) Deletion mutagenesis of human cystathionine beta-synthase. Impact on activity, oligomeric status, and S-adenosylmethionine regulation, *J Biol Chem 277*, 48386-48394.

[21] Kery, V., Bukovska, G., and Kraus, J. P. (1994) Transsulfuration depends on heme in addition to pyridoxal 5'-phosphate. Cystathionine beta-synthase is a heme protein, *J Biol Chem 269*, 25283-25288.

[22] Banerjee, R., Evande, R., Kabil, O., Ojha, S., and Taoka, S. (2003) Reaction mechanism and regulation of cystathionine beta-synthase, *Biochim Biophys Acta 1647*, 30-35.

[23] Mudd, S. H., Ebert, M. H., and Scriver, C. R. (1980) Labile methyl group balances in the human: the role of sarcosine, *Metabolism 29*, 707-720.

[24] Mudd, S. H., and Poole, J. R. (1975) Labile methyl balances for normal humans on various dietary regimens, *Metabolism 24*, 721-735.

[25] Finkelstein, J. D., Harris, B. J., Martin, J. J., and Kyle, W. E. (1982) Regulation of hepatic betaine-homocysteine methyltransferase by dietary methionine, *Biochem Biophys Res Commun 108*, 344-348.

[26] Finkelstein, J. D., Martin, J. J., Harris, B. J., and Kyle, W. E. (1983) Regulation of hepatic betaine-homocysteine methyltransferase by dietary betaine, *J Nutr 113*, 519-521.

[27] Taoka, S., Widjaja, L., and Banerjee, R. (1999) Assignment of enzymatic functions to specific regions of the PLP-dependent heme protein cystathionine beta-synthase, *Biochemistry 38*, 13155-13161.

[28] Storch, K. J., Wagner, D. A., Burke, J. F., and Young, V. R. (1988) Quantitative study in vivo of methionine cycle in humans using [methyl-2H3]- and [1-13C]methionine, *Am J Physiol 255*, E322-331.

[29] Davis, S. R., Stacpoole, P. W., Williamson, J., Kick, L. S., Quinlivan, E. P., Coats, B. S., Shane, B., Bailey, L. B., and Gregory, J. F., 3rd. (2004) Tracer-derived total and folate-dependent homocysteine remethylation and synthesis rates in humans indicate that serine is the main one-carbon donor, *Am J Physiol Endocrinol Metab 286*, E272-279.

[30] Storch, K. J., Wagner, D. A., Burke, J. F., and Young, V. R. (1990) [1-13C; methyl-2H3]methionine kinetics in humans: methionine conservation and cystine sparing, *Am J Physiol 258*, E790-798.

[31] Messerschmidt, A., Worbs, M., Steegborn, C., Wahl, M. C., Huber, R., Laber, B., and Clausen, T. (2003) Determinants of enzymatic specificity in the Cys-Met-metabolism PLP-dependent enzymes family: crystal structure of cystathionine gamma-lyase from yeast and intrafamiliar structure comparison, *Biol Chem 384*, 373-386.

[32] Imsand, E. M., Njeri, C. W., and Ellis, H. R. (2012) Addition of an external electron donor to in vitro assays of cysteine dioxygenase precludes the need for exogenous iron, *Arch Biochem Biophys 521*, 10-17.

[33] Njeri, C. W., and Ellis, H. R. (2014) Shifting redox states of the iron center partitions CDO between crosslink formation or cysteine oxidation, *Arch Biochem Biophys 558*, 61-69.

[34] Chai, S. C., Jerkins, A. A., Banik, J. J., Shalev, I., Pinkham, J. L., Uden, P. C., and Maroney, M. J. (2005) Heterologous expression, purification, and characterization of recombinant rat cysteine dioxygenase, *J Biol Chem 280*, 9865-9869.

[35] Yagi, T., Kagamiyama, H., and Nozaki, M. (1979) Cysteine sulfinate transamination activity of aspartate aminotransferases, *Biochem Biophys Res Commun 90*, 447-452.

[36] Kirsch, J. F., Eichele, G., Ford, G. C., Vincent, M. G., Jansonius, J. N., Gehring, H., and Christen, P. (1984) Mechanism of action of aspartate aminotransferase proposed on the basis of its spatial structure, *J Mol Biol 174*, 497-525.

[37] Singer, T. P., and Kearney, E. B. (1956) Intermediary metabolism of L-cysteinesulfinic acid in animal tissues, *Arch Biochem Biophys 61*, 397-409.

[38] Oertel, W. H., Schmechel, D. E., Weise, V. K., Ransom, D. H., Tappaz, M. L., Krutzsch, H. C., and Kopin, I. J. (1981) Comparison of cysteine sulphinic acid decarboxylase isoenzymes and glutamic acid decarboxylase in rat liver and brain, *Neuroscience 6*, 2701-2714.

[39] Guion-Rain, M. C., Portemer, C., and Chatagner, F. (1975) Rat liver cysteine sulfinate decarboxylase: purification, new appraisal of the molecular weight and determination of catalytic properties, *Biochim Biophys Acta 384*, 265-276.

[40] Stipanuk, M. H., Dominy, J. E., Jr., Lee, J. I., and Coloso, R. M. (2006) Mammalian cysteine metabolism: new insights into regulation of cysteine metabolism, *J Nutr 136*, 1652S-1659S.

[41] Stipanuk, M. H., Londono, M., Lee, J. I., Hu, M., and Yu, A. F. (2002) Enzymes and metabolites of cysteine metabolism in nonhepatic tissues of rats show little response to changes in dietary protein or sulfur amino acid levels, *J Nutr 132*, 3369-3378.

[42] Lee, J. I., Londono, M., Hirschberger, L. L., and Stipanuk, M. H. (2004) Regulation of cysteine dioxygenase and gamma-glutamylcysteine synthetase is associated with hepatic cysteine level, *J Nutr Biochem 15*, 112-122.

[43] Roman, H. B., Hirschberger, L. L., Krijt, J., Valli, A., Kozich, V., and Stipanuk, M. H. (2013) The cysteine dioxgenase knockout mouse: altered cysteine metabolism in nonhepatic tissues leads to excess H2S/HS(-) production and evidence of pancreatic and lung toxicity, *Antioxid Redox Signal 19*, 1321-1336.

[44] Bella, D. L., Hahn, C., and Stipanuk, M. H. (1999) Effects of nonsulfur and sulfur amino acids on the regulation of hepatic enzymes of cysteine metabolism, *Am J Physiol 277*, E144-153.

[45] Jerkins, A. A., Bobroff, L. E., and Steele, R. D. (1989) Hepatic cysteine sulfinic acid decarboxylase activity in rats fed various levels of dietary casein, *J Nutr 119*, 1593-1597.

[46] Bagley, P. J., and Stipanuk, M. H. (1994) The activities of rat hepatic cysteine dioxygenase and cysteinesulfinate decarboxylase are regulated in a reciprocal manner in response to dietary casein level, *J Nutr 124*, 2410-2421.

[47] Yin, J., Ren, W. K., Yang, G., Duan, J. L., Huang, X. G., Fang, R. J., Li, C. Y., Li, T. J., Yin, Y. L., Hou, Y. Q., Kim, S. W., and Wu, G. Y. (2016) L-Cysteine metabolism and its nutritional implications, *Mol Nutr Food Res 60*, 134-146.

[48] Stipanuk, M. H., and Ueki, I. (2011) Dealing with methionine/homocysteine sulfur: cysteine metabolism to taurine and inorganic sulfur, *J Inherit Metab Dis 34*, 17-32.

[49] Recasens, M., Benezra, R., Basset, P., and Mandel, P. (1980) Cysteine sulfinate aminotransferase and aspartate aminotransferase isoenzymes of rat brain. Purification, characterization, and further evidence for identity, *Biochemistry 19*, 4583-4589.

[50] Dunwell, J. M., Culham, A., Carter, C. E., Sosa-Aguirre, C. R., and Goodenough, P. W. (2001) Evolution of functional diversity in the cupin superfamily, *Trends Biochem Sci 26*, 740-746.

[51] Dunwell, J. M., Purvis, A., and Khuri, S. (2004) Cupins: the most functionally diverse protein superfamily?, *Phytochemistry 65*, 7-17.

[52] Uberto, R., and Moomaw, E. W. (2013) Protein similarity networks reveal relationships among sequence, structure, and function within the Cupin superfamily, *PLoS One 8*, e74477.

[53] Stipanuk, M. H., Simmons, C. R., Karplus, P. A., and Dominy, J. E., Jr. (2011) Thiol dioxygenases: unique families of cupin proteins, *Amino Acids 41*, 91-102.

[54] Souness, R. J., Kleffmann, T., Tchesnokov, E. P., Wilbanks, S. M., Jameson, G. B., and Jameson, G. N. (2013) Mechanistic implications of persulfenate and persulfide binding in the active site of cysteine dioxygenase, *Biochemistry 52*, 7606-7617.

[55] Opaleye, O., Rose, R. S., Whittaker, M. M., Woo, E. J., Whittaker, J. W., and Pickersgill, R. W. (2006) Structural and spectroscopic studies shed light on the mechanism of oxalate oxidase, *J Biol Chem 281*, 6428-6433.

[56] McCoy, J. G., Bailey, L. J., Bitto, E., Bingman, C. A., Aceti, D. J., Fox, B. G., and Phillips, G. N., Jr. (2006) Structure and mechanism of mouse cysteine dioxygenase, *Proc Natl Acad Sci U S A 103*, 3084-3089.

[57] Fetzner, S. (2012) Ring-cleaving dioxygenases with a cupin fold, *Appl Environ Microbiol 78*, 2505-2514.

[58] Simmons, C. R., Liu, Q., Huang, Q., Hao, Q., Begley, T. P., Karplus, P. A., and Stipanuk, M. H. (2006) Crystal structure of mammalian cysteine dioxygenase. A novel mononuclear iron center for cysteine thiol oxidation, *J Biol Chem 281*, 18723-18733.

[59] Fusetti, F., Schroter, K. H., Steiner, R. A., van Noort, P. I., Pijning, T., Rozeboom, H. J., Kalk, K. H., Egmond, M. R., and Dijkstra, B. W. (2002) Crystal structure of the copper-containing quercetin 2,3-dioxygenase from Aspergillus japonicus, *Structure 10*, 259-268.

[60] Dilovic, I., Gliubich, F., Malpeli, G., Zanotti, G., and Matkovic-Calogovic, D. (2009) Crystal structure of bovine 3-hydroxyanthranilate 3,4-dioxygenase, *Biopolymers 91*, 1189-1195.

[61] Chai, S. C., Bruyere, J. R., and Maroney, M. J. (2006) Probes of the catalytic site of cysteine dioxygenase, *J Biol Chem 281*, 15774-15779.

[62] Simmons, C. R., Hirschberger, L. L., Machi, M. S., and Stipanuk, M. H. (2006) Expression, purification, and kinetic characterization of recombinant rat cysteine dioxygenase, a non-heme metalloenzyme necessary for regulation of cellular cysteine levels, *Protein Expr Purif 47*, 74-81.

[63] Pierce, B. S., Gardner, J. D., Bailey, L. J., Brunold, T. C., and Fox, B. G. (2007) Characterization of the nitrosyl adduct of substrate-bound mouse cysteine dioxygenase by electron paramagnetic resonance: electronic structure of the active site and mechanistic implications, *Biochemistry 46*, 8569-8578.

[64] Stipanuk, M. H., Londono, M., Hirschberger, L. L., Hickey, C., Thiel, D. J., and Wang, L. (2004) Evidence for expression of a single distinct form of mammalian cysteine dioxygenase, *Amino Acids 26*, 99-106.

[65] Ito, N., Phillips, S. E., Stevens, C., Ogel, Z. B., McPherson, M. J., Keen, J. N., Yadav, K. D., and Knowles, P. F. (1991) Novel thioether bond revealed by a 1.7 A crystal structure of galactose oxidase, *Nature 350*, 87-90.

[66] Whittaker, M. M., Kersten, P. J., Nakamura, N., Sanders-Loehr, J., Schweizer, E. S., and Whittaker, J. W. (1996) Glyoxal oxidase from Phanerochaete chrysosporium is a new radical-copper oxidase, *J Biol Chem 271*, 681-687.

[67] Whittaker, M. M., Kersten, P. J., Cullen, D., and Whittaker, J. W. (1999) Identification of catalytic residues in glyoxal oxidase by targeted mutagenesis, *J Biol Chem 274*, 36226-36232.

[68] Schnell, R., Sandalova, T., Hellman, U., Lindqvist, Y., and Schneider, G. (2005) Siroheme- and [Fe4-S4]-dependent NirA from Mycobacterium tuberculosis is a sulfite reductase with a covalent Cys-Tyr bond in the active site, *J Biol Chem 280*, 27319-27328.

[69] Polyakov, K. M., Boyko, K. M., Tikhonova, T. V., Slutsky, A., Antipov, A. N., Zvyagilskaya, R. A., Popov, A. N., Bourenkov, G. P., Lamzin, V. S., and Popov, V. O. (2009) High-resolution structural analysis of a novel octaheme cytochrome c nitrite reductase from the haloalkaliphilic bacterium Thioalkalivibrio nitratireducens, *J Mol Biol 389*, 846-862.

[70] Itoh, S., Taki, M., and Fukuzumi, S. (2000) Active site models for galactose oxidase and related enzymes, *Coordin Chem Rev 198*, 3-20.

[71] Rogers, M. S., Baron, A. J., McPherson, M. J., Knowles, P. F., and Dooley, D. M. (2000) Galactose oxidase pro-sequence cleavage and cofactor assembly are self-processing reactions, *J Am Chem Soc 122*, 990-991.

[72] Baron, A. J., Stevens, C., Wilmot, C., Seneviratne, K. D., Blakeley, V., Dooley, D. M., Phillips, S. E., Knowles, P. F., and McPherson, M. J. (1994) Structure and mechanism of galactose oxidase. The free radical site, *J Biol Chem 269*, 25095-25105.

[73] Dominy, J. E., Jr., Hwang, J., Guo, S., Hirschberger, L. L., Zhang, S., and Stipanuk, M. H. (2008) Synthesis of amino acid cofactor in cysteine dioxygenase is regulated by substrate and represents a novel post-translational regulation of activity, *J Biol Chem 283*, 12188-12201.

[74] Yamaguchi, K., Hosokawa, Y., Kohashi, N., Kori, Y., Sakakibara, S., and Ueda, I. (1978) Rat liver cysteine dioxygenase (cysteine oxidase). Further purification, characterization, and analysis of the activation and inactivation, *J Biochem 83*, 479-491.

[75] Bella, D. L., Hirschberger, L. L., Hosokawa, Y., and Stipanuk, M. H. (1999) Mechanisms involved in the regulation of key enzymes of cysteine metabolism in rat liver in vivo, *Am J Physiol 276*, E326-335.

[76] Arjune, S., Schwarz, G., and Belaidi, A. A. (2015) Involvement of the Cys-Tyr cofactor on iron binding in the active site of human cysteine dioxygenase, *Amino Acids 47*, 55-63.

[77] Crawford, J. A., Li, W., and Pierce, B. S. (2011) Single turnover of substrate-bound ferric cysteine dioxygenase with superoxide anion: enzymatic reactivation, product formation, and a transient intermediate, *Biochemistry 50*, 10241-10253.

[78] Joseph, C. A., and Maroney, M. J. (2007) Cysteine dioxygenase: structure and mechanism, *Chem Commun (Camb)*, 3338-3349.

[79] Ye, S., Wu, X., Wei, L., Tang, D., Sun, P., Bartlam, M., and Rao, Z. (2007) An insight into the mechanism of human cysteine dioxygenase. Key roles of the thioether-bonded tyrosine-cysteine cofactor, *J Biol Chem 282*, 3391-3402.

[80] de Visser, S. P., and Straganz, G. D. (2009) Why do cysteine dioxygenase enzymes contain a 3-His ligand motif rather than a 2His/1Asp motif like most nonheme dioxygenases?, *J Phys Chem A 113*, 1835-1846.

[81] Davies, C. G., Fellner, M., Tchesnokov, E. P., Wilbanks, S. M., and Jameson, G. N. (2014) The Cys-Tyr cross-link of cysteine dioxygenase changes the optimal pH of the reaction without a structural change, *Biochemistry 53*, 7961-7968.

[82] Driggers, C. M., Kean, K. M., Hirschberger, L. L., Cooley, R. B., Stipanuk, M. H., and Karplus, P. A. (2016) Structure-Based Insights into the Role of the Cys-Tyr Crosslink and Inhibitor Recognition by Mammalian Cysteine Dioxygenase, *J Mol Biol 428*, 3999-4012.

[83] Li, W., Blaesi, E. J., Pecore, M. D., Crowell, J. K., and Pierce, B. S. (2013) Second-sphere interactions between the C93-Y157 cross-link and the substrate-bound Fe site influence the O(2) coupling efficiency in mouse cysteine dioxygenase, *Biochemistry 52*, 9104-9119.

[84] Njeri, C. W. (2014) The Efficiency of Enzymatic L-Cysteine Oxidation in Mammalian Systems Derives from teh Optimal Organization of the Active Site of Cysteine Dioxygenase, In *Chemistry and Biochemistry*, p 149, Auburn University, Auburn, AL.

[85] Driggers, C. M., Cooley, R. B., Sankaran, B., Hirschberger, L. L., Stipanuk, M. H., and Karplus, P. A. (2013) Cysteine dioxygenase structures from pH4 to 9: consistent cys-persulfenate formation at intermediate pH and a Cys-bound enzyme at higher pH, *J Mol Biol 425*, 3121-3136.

[86] Sorbo, B., and Ewetz, L. (1965) Enzymatic Oxidation of Cysteine to Cysteinsulfinate in Rat Liver, *Biochem Bioph Res Co 18*, 359-&.

[87] Ewetz, L., and Sorbo, B. (1966) Characteristics of Cysteinesulfinate-Forming Enzyme System in Rat Liver, *Biochimica Et Biophysica Acta 128*, 296-&.

[88] Straganz, G. D., and Nidetzky, B. (2006) Variations of the 2-His-1-carboxylate theme in mononuclear non-heme FeII oxygenases, *Chembiochem 7*, 1536-1548.

[89] Pochapsky, T. C., Pochapsky, S. S., Ju, T., Hoefler, C., and Liang, J. (2006) A refined model for the structure of acireductone dioxygenase from Klebsiella ATCC 8724 incorporating residual dipolar couplings, *J Biomol NMR 34*, 117-127.

[90] Emsley, P., and Cowtan, K. (2004) Coot: model-building tools for molecular graphics, *Acta Crystallogr D Biol Crystallogr 60*, 2126-2132.

[91] Gardner, J. D., Pierce, B. S., Fox, B. G., and Brunold, T. C. (2010) Spectroscopic and computational characterization of substrate-bound mouse cysteine dioxygenase: nature of

the ferrous and ferric cysteine adducts and mechanistic implications, *Biochemistry 49*, 6033-6041.

[92] Simmons, C. R., Krishnamoorthy, K., Granett, S. L., Schuller, D. J., Dominy, J. E., Jr., Begley, T. P., Stipanuk, M. H., and Karplus, P. A. (2008) A putative Fe2+-bound persulfenate intermediate in cysteine dioxygenase, *Biochemistry 47*, 11390-11392.

[93] Lombardi.Jb, Singer, T. P., and Boyer, P. D. (1969) Cysteine Oxygenase .2. Studies on Mechanism of Reaction with 18oxygen, *Journal of Biological Chemistry 244*, 1172-&.

[94] Li, W., and Pierce, B. S. (2015) Steady-state substrate specificity and O(2)-coupling efficiency of mouse cysteine dioxygenase, *Arch Biochem Biophys 565*, 49-56.

[95] Ferraroni, M., Matera, I., Steimer, L., Burger, S., Scozzafava, A., Stolz, A., and Briganti, F. (2012) Crystal structures of salicylate 1,2-dioxygenase-substrates adducts: A step towards the comprehension of the structural basis for substrate selection in class III ring cleaving dioxygenases, *J Struct Biol 177*, 431-438.

[96] Kleffmann, T., Jongkees, S. A., Fairweather, G., Wilbanks, S. M., and Jameson, G. N. (2009) Mass-spectrometric characterization of two posttranslational modifications of cysteine dioxygenase, *J Biol Inorg Chem 14*, 913-921.

[97] Siakkou, E., Rutledge, M. T., Wilbanks, S. M., and Jameson, G. N. (2011) Correlating crosslink formation with enzymatic activity in cysteine dioxygenase, *Biochim Biophys Acta 1814*, 2003-2009.

[98] Davidson, V. L. (2018) Protein-Derived Cofactors Revisited: Empowering Amino Acid Residues with New Functions, *Biochemistry*.

[99] Whittaker, M. M., and Whittaker, J. W. (2003) Cu(I)-dependent biogenesis of the galactose oxidase redox cofactor, *J Biol Chem 278*, 22090-22101.

CHAPTER FOUR

LITERATURE REVIEW: PART II

4.1 Sulfur metabolism in bacteria

Similar to mammals, sulfur plays an important metabolic role in bacterial organisms. Inorganic sulfite and cysteine are the primary sources of sulfur for bacteria [1]. Unfortunately, inorganic sulfite and cysteine are not often readily available in the environment exist. To counterbalance this shortcoming, many species of bacteria have the ability to scavenge inorganic sulfite from organosulfonates. Organosulfonates are typically small carbon-based molecules found in nature that contain a $R\text{-}SO_3^-$ functional group. Through a process called desulfonation, organosulfonates are used by bacteria as an alternate sulfur source. For organosulfonates like alkanesulfonate, desulfonation takes place through the cleavage of the carbon-sulfur bond, producing inorganic sulfite (SO_3^{-2}) and the corresponding aldehyde. Inorganic sulfite is then further incorporated into important biomolecules like L-cysteine [2].

4.2 Genes expressed during sulfate starvation

Many bacterial organisms have enzymes capable of scavenging sulfite from alkanesulfonates as well as sulfate and taurine. When sulfate is limited, the sulfate-starvation-induced (*ssi*) operons are upregulated [3]. In *Escherichia coli*, two *ssi* operons identified included *tauABCD* and *ssuEADCB*, which are responsible for desulfonation of taurine (2-

aminoethanesulfonate) and alkanesulfonates, respectively (**Figure 4.1**). In both the *tau* and *ssu* gene clusters, *tauABC* and *ssuABC* serve as the ABC-type transporter system responsible for uptake of taurine and alkanesulfonates into the cell [4-6]. Little is known regarding about the exact mechanism in which the substrates move across the external membrane and through the periplasm and cytoplasm. However the substrate transport order of enzymes has been identified (**Figure 4.2**). Biochemical studies support that TauA and SsuA are the periplasmic sulfonate binding proteins, whereas TauC and SsuC are integral in substrate transportation across the permease membrane, and TauB and SsuB are enzymes that hydrolyze ATP. Alkanesulfonates can be transported by both *ssuABC* and *tauABC*; however, taurine is transported exclusively by *tauABC* [7].

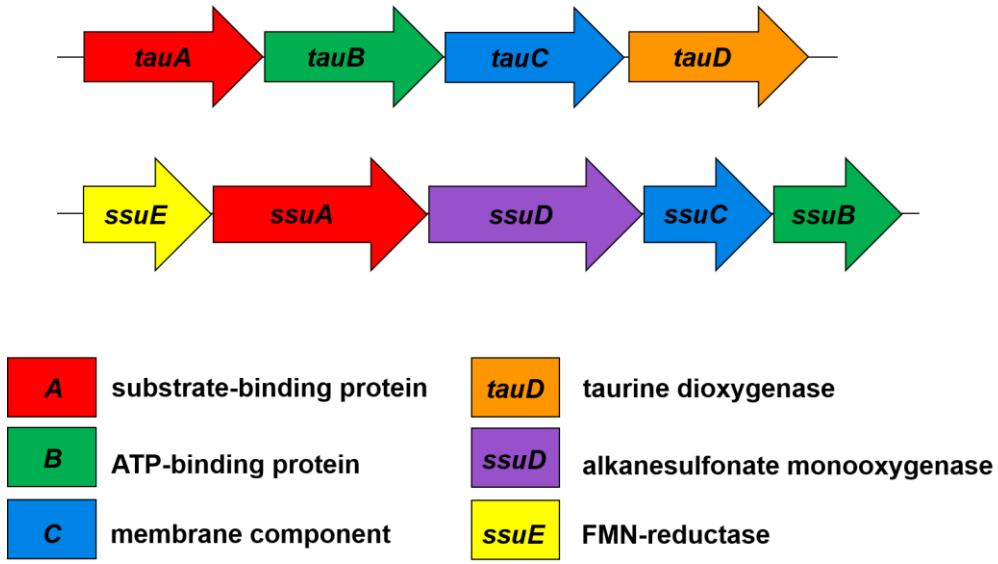

Figure 4.1. *tau* and *ssu* genes expressed during sulfate limiting conditions. Adapted from [2].

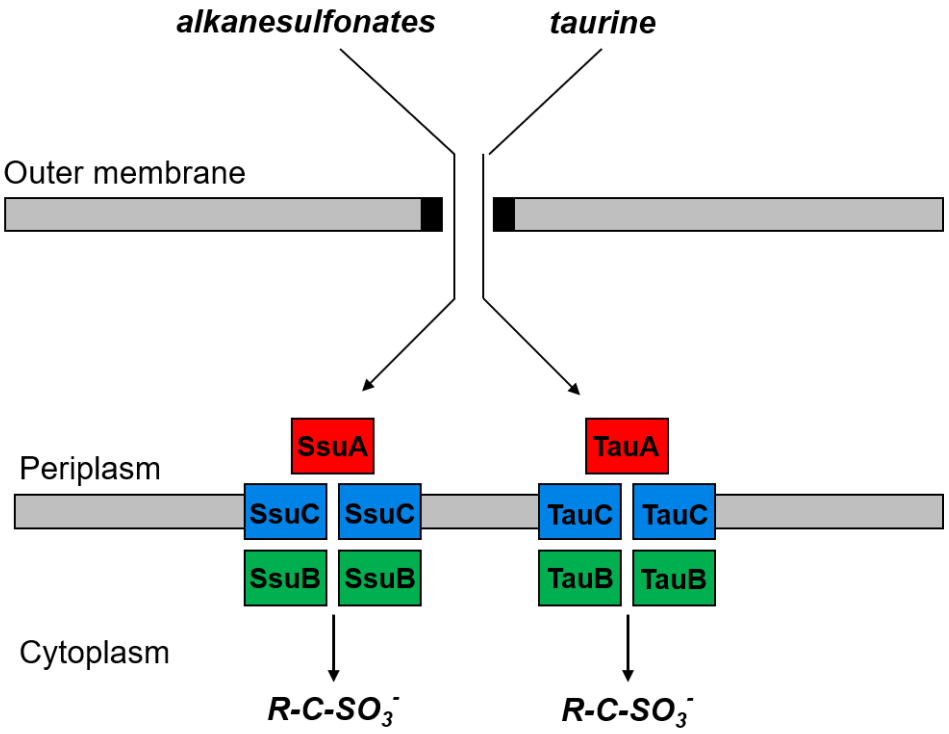

Figure 4.2. Uptake and transportation of alkanesulfonates and taurine in the *ssu* and *tau* gene clusters from *E. coli*. Adapted from [2].

Similarly, desulfonation of taurine is specific to the TauD enzyme. Taurine dioxygenase, or TauD, is an α-ketoglutarate dependent non-heme iron enzyme which converts taurine to aminoacetaldehyde and sulfite (**Figure 4.3**) [8]. Due to the involvement of α-ketoglutarate, succinate and carbon dioxide are additional products of the desulfonation reaction. In addition, TauD is also able to utilize some small aliphatic and aromatic sulfonates [8]. Alkanesulfonates are converted to sulfite and the corresponding aldehyde by SsuD. The **s**ulfonate-**s**ulfur **u**tilization enzyme alkanesulfonate monooxygenase, or SsuD, uses reduced flavin and oxygen to convert a wide range of alkanesulfonates to sulfite and the corresponding aldehyde [6]. Unlike TauD, SsuD requires $FMNH_2$, which is supplied by the FMN-reductase SsuE.

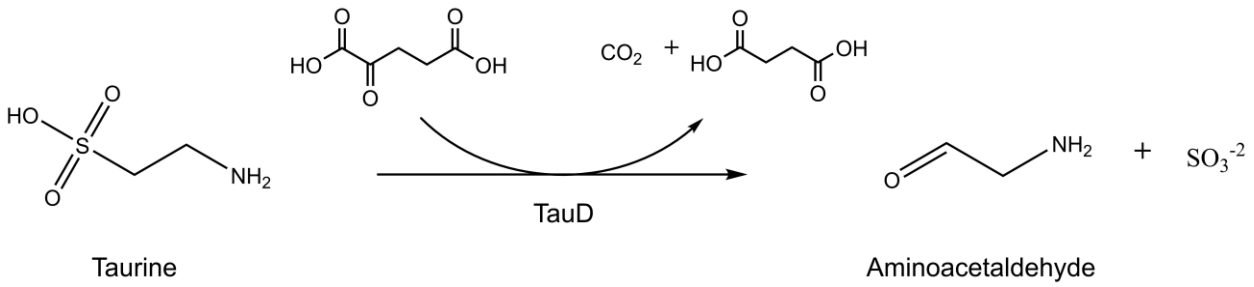

Figure 4.3. Conversion of taurine to aminoacetaldehyde and sulfite by TauD [8].

4.3 FMN-reductase SsuE

In *E. coli*, the FMN-reductase SsuE is responsible for providing reduced flavin to the alkanesulfonate monooxygenase SsuD. In most flavoproteins FMN is bound as a prosthetic group which provides stability and prevents autooxidation of $FMNH_2$. However, purified recombinant wild-type SsuE does not contain bound flavin as a prosthetic group [9]. It is interesting that flavin is used as a substrate in SsuE. Previous work has shown that SsuE has a higher affinity for FMN with a K_d value of 0.015 ± 0.004 μM, with one flavin bound per monomer [10]. Additionally, most FMN-reductases can utilize NADPH or NADH, but typically have a preference for only one. The SsuE enzyme can use either NADPH or NADH, with equal effectiveness, to reduce flavin (**Figure 4.4**) [9].

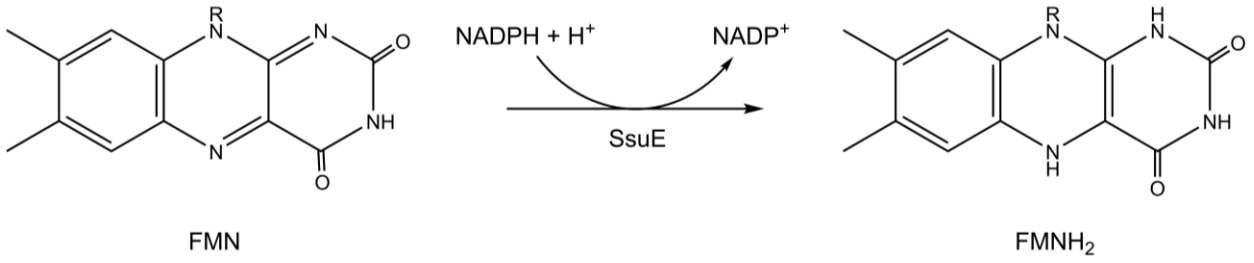

Figure 4.4. Reduction of FMN to $FMNH_2$ by SsuE.

Like many FMN-dependent reductases, kinetic studies revealed that SsuE reduces FMN through a ordered sequential mechanism (**Figure 4.5**). The NADPH substrate is first to bind followed by FMN, FMN is then reduced and released as $FMNH_2$ followed by the release of $NADP^+$ [10]. In addition, there is competitive inhibition between $NADP^+$ and NADPH, however high concentrations of NADPH can reverse the inhibitory effect.

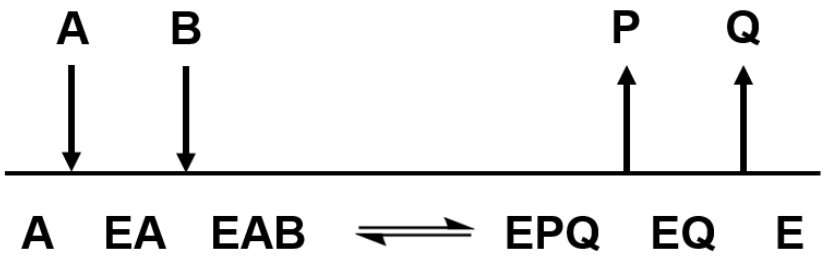

Figure 4.5. Ordered sequential mechanism of SsuE where A=NADPH; B=FMN; P=$FMNH_2$; and Q=$NADP^+$. Adapted from [10].

Rapid reaction kinetics studies of flavin reduction by SsuE revealed that flavin reduction occurs in three separate phases [11]. The first detectable phase is the interaction between NADPH and FMN, which is followed by electron transfer from the pyridine nucleotide of NADPH to FMN. The hydride transfer between NADPH and FMN was identified as the rate-limiting step, which was confirmed by [4(R)-^{2}H] NADPH isotope studies. The last step was determined to be either the release of products or the decline of the $FMNH_2$-$NADP^+$ complex [11].

Early oligomeric state analysis, as determined by gel filtration, shows recombinant wild-type SsuE exists as a homodimer [9]. However, three-dimensional structural analysis of wild-type

SsuE determined the flavin-bound and flavin free enzyme exists as a tetramer (**Figure 4.6**) [12]. Analytical ultracentrifugation studies confirmed that flavin-free wild-type SsuE exists as a tetramer, or more specifically a dimer of dimers [12]. Contrary to the structural investigations, in the presence of flavin wild-type SsuE undergoes a conformational shift from a tetramer to a dimer [12]. Crystallization of FMN-bound wild-type SsuE occurred in the presence of supra-physiological concentrations of enzyme and flavin, which could have an effect on the oligomeric state. Overall, it is suspected that binding of FMN weakens the tetramer, causing the enzyme to exist in a tetramer-dimer equilibrium.

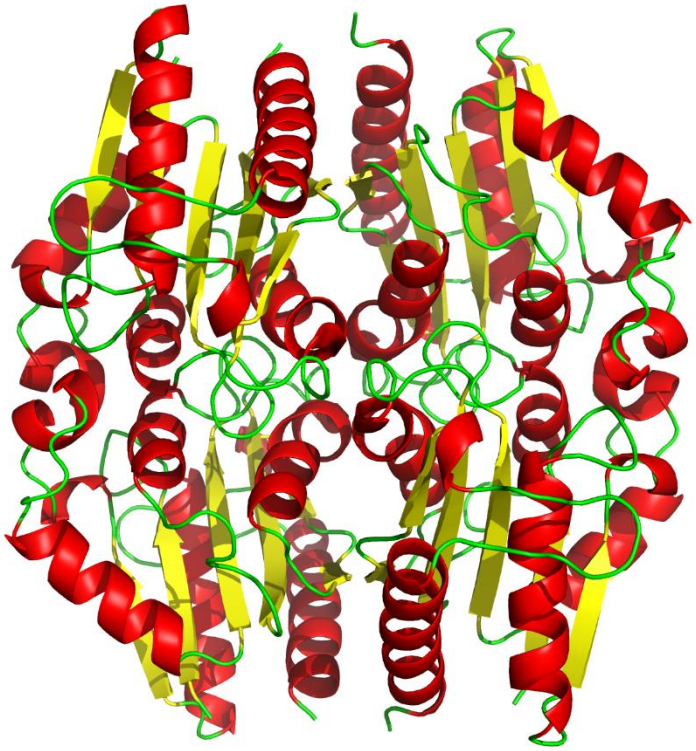

Figure 4.6. Crystal structure of the tetramer SsuE from *E. coli*.. α-helices (red), β-sheets (yellow), and turns/loops (green). PDB: 4PTY [12].

Primary differences among members of the NAD(P)H:FMN reductase family is the presence of a π-helix. A π-helix was identified at the tetramer interface of wild-type SsuE (**Figure 4.7**). A π-helix is characterized by an insertion of an amino acid residue resulting in 4.1 amino acids per turn, as compared to an α-helix consisting of only 3.6 amino acids per turn. Since π-helices have more amino acids per turn they are further characterized by a bulge protruding from the helix [13, 14]. In an enzyme, the occurrence of a π-helix usually signifies an evolutionary advancement such as enhanced function [13, 14]. In SsuE, the π-helix is due to an insertion of a tyrosine residue (Tyr118). Interestingly, the hydroxyl of Tyr118 forms a hydrogen bond across the helical interface to the oxygen atom in the carbonyl backbone of Ala78 [15]. In the FMN-bound SsuE crystal structure the polypeptide nitrogen of Ala78 hydrogen bonds to an oxygen (O4) of FMN (**Figure 4.8**).

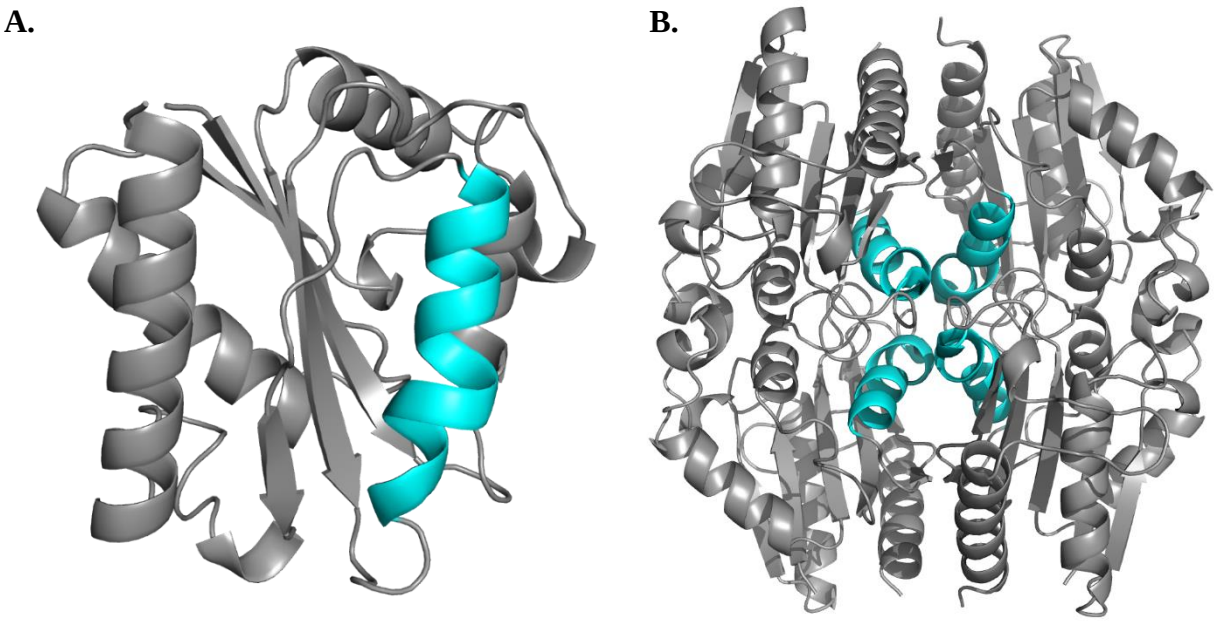

Figure 4.7. Three dimensional crystal structure of wild-type SsuE (PDB: 4PTY) . **A.** Monomer of wild-type SsuE highlighting the π-helix (cyan). **B.** Tetramer of wild-type SsuE with π-helices shown at the tetramer interface. [12]

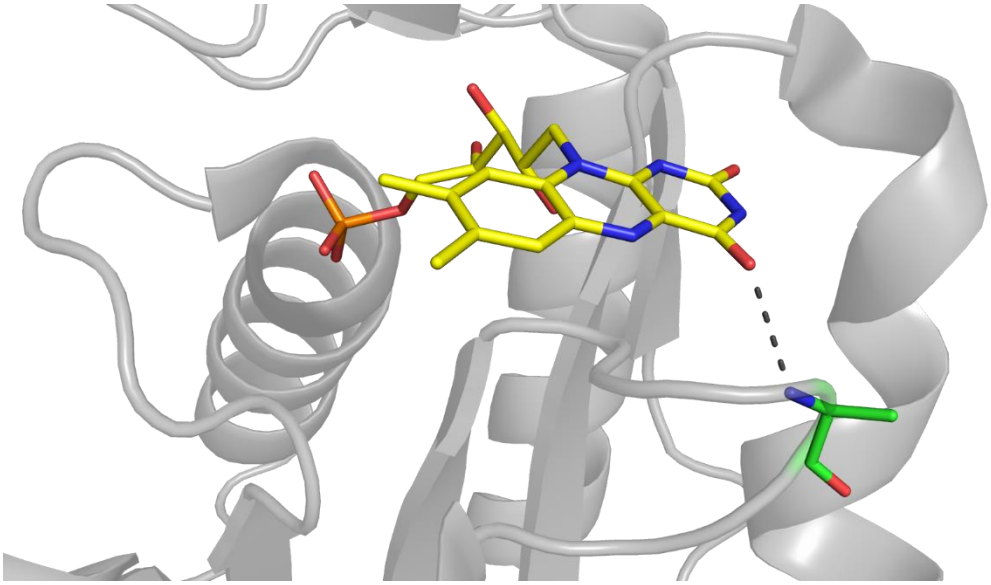

Figure 4.8. Three dimensional crystal structure of FMN-bound wild-type SsuE showing hydrogen bonding between FMN and Ala78. PDB: 4PTZ [12]

It has also been suggested, that due to its position within the π-helix, the conserved Tyr118 may play a role in oligomeric state changes that promote reduced flavin transfer to SsuD. Recent studies sought to investigate the role of Tyr118 and the π-helix in SsuE. In order to investigate the role of Tyr118, site-directed mutagenesis from tyrosine to an alanine was performed [16]. Mutation of tyrosine to alanine should disrupt the hydrogen bonding network between Tyr118 and Ala78. Since alanine lacks aromaticity, the bulge indicative of the π-helical secondary structure should be abolished. Three dimensional crystal structures of flavin-free Y118A SsuE confirmed the π-helix now exists as a typical α-helix [17]. Purified Y118A SsuE yielded a brightly yellow colored enzyme with absorbance maxima at 370 and 457 nm corresponding to a flavin-bound enzyme. FMN was liberated from Y118A SsuE through denaturation. Subsequent filtration retained the enzyme and left the yellow solution as the flow-thru. The ability to separate through denaturation

confirmed the yellow molecule was not covalently bound, and mass spectrometric analysis gave a molecular weight consistent with FMN. ApoY118A SsuE binds flavin in a 1:1 ratio, with an oxidized FMN dissociation constant (K_d) value of 8 ± 1 nM, which is two-fold lower than wild-type SsuE indicating tighter binding [16]. Results from anaerobic kinetic studies showed the Y118A SsuE variant is capable of flavin reduction. Upon exposure to air slow oxidation of reduced flavin occurred. These results suggest the usually reactive $FMNH_2$ is receiving protection against oxygen from Y11A SsuE. In coupled assays, Y118A SsuE is unable to support the transfer of reduced flavin to SsuD [16]. However, Y118A SsuE is able to transfer electrons to ferricyanide under aerobic conditions.

Further investigation into the three dimensional crystal structure of SsuE, showed π-π stacking interactions between Tyr118 residues across the tetramer interface (**Figure 4.9**) [15]. It is speculated that the protruding bulge of the π-helix facilitates the π-π stacking interactions, promoting a tetramer interface. Additional Tyr118 variants were constructed to further evaluate the role of the π-helix in oligomeric state changes. For simplicity, a qualitative summary of results for each variant, including previously discussed Y118A SsuE, is summarized in **Table 4.1** [15].

Table 4.1: Summary of results for wild-type and Y118 SsuE variants [15, 16].

	FMN-bound as purified	FMN binding compared to wild-type	Supports NADPH oxidase activity	Supports $FMNH_2$ transfer to SsuD	e^- transfer to FeCN	Oligomeric State
wild-type SsuE	no	---	yes	yes	yes	tetramer
Y118A	yes	similar	no	no	yes	dimer
Y118S	yes	similar	no	no	no	dimer
Y118F	no	similar	yes	yes	n/d*	tetramer
ΔY118	no	10-fold inc.	no	no	yes	tetramer

*n/d – was not determined

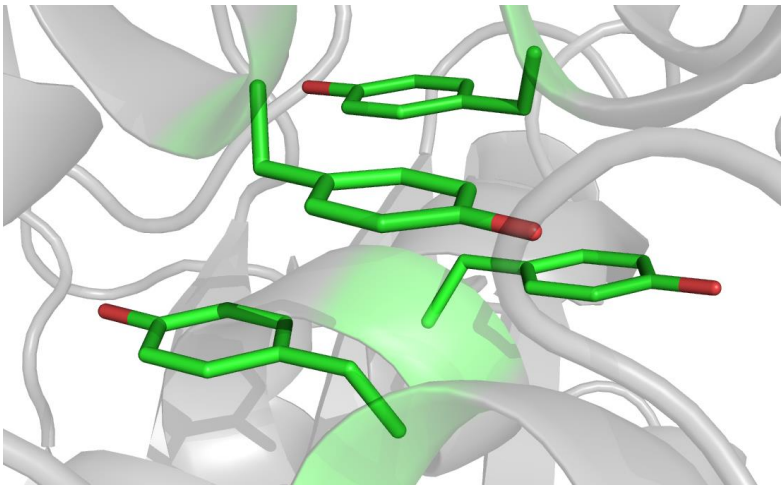

Figure 4.9. π-π stacking interactions between Tyr118 across the tetramer interface of wild-type SsuE. PDB: 4PTY [15]

Substitution of Y118 to serine (Y118S SsuE) could allow for the theoretical conservation of hydrogen bonding to Ala78 across the tetramer interface. However due to the absence of aromaticity provided by the benzene ring, π-π stacking cannot occur. Purified Y118S SsuE is flavin-bound and exists as a dimer. Depesite the preservation of the hydroxyl group, the shortened amino acid is not long enough to hydrogen bond across the tetramer interface. The Y118S SsuE variant is unable to support NADPH oxidation and flavin transfer to SsuD. Unlike Y118A SsuE, the serine variant is not able to support transfer to ferricyanide. Mutation of Y118 to phenylalanine (Y118F SsuE) maintains π-π stacking interactions, while compromising hydrogen bonding to Ala78. The Y118F SsuE variant exists as a tetramer and can support NADPH oxidation and flavin transfer to SsuD. The preservation of the native oligomeric state suggests that π-π interactions persisted. Due to the bulkiness of the benzene ring, the π-helix of Y118F SsuE may have remained intact as well [15].

Lastly, deletion of the tyrosine residue (ΔY118 SsuE) removed the insertional additional amino acid needed to form a π-helix. This deletion of the tyrosine residue restored the π-helix to an α-helix, with the overall oligomeric state of a tetramer [15]. ΔY118 SsuE had no measurable NADPH oxidase activity and was unable to support flavin transfer to SsuD. There was also a 10-fold increase in the FMN binding value compared to wild-type SsuE. These results provide evidence that ΔY118 is stable as a tetramer even in the presence of FMN. Unable to form a dimer, the active site remains concealed and flavin transfer would not occur. Overall, mutational studies suggest that insertion of the tyrosine residue plays a key role in the formation of the π-helix and π-π stacking interactions. Although the exact mechanism is currently unknown, these π-interactions play an important part in the secondary structure and the ability to transfer reduced flavin to SsuD.

4.4 Alkanesulfonate monooxygenases SsuD

Once reduced by SsuE, $FMNH_2$ is utilized by the alkanesulfonate monooxygenase SsuD to cleave the carbon-sulfur bond of a wide range of 1-alkanesulfonates. The alkanesulfonate monooxygenase system is the first reported system that is capable of cleaving the carbon-sulfur (C-S) bonds through a oxygenase mechanism [9]. Through the use of reduced flavin and molecular oxygen, SsuD desulfonates a wide variety of 1-alkanesulfonates into sulfite and the corresponding aldehyde (**Figure 4.10**).

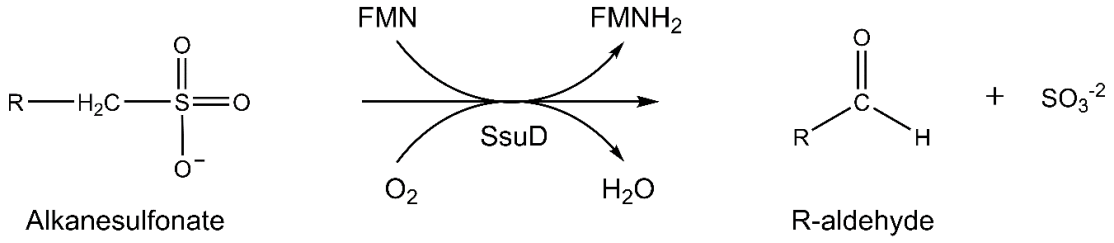

Figure 4.10. Conversion of alkanesulfonate to sulfite and R-aldehyde by SsuD.

Overall the cleavage of the C-S bond is dependent on dioxygen, which is activated by reduced flavin [18]. The substrate binding order in SsuD was determined through steady-state and rapid reaction kinetic studies. Results suggested that reduced flavin binds first, followed by the alkanesulfonate, with dioxygen binding last (**Figure 4.11**) [18]. It has also been suggested that dioxygen binds prior to the alkanesulfonate substrate octanesulfonate (OCS). However, a faster reaction rate and slower disassociation constant was observed when SsuD was premixed with $FMNH_2$ and octanesulfonate as compared to a premix of SsuD and $FMNH_2$ alone [18]. These results suggests that dioxygen likely binds last. It was also determined that OCS binds in a 1:1 ratio with SsuD-$FMNH_2$, with a K_d value of 17.5 ± 0.9 μM [18].

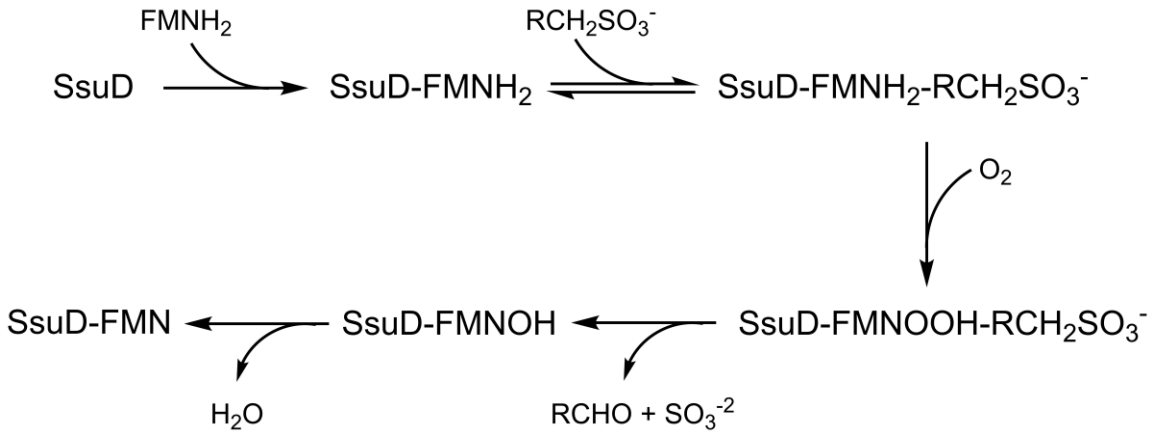

Figure 4.11. Proposed substrate binding order of $FMNH_2$ and alkanesulfonate for SsuD. Adapted from [18].

Additionally, rapid-reaction kinetics provided evidence for the existence of a C4a-(hydro)-peroxyflavin intermediate. This oxygenated C4a-flavin reaction intermediate is common among flavoprotein monooxygenase systems [19-21]. The proposed desulfonation reaction mechanism is shown in **Figure 4.12**. After dioxygen activation, the C4a-(hydro)-peroxyflavin initiates a nucleophilic attack on the sulfonate functional group of the alkanesulfonate forming an alkanesulfonate-peroxyflavin intermediate. A Baeyer-Villiger rearrangement of the flavin intermediate, followed by proton abstraction by a nearby base produces the sulfite and R-aldehyde [18].

As a member of the bacterial luciferase family, SsuD has the traditional triosephosphate isomerase (TIM)-barrel fold characterized by eight α-helices and eight parallel β-sheets. The active site is located at the C-terminal end of the β-barrel [22]. Like most TIM-barrel proteins, SsuD contains a loop region (residues 250-282) [22-25]. Due to the predicted flexible nature of this loop, it remains unresolved in three dimensional crystal structures [22]. The loop region is speculated to act as a lid-gating mechanism, protecting the reduced flavin from solvent exposure [26-31]. This type of substrate protection has previously been identified in bacterial luciferase [32-34]. In SsuD a conserved arginine residue, Arg297, is located on the loop region that is directly positioned over the active site [35]. Substitution of Arg297 to alanine and lysine in SsuD resulted in an inactive enzyme. Additionally, both arginine variants displayed a 4-fold decrease in the ability to bind reduced flavin. It was concluded that Arg297 does not significantly effect reduced flavin binding, but is more likely to play a role in overall loop closure [35]. Additionally, partial deletion of the loop regions of SsuD had no effect on reduced flavin binding, but did have an effect on desulfonation activity [36]. This data suggest that the loop aids in the exchange of reduced flavin transfer between SsuE and SsuD.

Recombinant wild-type SsuD exists as a homotetramer and contains only one cysteine residue (Cys54). The lack of cysteine residues is considered an advantage during sulfur limiting conditions. Interestingly, Cys54 is located within the active site of SsuD, and is considered a conserved residue, along with His228, Arg297, and Tyr331 (**Figure 4.13**). Structurally similar enzymes, bacterial luciferase and long-chain alkane monooxygenase (LadA), also contain the same active site residues [22, 37-41].

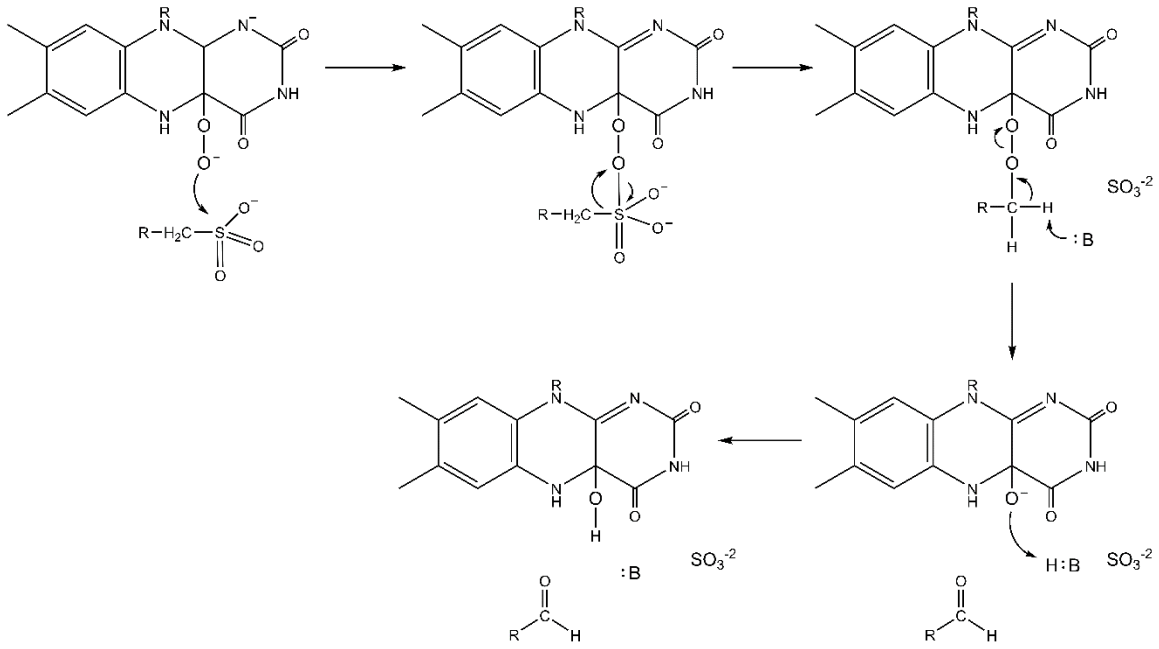

Figure 4.12. Proposed desulfonation mechanism of SsuD. Adapted from [18].

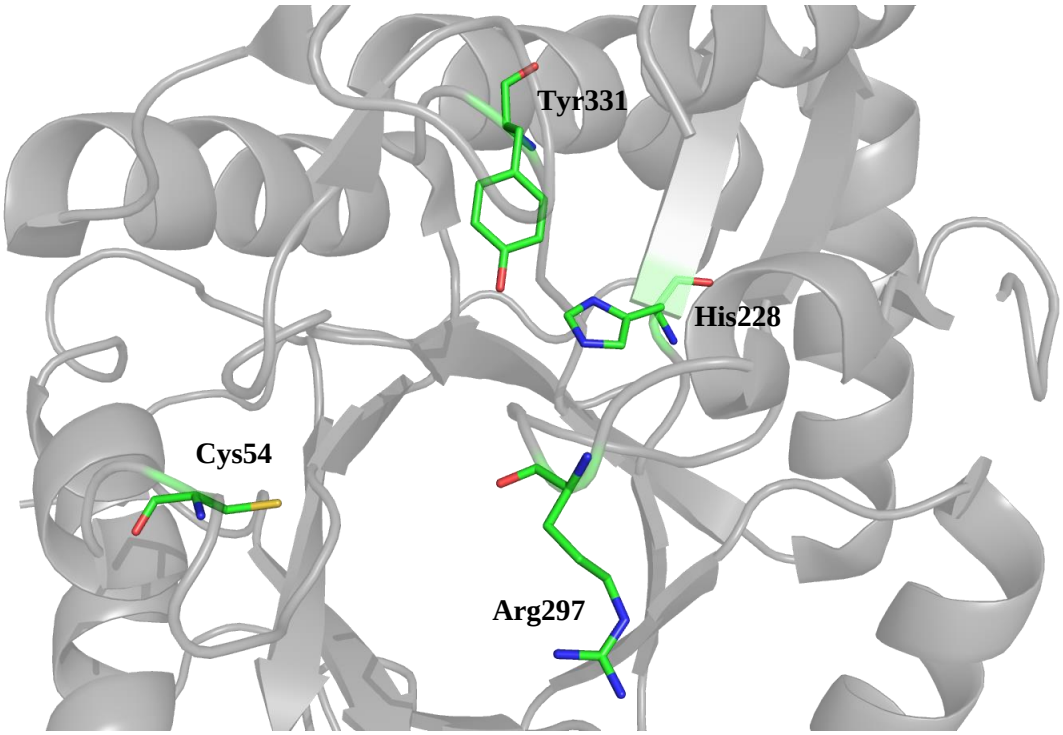

Figure 4.13. Location of conserved active site residues Cys54, His228, Arg297, and Tyr331 in wild-type SsuD. PDB: 1M41 [22].

Site directed mutagenesis of Cys54 to alanine (C54A) and serine (C54S) was used to evaluate the role of the conserved residue in SsuD [37]. Interestingly, the conservative substitution of cysteine to serine yielded an overall increase in catalytic efficiency with a k_{cat}/K_m value of 3.8 ± 0.7 $\mu M^{-1}min^{-1}$ compared to 1.2 ± 0.2 $\mu M^{-1}min^{-1}$ for wild-type SsuD. However, it should be noted that this increase is primarily due to the 6-fold decrease in K_m of C54S SsuD. Alternatively, C54A SsuD was determined to have a 9-fold decrease in k_{cat} with a value of 5.6 ± 0.1 min^{-1} versus 51.7 ± 2.1 min^{-1} for wild-type SsuD. This decrease led to an overall 6-fold decrease in k_{cat}/K_m with a value of 0.2 ± 0.1 $\mu M^{-1}min^{-1}$ [37]. Neither C54A or C54S SsuD had an effect on the binding of FMN or $FMNH_2$. However, both C54A and C54S showed an increased affinity for octanesulfonate

binding with K_d values of 4.97 ± 0.58 μM and 2.68 ± 0.60 μM, respectively, compared to 17.5 ± 0.9 μM for wild-type SsuD [37]. Results from rapid-reaction kinetics provided evidence that C54S SsuD was capable of forming the C4a-(hydro)-peroxyflavin intermediate, however the flavin intermediate was undetectable in experiments with C54A SsuD. Overall it was concluded, the thiol of Cys54 provides stabilization to C4a-(hydro)-peroxyflavin intermediate. It is most likely that stabilization occurs via hydrogen bonding. C54S SsuD retains the ability to hydrogen bond, and therefore provides similar stabilization to the reduced flavin intermediate as wild-type SsuE [37].

4.5. Flavin transfer and protein-protein interactions

Reduced flavin is known to readily oxidize, generating reactive oxygen species such as hydrogen peroxide or hydroxyl radicals [42-44]. Formation of these molecules can create a toxic environment within the cell and lead to permanent physiological damage. Therefore it is suggested that flavin transfer in bacteria is tightly controlled. Fluorescence binding studies determined that SsuE has a dissociation constant of 0.015 ± 0.004 μM for FMN, which is 600-fold lower than the K_d value of 10.2 ± 0.4 μM for SsuD [45]. Alternatively, SsuD has a K_d value of 0.32 ± 0.15 μM for $FMNH_2$, compared to the 40-fold higher than the K_d value of 15.5 ± 1.3 μM for SsuE [18]. The high degree of specificity for FMN by SsuE and $FMNH_2$ by SsuD may play a role in flavin transfer.

It has been proposed that flavin transfer between SsuE and SsuD can occur through a free diffusion or channeling mechanism (**Figure 4.14**) [45]. Transfer of flavin by free diffusion would be inefficient due to the highly probable autooxidation of $FMNH_2$. A channeling mechanism, that involves protein-protein interactions, would be more efficient due to structural protection of reduced flavin from non-enzymatic oxidation. Detection of protein-protein interactions in FMN-dependent two-component systems appears to be dependent on the enzymes being investigated [10, 46-50]. While evaluating the mechanism in which SsuE utilizes FMN and NADPH, Gao, et.

al. observed that in the presence of SsuD and octanesulfonate, SsuE switched from an ordered sequential mechanism to a rapid equilibrium ordered mechanism [10]. The altered mechanism of SsuE suggested that static interactions could occur between the two proteins.

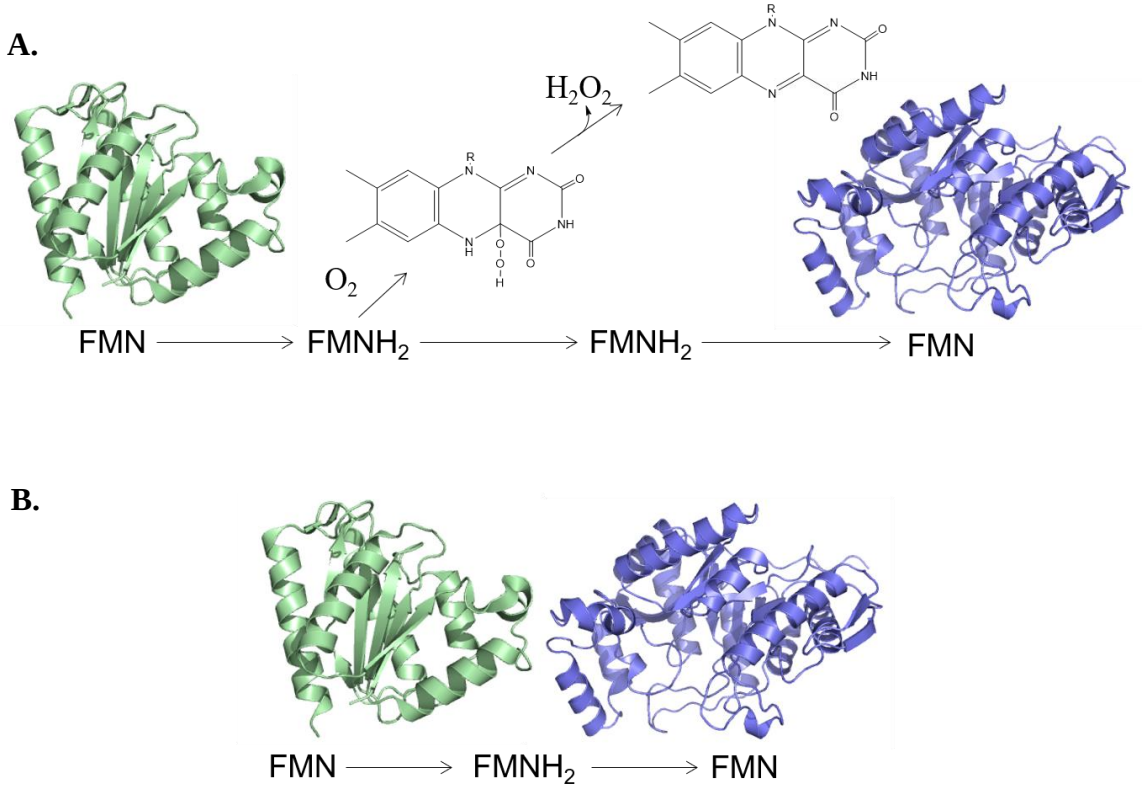

Figure 4.14. Two proposed mechanisms of flavin transfer between SsuE and SsuD. **A.** Flavin transfer by free diffusion or **B.** flavin transfer through a channeling mechanism [45].

Initial static interaction between the two proteins were observed in chromatographic separation experiments using His-tagged SsuD and a Ni-NTA column. After a high concentration imidazole wash, SDS-PAGE analysis confirmed the coelution of wild-type SsuE and His-tagged wild-type SsuD [45]. The observed static interaction were further evaluated by fluorescent spectroscopy to quantitatively determine binding affinity between the two proteins. Similar to substrate binding experiments, protein binding was determined by titrating wild-type SsuD into an FMN-bound SsuE solution while monitoring an increase in signal intensity. Results found that FMN-SsuE bound in a 1:1 ratio with SsuD, having a K_d value of 0.0022 ± 0.0010 μM [45].

In addition, studies were conducted to identify the specific regions involved in protein-protein interactions [51]. Amide hydrogen-deuterium exchange mass spectrometry (HDX-MS) is a technique used to study conformational dynamics of proteins by exchanging labile hydrogen atoms with deuterium (D_2O). The amount of deuterium that was exchanged for SsuE and SsuD individually was compared to the amount of deuterium exchanged for the SsuE-SsuD complex. In wild-type SsuE, a > 20% decrease in deuterium exchange was found in two regions corresponding to amino acids 78-89 (KAAYSGALKTLL) and 118-125 (YALKPVL). Similarly two regions of SsuD, 251-261 (DDETIAKAQAA) and 285-295 (EISPNLWAGVG) were also identified with a comparable decrease in deuterium [51]. The protected regions on SsuE correspond to two helices, one being the π-helix that contains Tyr118 (**Figure 4.15 A**). Similarly protected amino acids on SsuD are identified by two α-helices and one loop region positioned at the opening of the active site (**Figure 4.15 B**).

A.

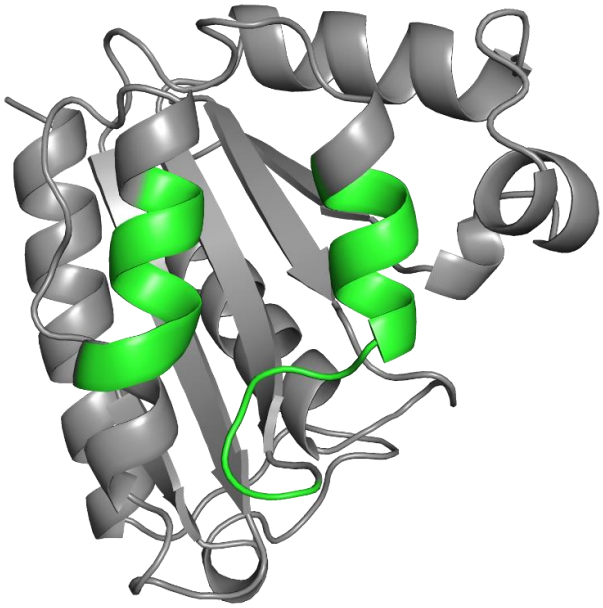

B.

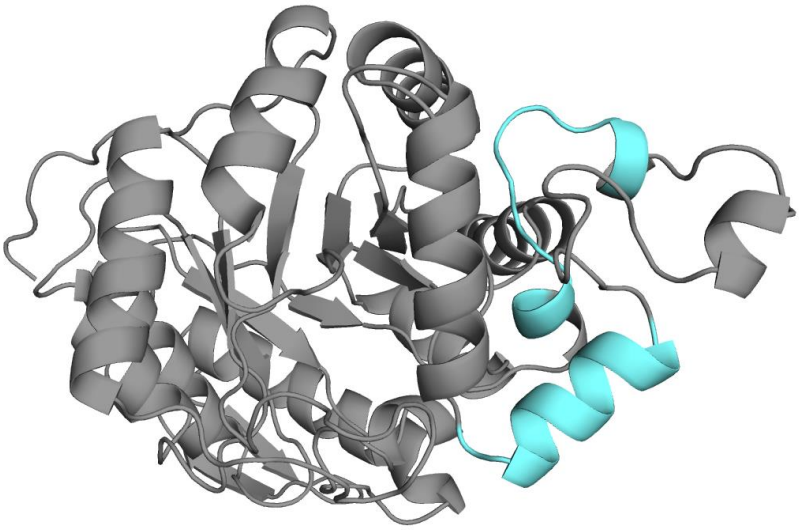

Figure 4.15. Protein-protein interaction sites as determined by HDX-MS. **A.** Interaction sites (green) for wild-type SsuE and **B.** Interaction sites (cyan) for wild-type SsuD.

As previously discussed wild-type SsuE exists as a tetramer, or more specifically a dimer of dimers, with the active site contained within the tetramer interface [12]. However in the presence of FMN, SsuE undergoes an oligomeric state change into a dimer exposing the active site. The vulnerability of the active site in SsuE could be key in the involvement of flavin transfer through protein-protein interactions. As previously discussed, mutation of Tyr118 to alanine in SsuE produced a tightly bound FMN variant incapable of transferring reduced flavin to SsuD [16]. Addition of Y118A SsuE into reactions of SsuE and SsuD could determine if flavin transfer occurred exclusively through a channeling mechanism. Y118A and wild-type SsuE would compete with each other for interaction sites of wild-type SsuD. Incubation of wild-type SsuE in the presence of increasing concentrations of Y118A SsuE and fixed concentrations of SsuD, showed a decline in sulfite production. Inhibition of sulfite production by Y118A reached a plateau at a 1:1 ratio of Y118A to wild-type SsuD [16]. The Y118A SsuE variant proved to be an valuable tool in investigating protein-protein interactions.

Interaction sites of SsuD are located in the dynamic loop region and contain negatively charged amino acids. Triple mutation of three negatively charged residues, Asp251/Asp252/Glu253, to alanine (DDE (251/252/253)AAA) and deletion of the α-helical region containing Asp251-Ala261 (ΔD251-A261) in SsuD were performed to better determine the role of these regions in protein-protein interactions. Circular dichroism spectroscopy determined that the triple mutation and deletion of the Asp251-Ala261 region had no effect on the overall gross secondary structure of SsuD. Steady-state kinetic analysis determined the DDE(251/252/253)AAA SsuD variant gave a 4-fold decrease in catalytic efficiency (k_{cat}/K_m) as compared to wild-type SsuD, whereas there was no detectable activity with (ΔD251-A261) SsuD [51].

The interaction sites were further investigated through mutagenesis studies. Pull-down experiments performed with His-tagged DDE(251/252/253)AAA and (ΔD251-A261) SsuD showed wild-type SsuE did not coelute with the variant enzymes [51]. The SsuD DDE(251/252/253)AAA variant had a 5-fold decrease in binding affinity compared to wild-type SsuE with a K_d value of 0.21 ± 0.03 μM as compared to 0.039 ± 0.015 μM for wild-type SsuD, and suggested that protein-protein interactions were compromised [51].

The positions of the protected residues, in both SsuE and SsuD, over the active sites suggest that protein-protein interactions would aid in the transfer of reduced flavin [51]. Additionally, each region contains a series of charged residues. The residues in SsuE are primarily positively charged (Lys77, Lys86, and Lys121), while the residues in SsuD are primarily negatively charged (Asp251, Asp252, Glu253, Gln259, Glu285, and Asn289). Through electrostatic interactions, the alternatively charged residues of SsuE and SsuD could play a role in protein-protein interactions [51]. Overall, studies described have provided strong evidence into the detection and identification of specific regions involved in protein-protein interactions of the alkanesulfonate monooxygenase system.

4.6. Two-component systems in *Pseudomonas sp.* involved in sulfur metabolism

Alternative desulfonation mechanisms to acquire sulfur from methanesulfonate and dimethyl sulfone have been identified in pseudomonads [52-54]. Methanesulfonate (MSA) and dimethyl sulfide (DMS) are commonly found in soil environments where bacterial organisms thrive. DMS is an oxidative byproduct of marine ecosystems, and is produced through the degradation of dimethylsulfoniopropionate. Ultimately DMS is incorporated into the terrestrial environment through precipitation [55-60]. DMS can be further oxidized into dimethyl sulfoxide (DMSO) and dimethyl sulfone ($DMSO_2$) (**Figure 4.16**). It is currently thought that oxidation of

DMS occurs in the atmosphere, however enzymatic oxidation has not been ruled out [61-63]. When sulfite is limiting in the environment, oxidative products of DMS can be used as sulfur sources in *Pseudomonas sp*..

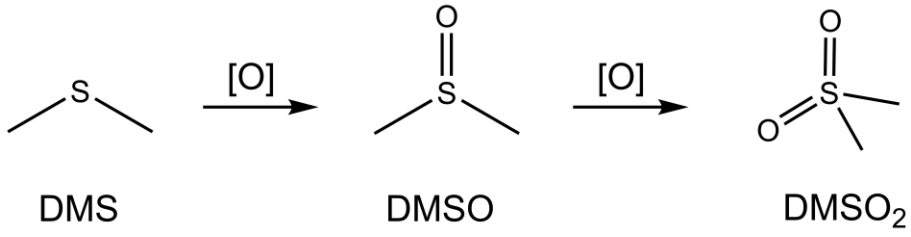

Figure 4.16. Non enzymatic oxidation of DMS to $DMSO_2$. DMS=dimethyl sulfide; DMSO=dimethyl sulfoxide; $DMSO_2$=dimethyl sulfone. Adapted from [63, 64].

The SsuE/SsuD alkanesulfonate monooxygenase system has been identified in *Pseudomonas aeruginosa* and *Pseudomonas putida* [65, 66]. The alkanesulfonate monooxygenase system in *Pseudomonas sp*. is homologous to the one found in *E. coli*. However in *Pseudomonas sp.*, a sixth gene was identified on the *ssu* operon. The additional gene, designated *ssuF*, is a small molybdopterin-binding protein. The exact role of SsuF has yet to be determined, but in the presence of SsuF, SsuD is capable of desulfonating organosulfates ($R\text{-}O\text{-}SO_3^-$) and aromatic alkanesulfonates as well as C-2 to C-10 aliphatic alkanesulfonates [65].

In *Pseudomonas aeruginosa* strain PAO1, an additional set of *ssi* genes that are involved in the desulfonation of methanesulfonate, *msuEDC* were identified (**Figure 4.17**) [52]. The *msuED* genes encode for an NADH-dependent FMN-reductase MsuE, which supplies reduced flavin to the $FMNH_2$-dependent monooxygenase MsuD. Unlike SsuD, MsuD reacts with a limited number

of alkanesulfonates, with methanesulfonate as the preferred substrate [52]. Additionally, the *msuC* gene encodes for a ~ 45 kDa enzyme with a unknown function, MsuC. Amino acid sequence comparison shows MsuC is closely related, > 40% identity, to DszC in *Rhodococcus erythropolis*. DszC catalyzes the initial oxidation of sulfinates ($R\text{-}SO_2^-$) to sulfonates ($R\text{-}SO_3^-$) [67]. A 1.5-fold increase in specific activity for desulfonation was found when MsuE and MsuD reaction occurred in the presence of MsuC. However, no measurable desulfonation activity was observed for MsuE and MsuC alone. MsuC was also found to be related to several acyl coenzyme A dehydrogenases (~ 25% identity) [52]. But, regardless of the specific function of MsuC, the addition of the *msuEDC* operon provides *Pseudomonas aeruginosa* an advantage in procuring sulfite compared to bacterial organisms only containing the *ssu* operon [52].

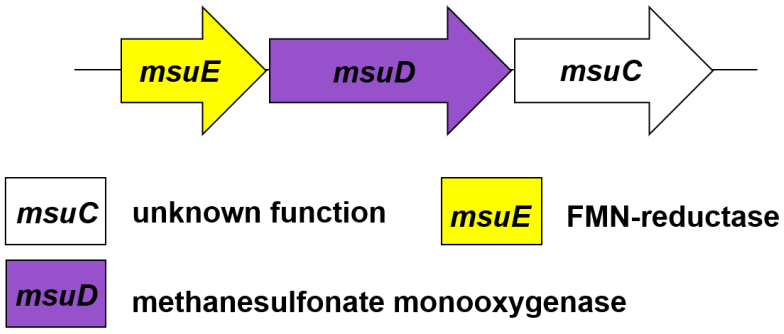

Figure 4.17. *msu* genes expressed during sulfur limiting conditions in *Pseudomonas aeruginosa*.

A pathway for utilization of dimethylsulfone has been identified in *Pseudomonas putida* strain DS1 [54]. The gene clusters *sfnECR*, and *sfnABFG* were shown to be induced under limited sulfate conditions (**Figure 4.18**) [53, 54, 68]. It is important to note that *Psuedomonas putida* lacks the *msu* genes. SfnE, NADH-dependent FMN-reductase, and SfnC, a hypothetical

monooxygenase, have a high amino acid sequence identity to MsuE (64 %) and MsuC (70 %) found in *Pseudomonas aeruginosa* [53]. Similar to MsuC, the role of SfnC has yet to be evaluated. Alternatively, SfnR was determined to be σ^{54}-dependent transcriptional activator that is required for the expression of *sfnABFG* [68].

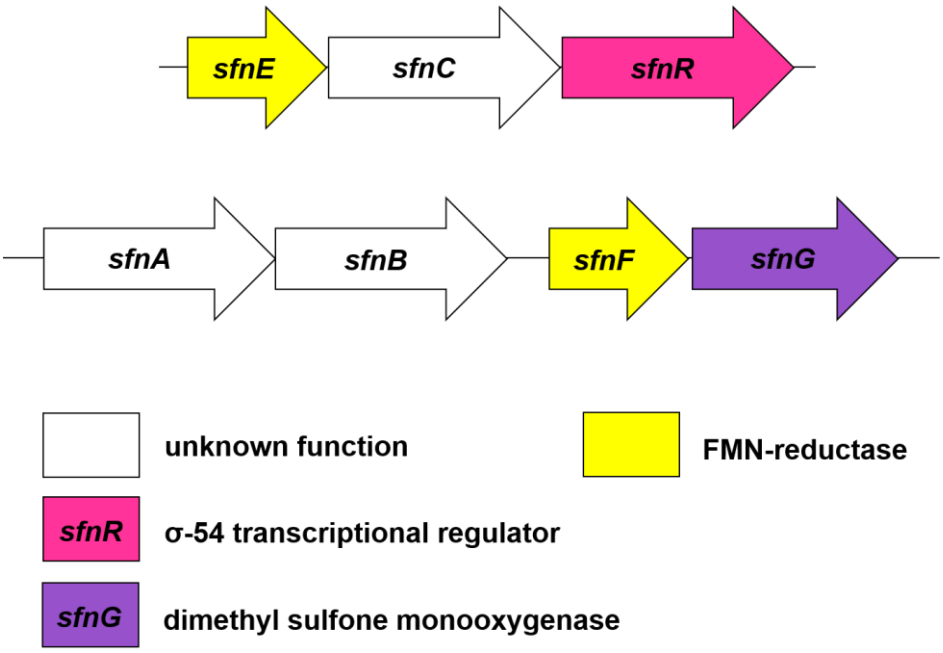

Figure 4.18. *sfn* genes expressed during sulfur limiting conditions in *Pseudomonas putida*.

The two genes, *sfnA* and *sfnB*, are located directly downstream from *sfnFG*, separated by a small intergenic region which binds the transcriptional activator, SfnR. SfnA and SfnB share amino acid identity (>30 %) with acyl coenzyme A dehydrogenase enzymes and DszC [68, 69]. Interestingly, SfnA and SfnB share 36% amino acid sequence identity with each other. SfnF, a hypothetical NAD(P)H-dependent FMN-reductase has 54% amino acid identity with MsuE, while SfnG, an $FMNH_2$-dependent monooxygenase, shares 37% amino acid identity with MsuD from

Pseudomonas aeruginosa [68]. Activity assays determined that SfnF is unable reduce or transfer flavin to SfnG [68]. However, SfnG successfully catalyzed the reaction of $DMSO_2$ to MSA when reduced flavin was supplied from SfnE (**Figure 4.19**).

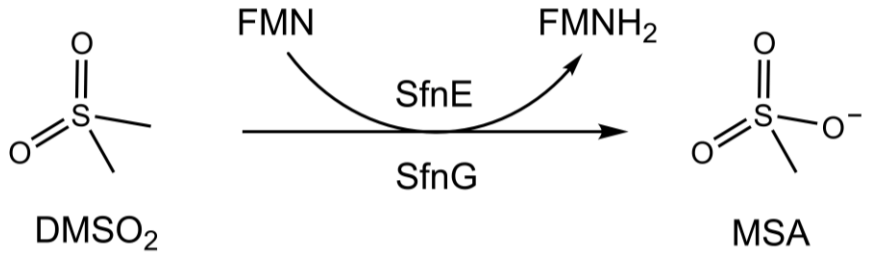

Figure 4.19. Conversion of $DMSO_2$ to MSA by SfnG, with reduced flavin supplied by SfnE as proposed by [68].

More recently, SfnG has been identified in *Pseudomonas fluorescens* strain Pf0-1. The *sfnG* gene is the only *sfn* gene present in *Pseudomonas fluorescens* [64]. Interestingly, the *msuEDC* gene cluster was also identified in *Pseudomonas fluorescens*. This is the first report of both *sfn* and *msu* genes present in a pseudomonad. In this study it was proposed that SfnG utilizes reduced flavin to catalyze the demethylation of $DMSO_2$ to yield methanesulfinate (**Figure 4.20**), and that the oxidation of methanesulfinate to MSA is non-enzymatic [64].

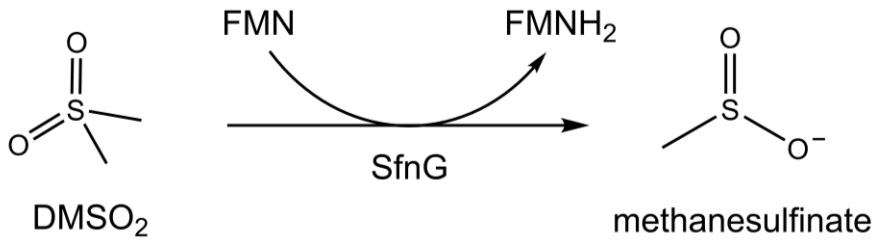

Figure 4.20. Conversion of $DMSO_2$ to methanesulfinate by SfnG as proposed by [64].

Since SfnG does not have a dedicated *sfn* FMN-reductase enzyme, MsuE was used to supply reduce flavin to SfnG. When SfnG was incubated in the presence of enzymatically generated $FMNH_2$ and $DMSO_2$, and the methanesulfonate product was identified. This is in agreeance with results of SfnG in *Pseudomonas putida*. However control experiments, excluding SfnG, showed that methanesulfonate was still able to form when methanesulfinate and FMN were incubated in the presence of MsuE [64]. Overall it was concluded that through an oxygen activated C4a-(hydro)peroxyflavin, superoxide radicals were generated causing the non enzymatic oxidation of methanesulfinate to MSA [64]. It was also speculated that *in vivo*, oxidation of methanesulfinate to MSA could occur through MsuC, whose function has yet to be identified. It is currently proposed that sulfite scavenging of $DMSO_2$ occurs through three enzymatic reactions involving SfnG, MsuC, and MsuD, with all enzymes requiring reduced flavin (**Figure 4.21**).

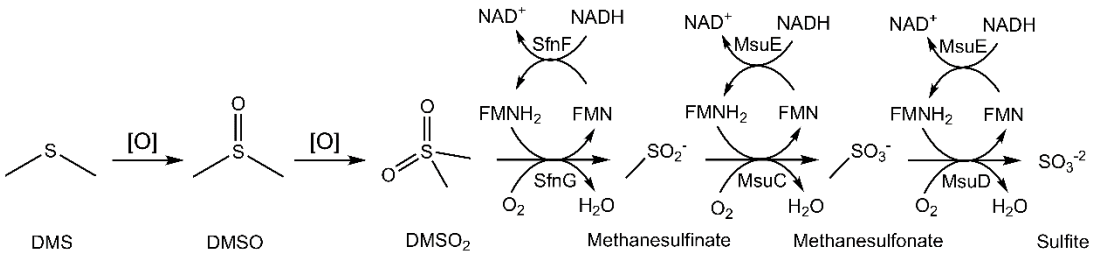

Figure 4.21. Proposed metabolic pathway of sulfite acquisition for DMS in *Pseudomonas putida*. Adapted from [64] and personal communication with D. Wicht.

4.7 Summary

Sulfur is a primary constituent of metabolically relevant small molecules and cofactors such as methionine and iron-sulfur clusters. Elemental sulfur is relatively low in abundance in the environment (~ 2%), and exists primarily as sulfate esters or organic sulfonates. Bacterial organisms require inorganic sulfite and cysteine for survival. Under sulfur limiting conditions bacteria possess the ability to encode for enzymes capable of scavenging inorganic sulfite from organosulfonate molecules. Two enzymes expressed during sulfur limiting conditions in E. coli, are a FMN-reductase (SsuE) and a monooxygenase (SsuD). Together, SsuE and SsuD comprise the FMN-dependent two-component monooxygenase systems that catabolizes C2 – C10 alkanesulfonates into inorganic sulfite and the corresponding aldehyde.

The FMN-dependent two-component systems are unlike most systems which utilize flavoproteins. SsuE and SsuD use flavin as their substrate, and the flavin is never covalently bound. Wild-type SsuE exists as a tetramer, but in the presence of FMN becomes a dimer. One unique structural feature of SsuE is the insertion of a tyrosine residue (Tyr118), which plays a key role in the formation of a π-helix. The hydroxyl group of Tyr118 hydrogen bonds across the tetramer

interface with the carboxyl-oxygen of Ala78. Additionally, the benzene ring of Tyr118 forms π-stacking interactions with adjacent Tyr118 residues. Mutational studies of Y118 concluded that both the π- helix and the π-π stacking interactions play important mechanistic roles in flavin transfer. In the reaction with SsuE, NADPH provides the enzyme with the electrons needed to reduce FMN to $FMNH_2$. The substrate binding order of SsuE follows an ordered sequential mechanism, with NADPH binding first followed by FMN. But, in the presence of SsuD and octanesulfonate, SsuE follows a rapid equilibrium ordered mechanism.

The monooxygenase SsuD employs reduced flavin, supplied from SsuE, to activate molecular oxygen, forming a C4a-(hydro)peroxyflavin intermediate capable of cleaving the carbon-sulfur bond in alkanesulfonates. Structurally SsuD exists as a tetramer, and is characterized by eight α-helices and eight parallel β-sheets that form the common TIM-barrel fold. Like most TIM-barrel proteins SsuD has a mobile loop region which acts as a gate, protecting reduced flavin from solvent exposure. The loop has been proposed to assist in the exchange of $FMNH_2$ by SsuE. Interestingly, SsuD only contains one cysteine residue (Cys54). Previous studies determined that the thiol group of Cys54 is important for stabilization of the reduced flavin intermediate.

Reduced flavin, and its catalytic intermediates, are reactive and can be easily oxidized. To prevent autooxidation the transfer of reduced flavin needs to be tightly controlled. Strong evidence has been provided that flavin transfer between SsuE and SsuD occurs through a channeling-type mechanism involving protein-protein interactions. Specific amino acid residues in SsuE and SsuD have been identified. Of the polar residues identified, SsuE contains the positively charged lysine residues, whereas SsuD contains the negatively charged amino acid residues, aspartate and glutamate. These oppositely charged residues most likely contribute to the static interactions that occur between the two proteins.

Additional FMN-dependent two-component systems capable of desulfonation have been identified in *Pseudomonas sp*.. Similar to *ssu*, when environmental sulfur sources are limiting *msu* and *sfn* genes encode for the expression of enzymes capable of foraging sulfite from alternative sources like dimethyl sulfoxide. Dimethyl sulfoxide ($DMSO_2$), is an oxidized form of dimethyl sulfide that is commonly found in the environment. The dimethyl sulfone monooxygenase (SfnG) uses reduced flavin to desulfonates $DMSO_2$ to methanesulfinate. Methanesulfinate undergoes oxidation to form methanesulfonate. Currently it is unclear whether this oxidation step occurs spontaneously or by enzymatic means. Regardless, methanesulfonate is then desulfonated by the $FMNH_2$-dependent methanesulfonate monooxygenase MsuD to produce sulfite. Both SfnG and MsuD require reduced flavin which is supplied by the NAD(P)H-dependent FMN-reductases SfnE and MsuE, respectively. A high degree of amino acid similarities exist between the this group of enzymes.

The remaining portion of the dissertation focuses on identifying and evaluating two-component enzymes in pseudomonads. Similar amino acid sequences and common functions between the enzymes suggest that protein-protein interactions may play a viable role in flavin transfer.

CHAPTER FIVE

Investigation of FMN-dependent Two-component Systems in *Pseudomonas aeruginosa* and *Pseudomonas putida*.

5.1 INTRODUCTION

Inorganic sulfur is an essential element for bacterial organisms. However, it is usually found in an inadequate supply in the environment in which bacteria live. Under sulfur limiting conditions bacterial organisms can express sulfur scavenging enzymes that allow the organism to acquire sulfur from alternative sources. In *E. coli*, the two-component alkanesulfonate system, comprised of a FMN-reductase (SsuE) and a monooxygenase (SsuD), are capable of desulfonating a wide range of C2 - C10 alkanesulfonates to produce inorganic sulfite and the corresponding aldehyde [6]. SsuE utilizes NADPH to reduce flavin to $FMNH_2$, which is then transferred to SsuD. Molecular oxygen is activated by $FMNH_2$-bound SsuD into a C4a-(hydro)peroxyflavin which cleaves the carbon-sulfur bond of the alkanesulfonate substrate, producing sulfite (**Figure 5.1**). Inorganic sulfite is further catabolized to sulfide, where it is incorporated into nucleosides, cofactors, and cysteine.

The mechanism of reduced flavin transfer can occur through free diffusion or through a channeling-type mechanism which requires protein-protein interactions. Due to the highly reactive

nature of reduced flavin in forming reactive oxygen species, flavin transfer through a channeling mechanism is thought to be favored [45].

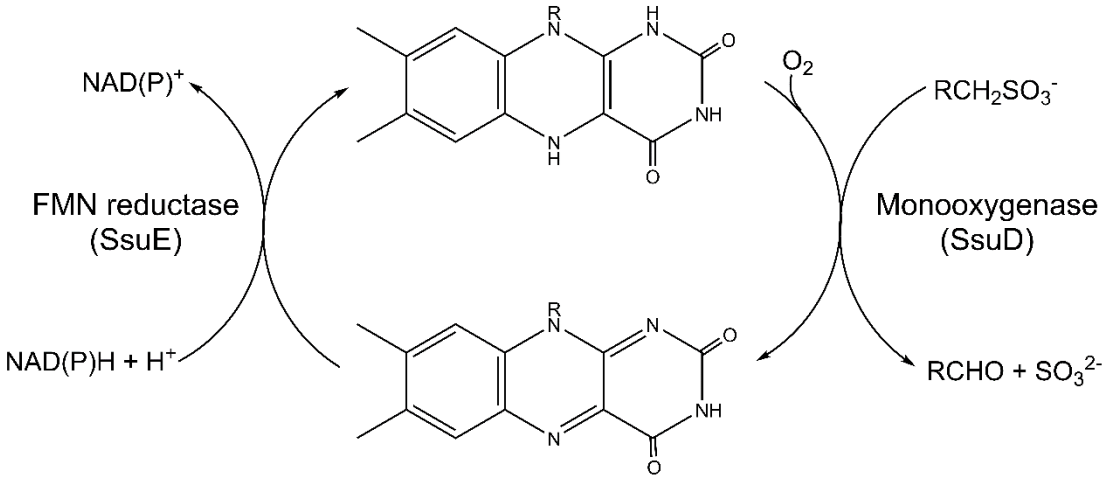

Figure 5.1. FMN-dependent two-component alkanesulfonate system reaction.

Static protein-protein interactions in the alkanesulfonate monooxygenase system have been identified through both chemical and spectroscopical methods [10, 45]. Recently, results from hydrogen-deuterium exchange mass spectrometry (HDX-MS) has identified the potential interaction sites between SsuE and SsuD [51]. Oppositely charged residues were present in the identified regions, which may form electrostatic interactions between the SsuE/SsuD protein complex.

The sulfate starvation induced (*ssi*) operon, containing the alkanesulfonate monooxygenase system, has also been identified in *Pseudomonas sp* [53, 54, 64, 65]. Interestingly, pseudomonads have additional genes that allow sulfite to be scavenged from molecules in the dimethyl sulfide (DMS) pathway. DMS originates as a byproduct generated by marine organisms. Through

evaporation and subsequent precipitation DMS is abundantly located in soil environments [55-60]. Autooxidation of DMS to dimethyl sulfoxide (DMSO) and dimethyl sulfone ($DMSO_2$) has been proposed to occur in the atmosphere.

The *msu* and *sfn* operons encode for the FMN-dependent two-component methanesulfonate and dimethyl sulfone monooxygenase systems, respectively [53, 54, 64]. Like the alkanesulfonate monooxygenase system, the *msu* and *sfn* pathways consist of a NAD(P)H dependent FMN-reductase and a corresponding monooxygenase. The proposed pathway in which Sfn and Msu enzymes scavenge sulfur from DMS is outlined in **Figure 5.2**. Given the structural similarity of Sfn and Msu to Ssu enzymes, they may also form protein-protein interaction. The primary objective of this study is to determine if any protein-protein interactions exist within the methanesulfonate and dimethyl sulfone monooxygenase systems in *Pseudomonas* species.

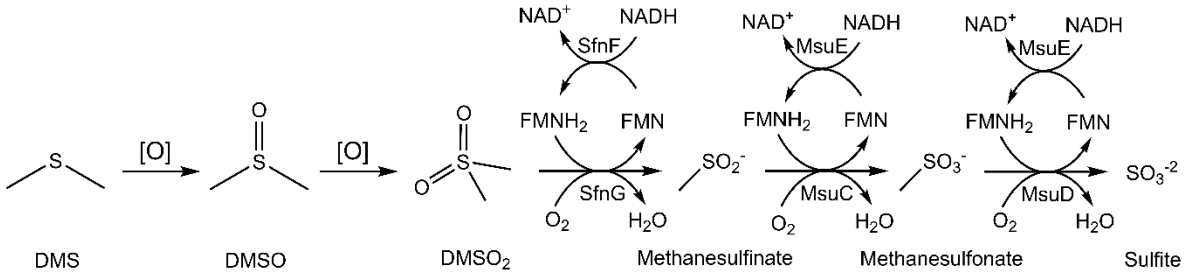

Figure 5.2. Proposed metabolic pathway of sulfite acquisition for DMS in *Pseudomonas sp*. Adapted from [64] and personal communication with D. Wicht.

5.2 METHODS AND MATERIALS

5.2.1 Materials

Potassium phosphate, dimethyl sulfoxide, β-nicotinamide adenine dinucleotide (NADH), β-nicotinamide adenine dinucleotide 2'-phosphate (NADPH), riboflavin 5'-monophosphate (FMN), Tris-HCl, octanesulfonate, DTNB, urea, ammonium sulfate, ampicillin, streptomycin sulfate, lysozyme, and brilliant blue R were purchased from Sigma (St. Louis, MO). Phenyl Sepharose 6 Fast Flow was purchased from GE Healthcare Life Sciences (Pittsburg, PA). Herculase II fusion polymerase was purchased from Agilent (Santa Clara, CA). T4 DNA ligase was purchased from New England BioLabs (Ipswich, MA). Isopropyl-β-D-thiogalactoside (IPTG) was purchased from Gold Biotechnology (St. Louis, MO). Glycerol and sodium chloride were purchased from Macron Fine Chemicals (Center Valley, PA). Difco-brand Luria-Bertani (LB) media was purchased from Becton, Dickinson and Company (Sparks, MD). Macro-Prep® High Q Support column media and size-exclusion gel filtration standard were purchased from Bio-Rad Laboratories (Hercules, CA). *Pseudomonas putida* strain KT2440 and *Pseudomonas putida* strain GB-1 was purchased from ATCC (Manassas, VA).

5.2.2 Construction of Two-component Genes in Pseudomonas sp.

Each gene was obtained from genomic DNA prepared directly from the *Pseudomonas* organism. All genes were PCR-amplified with Herculase II Fusion DNA polymerase using primers that included *Nde*I and *Xho*I restriction sites (**Table 5.1**). Ligation into the pET21a expression vector was performed with T4 DNA Ligase. Each resulting vector was transformed into *E. coli* XL-1 and BL21(DE3) expression cells. Plasmids were submitted for sequencing analysis at Eurofins Genomic. Cell cultures were stored as 50% glycerol stocks at – 80 °C.

Table 5.1: List of forward and reverse primers used to clone each gene.

	Organism	Forward (F) and Reverse (R) primers (5' to 3')
sfnF	*P. putida* KT2440	**F:** CGA GGG CAT ATG GTT CAA CAG CTT **R:** CTG TAA CTC GAG TCA GGC CGC
sfnG	*P. putida* KT2440	**F:** CA GGA GAC ATC CAT ATG AGC CAA CCG ATC AAA **R:** A TGG CCG CTC GAG TCA GGC CAC AGC G
ssuE	*P. aeruginosa* PAO1	**F:** GAT GAT CAT ATG CTC GTC GTT TCC **R:** GAT GAT CTC GAG TCA GAT GCT CCA
ssuD	*P. aeruginosa* PAO1	**F:** GAT GAT CAT ATG AGC CTC GAG **R:** GAT GAT CTC GAG TCA ACT CTG CGC
sfnG	*P. aeruginosa* PAO1	**F:** TA CCC CAT ATG AGC CAA GAG CAA C **R:** CGT CTC GAG TCA GGC CGC TTC
msuC	*P. aeruginosa* PAO1	**F:** G AAA CCC CAT ATG AAT GCG AAG AC **R:** TAT GGG TAG CTC GAG TCA TGA GTA G
sfnE	*P. putida* GB-1	**F:** GAT GAT CAT ATG GAG CAC CCC CAC TG **R:** GAT GAT CTC GAG TCA GGC GCT TTT

5.2.3 Expression and Purification of Two-component Enzymes in Pseudomonas sp.

All enzymes were expressed from the pET21a expression vector in *E. coli* strain BL21(DE3). One liter LB cultures were grown at 37 °C until the A_{600} value reached 0.6 – 0.8. At that time, a final concentration of 0.4 mM isopropyl-β-D-thiogalactoside (IPTG) was added and the incubation temperature was lowered to 18 °C for six hours. Cells were harvested by centrifugation at 5 000 rpm for 15 minutes at 4 °C. Cell pellets were then stored at – 80 °C overnight. Cell pellets were resuspended with 100 mL 25 mM potassium phosphate, pH 7.5, 10% glycerol with 0.02 mg/mL lysozyme in 10 mM Tris-Cl, pH 8.5. The resuspended cell mixture was lysed by sonication followed by centrifugation at 10 000 rpm, 4 °C for 15 min. Addition of 1.5% streptomycin sulfate (w/v) was added to the supernatant, and the solution was slowly stirred at 4 °C for 1 hour. The solution containing precipitated nucleic acids were centrifuged at 10 000 rpm at 4 °C for 20 min.

For the FMN-reductase enzymes, ammonium sulfate precipitation was from 20 - 45%. The resultant pellet was resuspended in 100 mL 25 mM potassium phosphate, pH 7.5, 10% glycerol, and 20% ammonium sulfate and loaded on a phenyl sepharose column. Protein was eluted from the column using a linear gradient from 20 – 0% ammonium sulfate in 25 mM potassium phosphate, pH 7.5, 10% glycerol. Fraction purity was determined by A_{280} values and SDS-PAGE (5% stacking with 12% resolving). Fractions determined to be of the highest purity were pooled and loaded onto a Macro-Prep High Q Support anion exchange column. Protein was eluted from the column using a linear gradient from 0 - 150 mM sodium chloride in 25 mM potassium phosphate, pH 7.5, 10% glycerol. Fraction purity was determined as described above, and pooled protein was dialyzed twice against one liter 25 mM potassium phosphate, pH 7.5, 10% glycerol, and 100 mM sodium chloride. Following dialysis, protein was centrifuged at 10 000 rpm, 4 °C for 15 minutes to remove any precipitated protein. Aliquots of the protein were flash frozen with liquid nitrogen, and stored at -80 °C.

The purification procedure for the monooxygenase enzymes was similar to purification of FMN-reductases, with minor modifications. Ammonium sulfate precipitation was from 30 – 60%. The pelleted protein was resuspended in 30 mL of 25 mM potassium phosphate, pH 7.5, 10% glycerol and dialyzed twice against one liter of 25 mM potassium phosphate, pH 7.5, 10% glycerol to equilibrate the buffer solution. After dialysis, protein was diluted with 100 mL 25 mM potassium phosphate, pH 7.5, 10% glycerol and loaded onto a Macro-Prep High Q Support anion exchange column. Protein was eluted from the column using a linear gradient from 0 - 150 mM sodium chloride in 25 mM potassium phosphate, pH 7.5, 10% glycerol. Fraction purity was determined based on A_{280} values and SDS-PAGE. Ammonium sulfate (20 %) was added to pooled protein and diluted with 100 mL 25 mM potassium phosphate, pH 7.5, 10% glycerol, 20% ammonium sulfate.

Protein was then loaded on a phenyl sepharose column, and eluted from the column using a linear gradient from 20 – 0% ammonium sulfate in 25 mM potassium phosphate, pH 7.5, 10% glycerol. Fraction purity was determined and pooled protein was dialyzed twice against one liter of 25 mM potassium phosphate, pH 7.5, 10% glycerol with 100 mM sodium chloride. Precipitated protein was removed by centrifugation and protein aliquots were flash frozen with liquid nitrogen and stored at – 80 °C.

In this study a total of ten enzymes, six FMN-reductases and four monooxygenases, were investigated from three species of *Pseudomonas*. For simplicity, each enzyme name, the organism in which they are found, their theoretical molecular weight as calculated by the amino acid sequence, and the in-text abbreviation that will be used are listed in **Table 5.2**.

Table 5.2: The ten enzymes evaluated in this study along with the organism they originated from, their theoretical molecular weight (MW), and the in-text abbreviation.

	Organism	Function	MW	Abbreviation
SsuE	*E. coli*	FMN-reductase	21,253 ± 1[a]	$SsuE_{Ec}$
SsuE	*P. put.*	FMN-reductase	21,570	$SsuE_{Pp}$
SsuE	*P. aer.*	FMN-reductase	21,517	$SsuE_{Pa}$
MsuE	*P. aer.*	FMN-reductase	20,028	$MsuE_{Pa}$
SfnE	*P. put.*	FMN-reductase	20,174	$SfnE_{PpG}$
SfnF	*P. put.*	FMN-reductase	25,504	$SfnF_{Pp}$
SsuD	*E. coli*	monooxygenase	41,605 ± 2[a]	$SsuD_{Ec}$
SsuD	*P. put.*	monooxygenase	41,506	$SsuD_{Pp}$
MsuD	*P. aer.*	monooxygenase	41,596	$MsuD_{Pa}$
SfnG	*P. put.*	monooxygenase	40,271	$SfnG_{Pp}$

[a]previously calculated based on mass spectrometry [10].

5.2.4 Circular Dichroism

Far-UV circular dichroism spectra were recorded on a JASCO J-810 spectropolarimeter. Spectra of all enzymes (5 μM) were taken in 0.1 nm increments in continuous scanning mode from 300 to 185 nm in a 0.1 cm cuvette with a bandwidth of 1 nm and scanning speed of 20 nm/min. Each spectra is an average of six scans. Background subtraction and smoothing of the data were performed using the software provided. Final data was plotted using KaleidaGraph™ software (Synergy Software, Reading, PA).

5.2.5 Fluorometric Titration of FMN-reductase Enzymes

Flavin binding to FMN-reductases was determined through spectrofluorometric titrations on a Cary Eclipse Agilent Fluorescence Spectrophotometer (Santa Clara, CA). A 1.0 mL solution containing 0.20 μM FMN in 25 mM potassium phosphate buffer 0.1 M sodium chloride, pH 7.5 was titrated with $SsuE_{Pp}$ (0.08 – 1.2 μM) or $MsuE_{Pa}$ (0.2 – 3.5 μM). A decrease in the relative intensity of the FMN spectra was monitored from 470 – 650 nm, with a λ_{max} = 526 nm, and excitation wavelength of 450 nm. The K_d values for FMN binding was determined as previously described [45].

5.2.6 Steady-state Kinetic Analyses

Kinetic parameters for each FMN-reductase were determined by monitoring a decrease in absorbance at 340 nm due to the oxidation of NAD(P)H to $NAD(P)^+$. Each reaction was initiated by the addition of 0.04 μM enzyme (0.1 μM for $SsuE_{Pp}$) to a cuvette containing FMN and NAD(P)H in 25 mM Tris-HCl, 0.1 M sodium chloride, pH 7.5 at 25 °C. Reactions where FMN was varied, NAD(P)H was held constant at 200 μM with an FMN range of 0.5 – 20 μM for $SfnE_{PpG}$, 0.1 – 3 μM FMN for $SsuE_{Ec}$, and 1 – 30 μM FMN for $SsuE_{Pp}$ or $MsuE_{Pa}$. For assays where

NAD(P)H was varied, FMN was held constant at 2 μM for $SsuE_{Ec}$ or $SfnE_{PpG}$ and 20 μM for $SsuE_{Pp}$ or $MsuE_{Pa}$ with an NAD(P)H range of 10 – 250 μM for all enzymes.

Kinetic parameters for each monooxygenase were determined by measuring the production of sulfite. Sulfite was reacted with DTNB to form the TNB anion which can be spectrophotometrically determined at 412 nm ($\varepsilon = 12,000\ M^{-1}cm^{-1}$). Each reaction was performed with 0.2 μM monooxygenase enzyme into a solution of 10 – 1000 μM octanesulfonate (or 10 – 500 μM methanesulfonate for $MsuD_{Pa}$) in 25 mM Tris-HCl, 0.1 M sodium chloride, pH 7.5 for a total reaction volume of 500 μL. For reactions with $SsuD_{Ec}$ and $MsuD_{Pa}$, flavin reductase enzymes were supplied in a 3:1 excess at 0.6 μM; for reactions with $SsuD_{Pp}$, flavin reductase enzymes were supplied in a 1:1 ratio at 0.2 μM. The concentration of FMN in each reaction depended on the concentration of the FMN-reductase. For $SsuE_{Ec}$ each reaction contained a final concentration of 2 μM, and reactions with $SsuE_{Pp}$ and $MsuE_{Pa}$ contained a final concentration of 10 μM FMN. All reactions were initiated with the addition of 500 μM NAD(P)H and proceeded for 3 minutes at 25 °C, and were quenched with 167 μL 8 M urea. A final concentration of 1 mM DTNB was added to each reaction and was allowed to develop for 1 – 3 minutes prior to being measured.

5.2.7 Rapid reaction Kinetic Analyses

Single-turnover experiments were performed on an Applied Photophysics SX.18 MV stopped-flow spectrophotometer by monitoring flavin reduction and subsequent oxidation as a change in absorbance at 450 nm over 100 seconds. Each experiment was performed in single-mixing mode by reacting equal volumes of solution from each syringe. The reaction was initiated by mixing 35 μM $SsuE_{Pp}$, 35 μM $SsuD_{Pp}$, with 30 μM FMN in 50 mM potassium phosphate, 10% glycerol, pH 7.5 against 50 μM octanesulfonate, 250 μM NADPH in 10 mM Tris-HCl. 0.1 M sodium chloride, pH 8.5 at 4 °C. Control experiments were performed as described above to

measure the reduction of flavin in the absence of SsuD$_{Pp}$. Kinetic traces were normalized and plotted as a log-log scale in Kaleidagraph software.

5.3 RESULTS

5.3.1 Determination of Genes in Pseudomonas sp.

Identification of FMN-reductase and monooxygenase genes in *Pseudomonas* species were determined by comparison of percent amino acid sequence identity to previously determined *ssu*, *sfn,* and *msu* genes from *E. coli* strain K12, *P. aeruginosa* strain PAO1, and *P. fluorescence* strain Pf0-1 [3, 64-66, 68]. The percent amino acid identity and similarity for identified FMN-reductase and monooxygenase enzymes as compared to $SsuE_{Ec}$ and $SsuD_{Ec}$ are listed in **Table 5.3** and **Table 5.4**. The gene numbers listed correspond to the notation used with the Pseudomonas Genome Database (www.pseudomonas.com) [70]. For simplicity, genes currently and previously identified in *Pseudomonas* species are listed in **Table 5.5**.

In *Pseudomonas putida* strain KT2440, two *sfn* operons were identified. The first operon contains the NAD(P)H-dependent FMN-reductase SfnF (PP_2764), and its partner dimethylsulfone monooxygenase SfnG (PP_2765). The second *sfn* operon contains the σ-54 dependent transcriptional regulator SfnR (PP_2771), a proposed monooxygenase SfnC (PP_2772), and its FMN-reductase partner SfnE (PP_2773). Currently in the Pseudomonas Genome Database, SfnF (PP_2764) and SfnG (PP_2765) are misannotated as MsuE and MsuD [70]. However, amino acid sequence identity comparison shows that PP_2765 is 80% identical to SfnG *P. flu*, and only 29% identical to MsuD *P. flu*. Additionally, the gene directly upstream from the misannotated genes is identified as the acyl-CoA dehydrogenase SfnA (PP_2762).

Table 5.3: Percent identity and similarity of FMN-reductases compared to $SsuE_{Ec}$

	% identity	% similarity
$SsuE_{Pa}$	57	69
$SsuE_{Pp}$	57	70
$MsuE_{Pa}$	28	48
$SfnE_{PpG}$	31	46
$SfnF_{Pp}$	31	38

Table 5.4: Percent identity and similarity of monooxygenase enzymes compared to $SsuD_{Ec}$.

	% identity	% similarity
$SsuD_{Pa}$	78	88
$SsuD_{Pp}$	79	88
$MsuD_{Pa}$	67	76
$SfnG_{Pp}$	28	45

Table 5.5: *ssu*, *sfn*, and *msu* genes identified in *Pseudomonas sp*. Genes in bold were identified in this study.

	P. put. KT2440	*P. put.* GB-1	*P. aer.* PAO1	*P. flu* Pf0-1
ssuE	0236	**0260**	3446	5415
ssuD	0238	**0262**	3444	5413
sfnF	**2764**	---	---	---
sfnG	**2765**	**1798**	**3954**	2879
sfnE	**2773**	**2164**	---	---
sfnC	**2772**	**2163**	---	---
sfnR	**2771**	**2162**	2354	---
msuC	---	---	2355	3917
msuD	---	---	2356	3916
msuE	---	---	2357	3915

In *Pseudomonas putida* strain GB-1, the *ssu* operon contains the FMN-reductase SsuE (PputGB1_0260) and an alkanesulfonate monooxygenase SsuD (PputGB1_0262), as well as SsuA, SsuB, SsuC, and SsuF. The *sfn* operon, *sfnECR*, contains a FMN-reductase SfnE (PputGB1_2164), an acyl-CoA dehydrogenase SfnC (PputGB1_2163), and a σ-54 dependent transcriptional regulator SfnR (PputGB1_2162). Interestingly, the dimethylsulfone monooxygenase SfnG (PputGB1_1798) exists as a single gene with the absence of *sfnABF*. Similarly, *Pseudomonas aeruginosa* strain PAO1 also lacked the *sfnABF* and *sfnECR* genes, and only contains dimethylsulfone monooxygenase SfnG (PA3954).

5.3.2 Purification and Determination of Secondary Structures

Following purification, the apparent molecular weight and purity of each enzyme was determined by SDS-PAGE (**Figure 5.3**). Each apparent molecular corresponded to the theoretical molecular weight as determined by the amino acid sequence. The $SfnF_{Pp}$ enzyme was soluble following purification (**Figure 5.3 C**). However, despite multiple attempts under diverse conditions, purification of $SfnF_{Pp}$ was unsuccessful. Additionally, far-UV circular dichroism spectra of FMN-reductases and monooxygenases were compared to determine the overall gross secondary structure. The FMN-reductases had similar overall gross secondary structures as compared to $SsuE_{Ec}$ (data not shown). Similarly, the monooxygenase enzymes had comparable gross secondary structures to $SsuD_{Ec}$ (**Figure 5.4**).

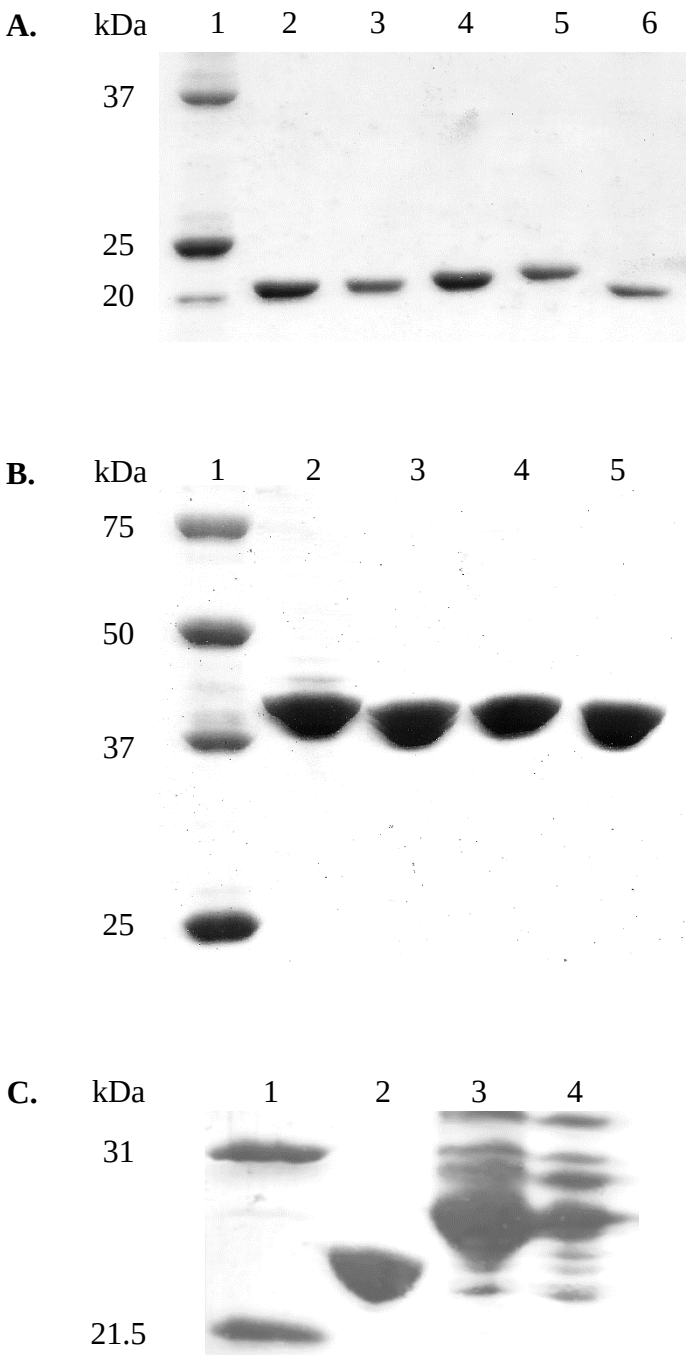

Figure 5.3. SDS-PAGE of purified enzymes involved in desulfonation in *E. coli* and *Pseudomonas sp*. **A.** FMN-reductase enzyme (1) Molecular weight marker, (2) $SsuE_{Ec}$, (3) $SsuE_{Pp}$, (4) $SsuE_{Pa}$, (5) $MsuE_{Pa}$, (6) $SfnE_{PpG}$, and **B.** Monooxygenase enzymes (1) Molecular weight marker, (2) $SsuD_{Ec}$, (3) $SsuD_{Pp}$, (4) $MsuD_{Pa}$, (5) $SfnG_{Pp}$. **C.** Expression of SfnF (1) Molecular weight marker, (2) wild-type $SsuE_{Ec}$, (3) $SfnF_{Pp}$ cell lysate (4) $SfnF_{Pp}$ cell free extract.

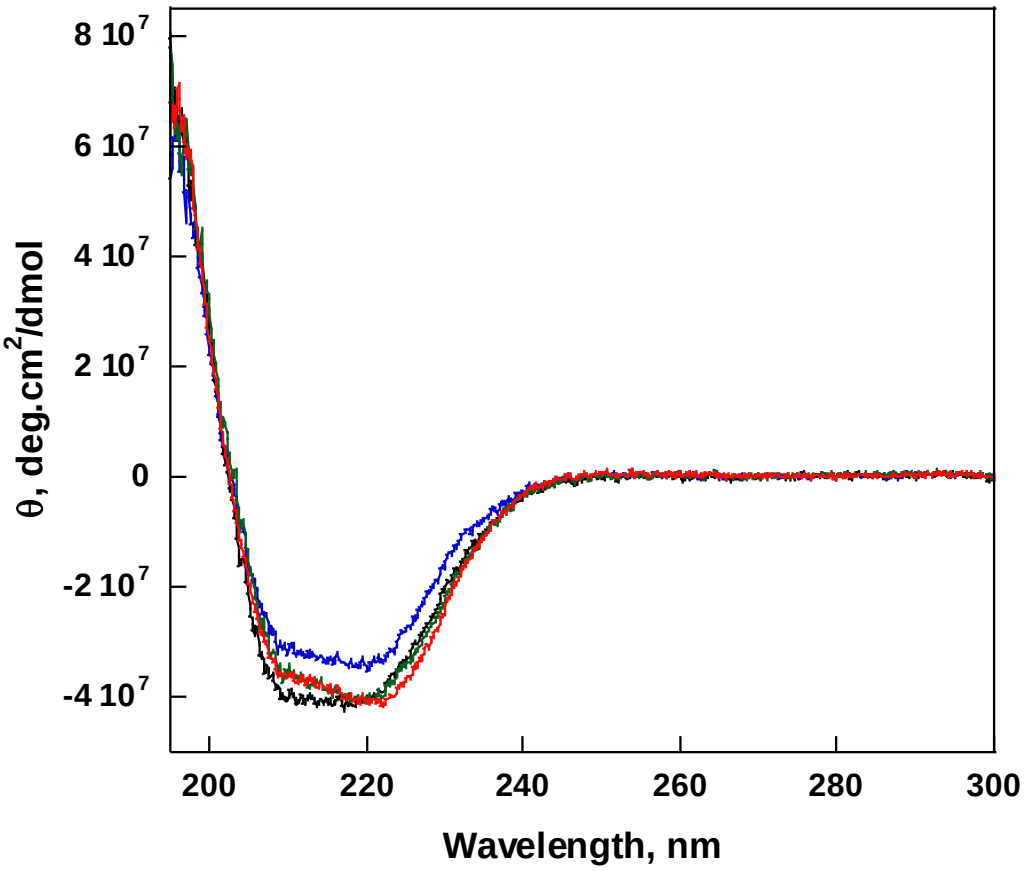

Figure 5.4. Circular dichroism spectra of SsuD$_{Ec}$ (black), SsuD$_{Pp}$ (blue), MsuD$_{Pa}$ (green), and SfnG$_{Pp}$ (red). Spectra were taken with 5 μM protein in 10 mM potassium phosphate, pH 7.5.

5.3.3 Flavin affinity and FMN binding

Flavin affinity and binding stoichiometry of each FMN-reductase for oxidized FMN was determined by fluorescence spectroscopy. A decrease in the absorbance of FMN at 526 nm can be observed when FMN binds to the reductase enzyme (**Figure 5.5**). The concentration of FMN bound-enzyme was plotted against total enzyme concentration to obtain a dissociation constant (K_d) for each FMN-reductase (**Figure 5.6** and **Table 5.6**). SsuE$_{Ec}$ had the lowest K_d value of 0.015 ± 0.004 μM, and SsuE$_{Pp}$ and MsuE$_{Pa}$ were one to two orders of magnitude higher with K_d values of 0.18 ± 0.01 μM and 2.0 ± 0.2 μM, respectively. A 1:1 ratio of enzyme to FMN was determined for SsuE$_{Ec}$ and SsuE$_{Pp}$, whereas MsuE$_{Pa}$ had a 1:1.7 enzyme to FMN ratio.

Table 5.6: Flavin binding in *E. coli* and *Pseudomonas sp.*

	K_d (μM)	FMN Binding (Enzyme:FMN)
SsuE$_{Ec}$ [a]	0.015 ± 0.004	1:1
SsuE$_{Pp}$	0.18 ± 0.01	1:1
MsuE$_{Pa}$.	2.0 ± 0.2	1:1.7

[a]previously reported [10].

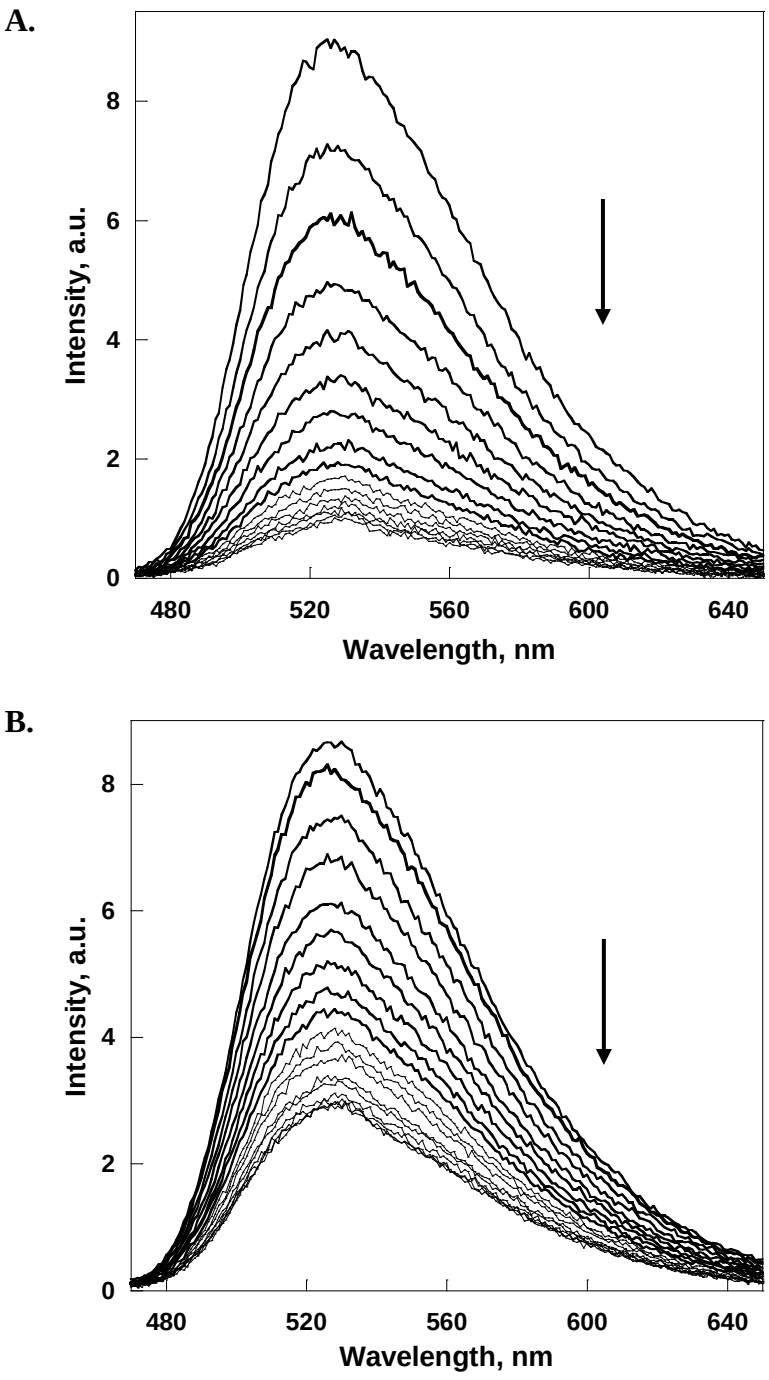

Figure 5.5. Fluorometric titration of FMN with a decrease in the relative signal intensity upon the addition of **A.** SsuE$_{Pp}$ and **B.** MsuE$_{Pa}$.

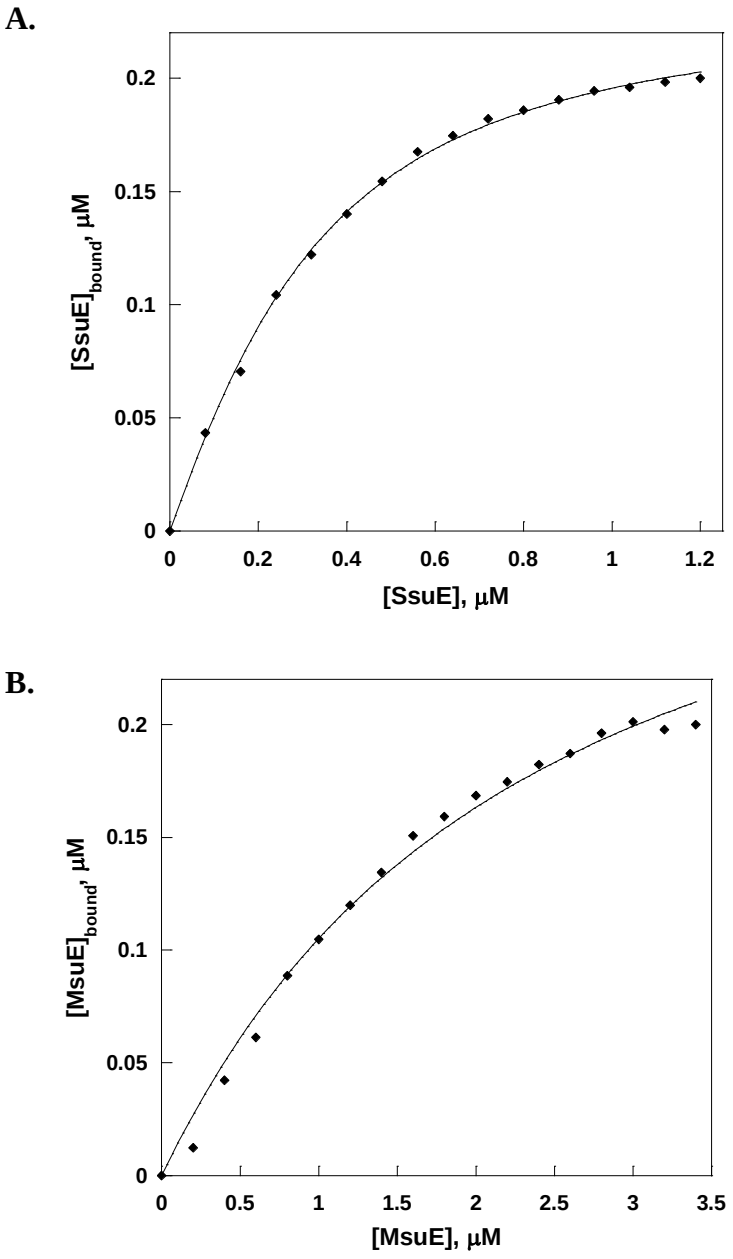

Figure 5.6. Fluorometric data of FMN-bound enzyme (**A**) SsuE$_{Pp}$ and (**B**) MsuE$_{Pa}$. Concentration of FMN-bound enzyme was plotted against the concentration of total enzyme and fit to the binding equation from [45].

5.3.4 Steady-state Kinetics of FMN-reductases

FMN-reductase assays were performed to determine the steady-state kinetic parameters for each enzyme. Since $FMNH_2$ is susceptible to auto-oxidation, flavin reduction was measured by monitoring the oxidation of NAD(P)H. Overall, it was found that NADPH was the preferred pyrimidinic substrate for SsuE$_{Ec}$ and SsuE$_{Pp}$, whereas NADH was the preferred substrate for MsuE$_{Pa}$ (**Table 5.7**). The SsuE$_{Pa}$ enzyme had no observable oxidase activity with NADPH or NADH in the presence of FMN or FAD.

Table 5.7: Steady-state kinetic parameters for MsuE$_{Pa}$ with NADH and NADPH.

	k_{cat} (min^{-1})	K_m (μM)	k_{cat}/K_m (μM^{-1} min^{-1})
NADH	409 ± 20	29 ± 5	14 ± 3
NADPH	94 ± 12	129 ± 34	0.7 ± 0.2

Under varied concentrations of FMN and fixed concentration of NAD(P)H, SsuE$_{Pp}$ has a ~ 5-fold decrease in turnover, with a k_{cat} (127 ± 4 min^{-1}) compared to SsuE$_{Ec}$ (516 ± 26 min^{-1}), SfnE$_{PpG}$ (787 ± 25 min^{-1}), and MsuE$_{Pa}$ (608 ± 39 min^{-1}). Additionally, SsuE$_{Pp}$ and MsuE$_{Pa}$ have an overall 10-fold decrease in catalytical efficiency with k_{cat}/K_{FMN} values of 102 ± 21 μM^{-1} min^{-1} and 96 ± 20 μM^{-1} min^{-1}, respectfully, as compared to k_{cat}/K_{FMN} values of 1326 ± 255 μM^{-1} min^{-1} and 1187 ± 181 μM^{-1} min^{-1} for SsuE$_{Ec}$ and SfnE$_{PpG}$ (**Table 5.8**). When the concentration of FMN was fixed and NAD(P)H was varied SsuE$_{Pp}$ had a 10-fold decrease in activity with a k_{cat}/K_{NADPH} value of 1.0 ± 0.5 μM^{-1} min^{-1} compared to 12 ± 2 μM^{-1} min^{-1}, 14 ± 3 μM^{-1} min^{-1}, and 12 ± 1 μM^{-1} min^{-1} for SsuE$_{Ec}$, MsuE$_{Pa}$, and SfnE$_{PpG}$, respectfully (**Table 5.9**).

Table 5.8: FMN steady-state kinetic parameters for FMN-reductases found in *E. coli* and *Pseudomonas sp*.

	k_{cat} (min^{-1})	K_{FMN} (μM)	k_{cat}/K_{FMN} (μM^{-1} min^{-1})
$SsuE_{Ec}$	516 ± 26	0.39 ± 0.07	1326 ± 255
$SsuE_{Pp}$	127 ± 4	1.3 ± 0.3	102 ± 21
$MsuE_{Pa}$	608 ± 39	6.3 ± 1.2	96 ± 20
$SfnE_{PpG}$	787 ± 25	0.7 ± 0.1	1187 ± 181
$SsuE_{Pa}$	---	---	---

Table 5.9: NAD(P)H steady-state kinetic parameters for FMN-reductases found in *E. coli* and *Pseudomonas sp*.

	k_{cat} (min^{-1})	$K_{NAD(P)H}$ (μM)	$k_{cat}/K_{NAD(P)H}$ (μM^{-1} min^{-1})
$SsuE_{Ec}$	670 ± 46	58 ± 12	12 ± 2
$SsuE_{Pp}$	491 ± 130	476 ± 172	1.0 ± 0.5
$MsuE_{Pa}$	409 ± 20	29 ± 5	14 ± 3
$SfnE_{PpG}$	767 ± 24	62 ± 6	12 ± 1
$SsuE_{Pa}$	---	---	---

5.3.5 Steady-state Kinetics of Monooxygenase Enzymes

Steady-state kinetic analyses were performed with $SsuD_{Ec}$, $SsuD_{Pp}$, and $MsuD_{Pa}$ in the presence of a FMN-reductase to determine if reduced flavin could be transferred to the monooxygenase partner. The steady-state kinetic parameters for each monooxygenase were determined by measuring the amount of TNB anion formed from the reaction of DTNB with the sulfite product produced by the monooxygenase. For reactions with $SsuD_{Ec}$, optimal sulfite production was determined with each FMN-reductase present in a 3:1 FMN-reductase/monooxygenase ratio to ensure $FMNH_2$ was saturating. Kinetic parameters for $SsuD_{Ec}$ in the presence of $SsuE_{Ec}$, $SsuE_{Pp}$, $MsuE_{Pa}$, and $SfnE_{PpG}$ were all comparable to each other (**Table 5.10**). Similar to results from NAD(P)H oxidase assays, $SsuE_{Pa}$ was unable to produce and transfer reduced flavin to $SsuD_{Ec}$.

Table 5.10: Steady-state kinetic parameters for $SsuD_{Ec}$ with FMN-reductases.

	k_{cat} (min^{-1})	K_m (μM)	k_{cat}/K_m (μM^{-1} min^{-1})
$SsuE_{Ec}$	34 ± 1	35 ± 4	1.0 ± 0.1
$SsuE_{Pp}$	34 ± 1	25 ± 3	1.4 ± 0.2
$MsuE_{Pa}$	54 ± 1	41 ± 4	1.3 ± 0.1
$SfnE_{PpG}$	35 ± 1	29 ± 2	1.2 ± 0.1
$SsuE_{Pa}$	---	---	---

When coupled with $MsuE_{Pa}$ and $SfnE_{PpG}$ in the presence of the NADPH , $SsuD_{Ec}$ displayed a two-fold increase in sulfite production with k_{cat}/K_m values of 1.3 ± 0.1 μM^{-1} min^{-1} with $MsuE_{Pa}$ and 1.2 ± 0.1 μM^{-1} min^{-1} with $SfnE_{PpG}$ as compared to the preferred oxidase substrate NADH, with values of 0.6 ± 0.1 μM^{-1} min^{-1} and 0.56 ± 0.06 μM^{-1} min^{-1}, respectively (**Table 5.11**).

Table 5.11: Steady-state kinetic parameters for $SsuD_{Ec}$ with $MsuE_{Pa}$ and $SfnE_{PpG}$.

	k_{cat} (min^{-1})	K_m (μM)	k_{cat}/K_m (μM^{-1} min^{-1})
$MsuE_{Pa}$ (NADH)	35 ± 1	55 ± 8	0.6 ± 0.1
$MsuE_{Pa}$ (NADPH)	54 ± 1	41 ± 4	1.3 ± 0.1
$SfnE_{PpG}$ (NADH)	33 ± 1	60 ± 7	0.56 ± 0.06
$SfnE_{PpG}$ (NADPH)	35 ± 1	29 ± 2	1.2 ± 0.1

Alternatively, optimal sulfite production in reactions with $SsuD_{Pp}$ occurred at a a 1:1 FMN-reductase/$SsuD_{Pp}$ ratio. A decline in kinetic activity was seen with an increased FMN-reductase/$SsuD_{Pp}$ ratio. Kinetic values for $SsuD_{Pp}$ in the presence of $SsuE_{Ec}$, $SsuE_{Pp}$, and $MsuE_{Pa}$ were all comparable to each other with k_{cat}/K_m values of $0.4 \pm 0.1\ \mu M^{-1}\ min^{-1}$, $0.6 \pm 0.1\ \mu M^{-1}\ min^{-1}$, and $0.3 \pm 0.1\ \mu M^{-1}\ min^{-1}$, respectively (**Table 5.12**).

Table 5.12: Steady-state kinetic parameters for $SsuD_{Pp}$ with FMN-reductases.

	k_{cat} (min^{-1})	K_m (μM)	k_{cat}/K_m (μM^{-1} min^{-1})
$SsuE_{Ec}$	12.3 ± 0.6	30 ± 7	0.4 ± 0.1
$SsuE_{Pp}$	14.9 ± 0.3	26 ± 3	0.6 ± 0.1
$MsuE_{Pa}$ (NADPH)	9.4 ± 0.6	27 ± 8	0.3 ± 0.1

When sulfite production of $MsuD_{Pa}$ was coupled with its FMN-reductase counterpart, $MsuE_{Pa}$, $MsuD_{Pa}$ displayed a 5-fold increase in sulfite production with a k_{cat}/K_m value of $0.5 \pm 0.1\ \mu M^{-1}\ min^{-1}$ with NADPH as compared a k_{cat}/K_m value of $0.11 \pm 0.01\ \mu M^{-1}\ min^{-1}$ with the preferred oxidase substrate NADH (**Table 5.13**).

Table 5.13: Steady-state kinetic parameters for $MsuD_{Pa}$ with $MsuE_{Pa}$.

	k_{cat} (min^{-1})	K_m (μM)	k_{cat}/K_m (μM^{-1} min^{-1})
NADH	4.3 ± 0.1	38 ± 4	0.11 ± 0.01
NADPH	17 ± 1	31 ± 10	0.5 ± 0.1

5.3.6 $MsuE_{Pa}$ NAD(P)H Oxidase Assay in the Presence of $MsuD_{Pa}$

NADPH oxidase assays with $MsuE_{Pa}$ were revisited to determine why $MsuE_{Pa}$ transfers flavin more efficiently to $MsuD_{Pa}$ in the presence of NADPH, rather than the preferred substrate NADH. $MsuE_{Pa}$ and $MsuD_{Pa}$ were titrated into a cuvette containing excess FMN and varying amounts of NAD(P)H. Overall $MsuE_{Pa}/MsuD_{Pa}$ with NADH and NADPH have a similar catalytic efficiency with k_{cat}/K_m values of 318 ± 57 μM^{-1} min^{-1} and 238 ± 21 μM^{-1} min^{-1}, respectively (**Table 5.14**). However, the k_{cat} value for NADH (1348 ± 68 min^{-1}) is 7-fold higher than the k_{cat} value for NADPH (188 ± 4 min^{-1}). Additionally, the K_m value of 0.79 ± 0.07 μM for NADPH is 5-fold lower than the K_m value of 4.24 ± 0.72 μM for the preferred substrate NADH.

Table 5.14: Steady-state kinetic parameters for $MsuE_{Pa}$ coupled with $MsuD_{Pa}$ with NADH and NADPH.

	k_{cat} (min^{-1})	K_m (μM)	k_{cat}/K_m (μM^{-1} min^{-1})
NADH	1348 ± 68	4.24 ± 0.72	318 ± 57
NADPH	188 ± 4	0.79 ± 0.07	238 ± 21

5.3.7 Y118A $SsuE_{Ec}$ Coupled Kinetics with $SsuD_{Pp}$

It has been previously determined that the $SsuE_{Ec}$ variant Y118A can reduce FMN to $FMNH_2$, but is unable to transfer $FMNH_2$ to its monooxygenase counterpart. Therefore, Y118A $SsuE_{Ec}$, has been instrumental in determining protein-protein interaction between $SsuE_{Ec}$ and $SsuD_{Ec}$. It has been shown that wild-type and Y118A $SsuE_{Ec}$ compete for protein-protein interaction sites on wild-type $SsuD_{Ec}$. When concentrations of Y118A $SsuE_{Ec}$ are increased in the presence of $SsuE_{Ec}$ and $SsuD_{Ec}$, overall sulfite production decreases due to the competition of interaction sites with $SsuD_{Ec}$. In order to investigate if protein-protein interaction occur between $SsuE_{Pp}$ and $SsuD_{Pp}$, Y118A $SsuE_{Ec}$ was incubated in the reaction mixtures. There was no measurable sulfite production in the reaction containing only Y118A $SsuE_{Ec}$ and $SsuD_{Pp}$ (**Figure 5.7 A**). The reaction mixture containing $SsuE_{Pp}$ and $SsuD_{Pp}$, along with increasing concentrations of Y118A $SsuE_{Ec}$, showed consistent sulfite production, meaning Y118A SsuE does not protein-protein interact (**Figure 5.7 B**).

5.3.8 Rapid reactions Kinetics with $SsuE_{Pp}$ and $SsuD_{Pp}$

To further evaluate possible protein-protein interactions between $SsuE_{Pp}$ and $SsuD_{Pp}$ rapid reaction kinetics were employed. If protein-protein interactions occur there should be a noticeable lag in the spectra for $SsuD_{Pp}$ oxidation of $FMNH_2$ as compared to auto-oxidation of $FMNH_2$. When compared to the reduction of FMN by $SsuE_{Ec}$, $SsuE_{Pp}$ displayed a similar spectra for flavin reduction with a longer delay time for flavin reduction (**Figure 5.8 A**). Overlay of the reduction of FMN by $SsuE_{Pp}$ compared to the reduction of FMN by $SsuE_{Pp}$ in the presence of $SsuD_{Pp}$ showed no discernable lag phase associated with protein-protein interactions (**Figure 5.8 B**).

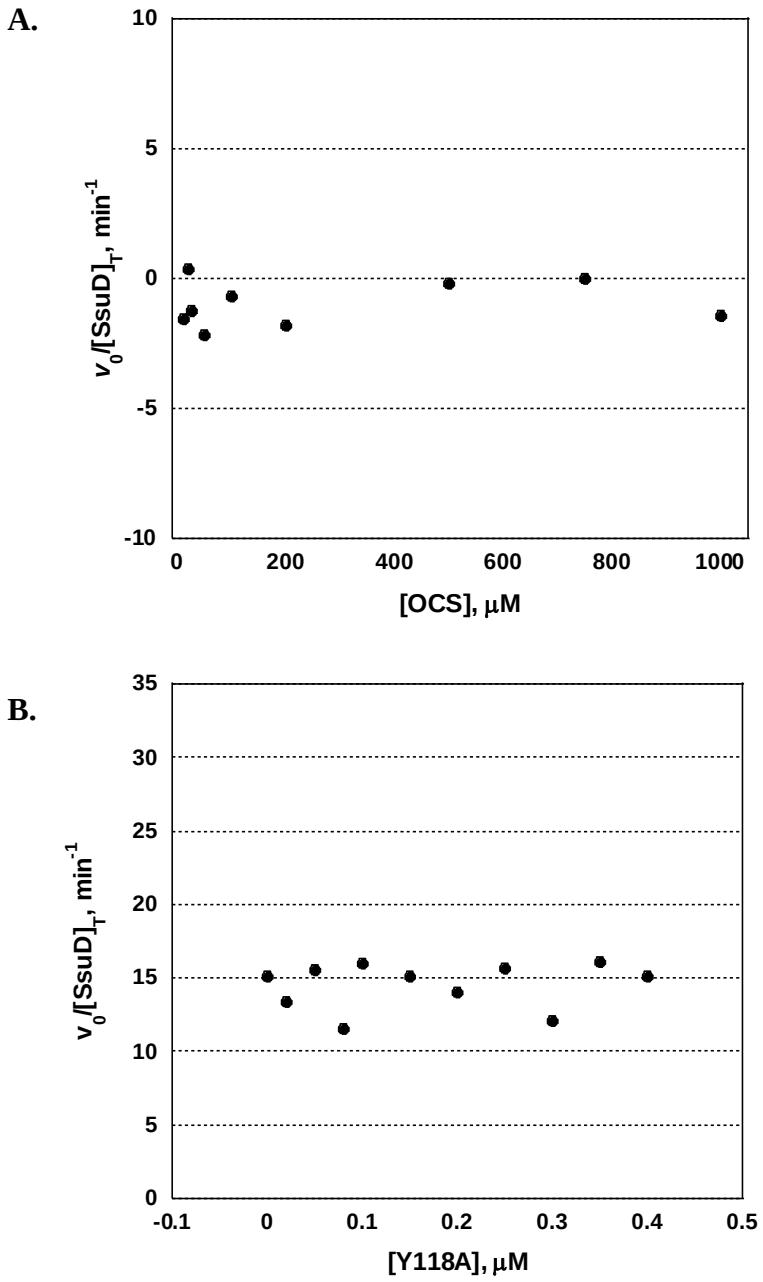

Figure 5.7. Competition assays with Y118A SsuE$_{Ec}$. **A.** Sulfite production from reaction with Y118A SsuE$_{Ec}$ and SsuD$_{Pp}$. **B.** Sulfite production from reaction with SsuE$_{Pp}$ and SsuD$_{Pp}$ with increasing concentrations of Y118A SsuE$_{Ec}$.

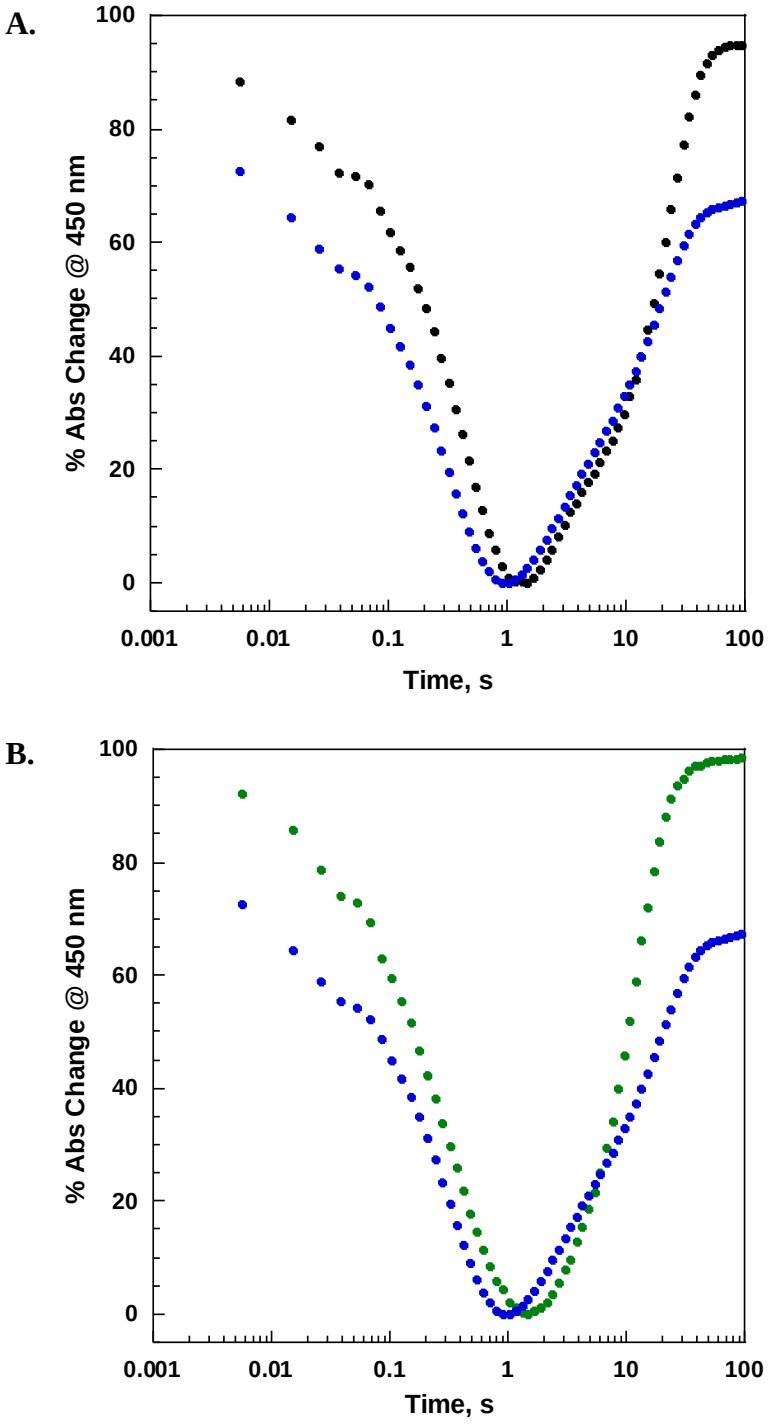

Figure 5.8. Rapid reaction kinetics monitoring the reduction of FMN to $FMNH_2$ with **A.** $SsuE_{Ec}$ (black trace) and $SsuE_{Pp}$ (blue trace) and **B.** $SsuE_{Pp}$ (blue trace) with $SsuD_{Pp}$ (green trace).

5.4 DISCUSSION

Several *ssi* NAD(P)H dependent two-component systems have been identified in *Pseudomonas putida* and *Pseudomonas aeruginosa*. Bacteria that possess the *sfn* and *msu* operons are able to acquire sulfite from methanesulfonate. The *msu* and *sfn* genes were identified based on amino acid sequence comparison (28 – 79% identity) with the FMN-reductase (SsuE) and the alkanesulfonate monooxygenase (SsuD) from *E. coli*. $SsuE_{Ec}$ and $SsuD_{Ec}$ have to been shown to transfer reduced flavin through protein-protein interactions [15, 36, 45, 51]. Recently, specific amino acid interaction sites have been identified within the two enzymes [51]. $SsuE_{Ec}$ contains two distinct interaction sites composed of 22 amino acids, four of which are positively charged. $SsuD_{Ec}$ also has two distinct interaction site of 22 amino acids. However, the six polar amino acids in $SsuD_{Ec}$ are negatively charged. Oppositely charged amino acid residues in $SsuE_{Ec}$ and $SsuD_{Ec}$ promote an environment for electrostatic interactions to occur. Amino acid sequence alignment of the interaction sites of $SsuE_{Ec}$ and $SsuD_{Ec}$ were compared to Msu and Sfn enzymes (**Figure 5.9**). Comparison shows the FMN-reductase and monooxygenase enzymes have similarly charged residues suggesting that protein-protein interactions could occur between these enzymes as well.

With the exception of $SsuE_{Pa}$ and $SfnF_{Pp}$ all purified FMN-reductases were capable of flavin reduction and transfer. There are no observable changes in the overall gross secondary structure of $SsuE_{Pa}$ compared to the other FMN-reductases, so it is currently unclear why flavin reduction is not supported. Additionally, a cell free extract of $SfnF_{Pp}$ was unable to support flavin reduction and transfer to $SsuD_{Pp}$ (data not shown). The inability of $SfnF_{Pp}$ to reduce flavin is not uncommon. In a previous study, SfnF from *Pseudomonas putida* strain DS1, was unable to support flavin reduction and transfer to SfnG [68].

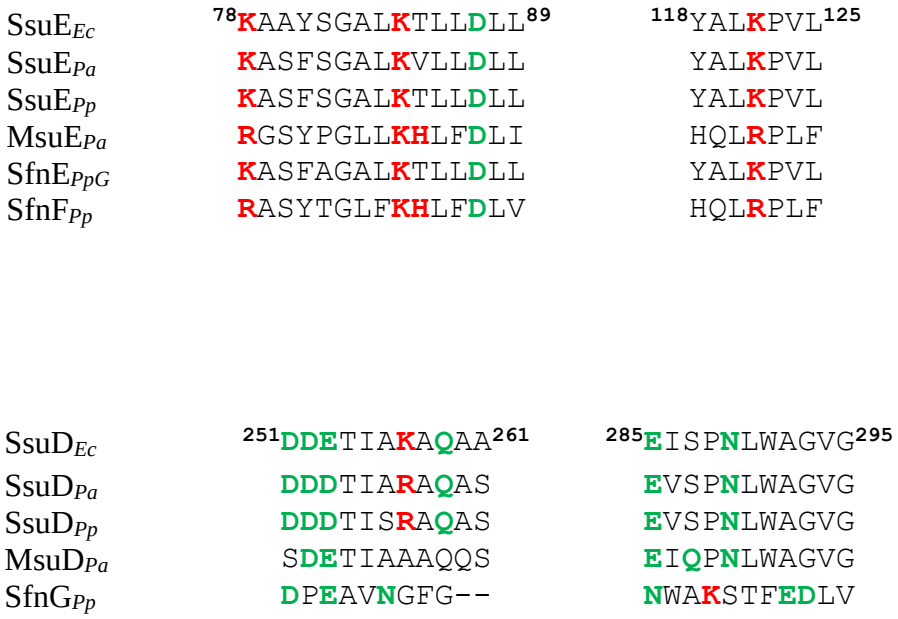

Figure 5.9. Amino acid sequence comparison of the SsuE$_{Ec}$ and SsuD$_{Ec}$ interaction sites with FMN-reductases and monooxygenases found in *Pseudomonas sp*. Red = positively charged amino acids and green = negatively charged amino acids.

Previous results have shown that SsuE$_{Ec}$ can utilize either NADH or NADPH to reduce flavin, with preference to NADPH [9]. Results from this study show SsuE$_{Pp}$ appears to be specific to NADPH, whereas SfnE$_{PpG}$ can utilize either NADPH or NADH, with a preference for the latter. Steady-state kinetic assays, where NADH was varied, yielded a 10-fold decrease in catalytic efficiency for SsuE$_{Pp}$ compared to the other FMN-reductase enzymes. Similarly, there was a 12-fold increase in the flavin binding affinity for SsuE$_{Pp}$ and a > 130-fold increase with MsuE$_{Pa}$ as compared to SsuE$_{Ec}$. Flavin binding to MsuE$_{Pa}$ occurs in a 1.7:1 flavin to enzyme ratio, unlike the 1:1 ratio seen with SsuE$_{Ec}$ and SsuE$_{Pp}$.

Similarly, MsuE$_{Pa}$ can utilize either NADH or NADPH. However, there is a 20-fold decrease in catalytic efficiency when NADPH is used, making NADH the preferred nicotinamide substrate. Interestingly, when the MsuE$_{Pa}$ NAD(P)H oxidase assay was performed in the presence of MsuD$_{Pa}$, the catalytic efficiency for NADPH and NADH were comparable (**Table 5.5** and **5.12**). Previous studies performed with SsuE$_{Ec}$, only showed a increase in NADPH oxidase activity when SsuD$_{Ec}$ and the alkanesulfonate substrate was present [10]. Additionally, there is a 4-fold increase in sulfite production for MsuD$_{Pa}$ when the non-preferred NADPH substrate is used (**Table 5.11**). Currently it is unclear why there is 20-fold decrease in NADPH oxidase activity with MsuE$_{Pa}$, but in coupled assays with MsuD$_{Pa}$ the catalytic activity is similar. A more in-depth look into the role of NAD(P)H in the methanesulfonate monooxygenase system will need to be performed before protein-protein interactions can be properly evaluated.

Since SsuE$_{Pp}$ appears to be specific to only NADPH, we shifted our attention and evaluated protein-protein interaction for this alkanesulfonate system. The ability of SsuE$_{Pp}$ to transfer reduced flavin was determined by measuring sulfite production by $FMNH_2$-dependent SsuD$_{Pp}$. Steady-state kinetic parameters for SsuD$_{Pp}$ was similar with SsuE$_{Pp}$ or SsuE$_{Ec}$, indicating that both

FMN-reductases were capable of flavin transfer. Previous studies of protein-protein interactions were identified through fluorometric titrations, rapid-reaction kinetics, and pull-down assays [36, 45]. Titrations of $SsuD_{Pp}$ into a solution of FMN-bound $SsuE_{Pp}$ displayed no observable increase in flavin absorbance (data not shown) as previously seen with $SsuE_{Ec}$/$SsuD_{Ec}$ [45]. When single-turnover of flavin reduction was monitored in the alkanesulfonate monooxygenase system from *E. coli* a distinct lag phase occurred prior to flavin oxidation, compared to oxidation of flavin with $SsuE_{Ec}$ alone [36]. This lag phase corresponds to the time it takes for the two proteins to interact and transfer reduce flavin. There was no observable lag phase between flavin reduction and subsequent oxidation with $SsuE_{Pp}$/$SsuD_{Pp}$ indicating the absence of protein-protein interactions (**Figure 5.8**). Previously Ni-NTA column chromatography was used to identify interactions between His-tagged $SsuD_{Ec}$ and native $SsuE_{Ec}$. After a high concentration imidazole wash, $SsuE_{Ec}$ and $SsuD_{Ec}$ co-eluted from the column [45]. To detect protein-protein interactions between $SsuE_{Pp}$ and $SsuD_{Pp}$, the pair was coupled and subjected to size exclusion chromatography where each enzyme eluted at two distinct retention times further suggesting that protein-protein interactions do not occur.

Overall there is a 57% identity and 70% similarity in amino acid sequence between $SsuE_{Pp}$ and $SsuE_{Ec}$, and a 79% and 88% identity and similarity between $SsuD_{Pp}$ and $SsuD_{Ec}$. Alignment of the specific protein-protein interaction sites identified by HDX-MS in the alkanesulfonate monooxygenase system of *E. coli*, shows a 91% identity and 100% similarity to the FMN-reductases $SsuE_{Ec}$ and $SsuE_{Pp}$ with all the charged amino acids remaining conserved. There is a 77% and 100% identity and similarity between the $SsuD_{Ec}$ and $SsuD_{Pp}$ monooxygenases, with two conserved mutations of glutamate to aspartate and lysine to arginine occurring within the charged

region (**Figure 5.9**). Substitution of these charged residues in SsuD$_{Pp}$ could influence protein-protein interactions with SsuE$_{Pp}$.

Unfortunately there is no single method for identifying static interactions between two proteins, and often times results vary. Based on the evidence provided here, preliminary investigations suggest that SsuE$_{Pp}$ and SsuD$_{Pp}$ do not transfer flavin through a channeling mechanism. Additional inquiry into FMN-dependent two-component systems of Sfn and Msu could provide a better indication of how the mechanism of flavin transfer relates to the structure of each enzyme. Furthermore investigation into the function of SsuF, an *ssu* enzyme only found in pseudomonads, could provide clarity into the full function of the alkanesulfonate monooxygenase system in *Pseudomonas* species.

REFERENCES: CHAPTERS 4 – 5

[1] Kertesz, M. A. (2000) Riding the sulfur cycle--metabolism of sulfonates and sulfate esters in gram-negative bacteria, *FEMS Microbiol Rev 24*, 135-175.

[2] van der Ploeg, J. R., Eichhorn, E., and Leisinger, T. (2001) Sulfonate-sulfur metabolism and its regulation in Escherichia coli, *Arch Microbiol 176*, 1-8.

[3] van der Ploeg, J. R., Weiss, M. A., Saller, E., Nashimoto, H., Saito, N., Kertesz, M. A., and Leisinger, T. (1996) Identification of sulfate starvation-regulated genes in Escherichia coli: a gene cluster involved in the utilization of taurine as a sulfur source, *J Bacteriol 178*, 5438-5446.

[4] Neumann, J., Rose-Sperling, D., and Hellmich, U. A. (2017) Diverse relations between ABC transporters and lipids: An overview, *Biochim Biophys Acta 1859*, 605-618.

[5] Hollenstein, K., Frei, D. C., and Locher, K. P. (2007) Structure of an ABC transporter in complex with its binding protein, *Nature 446*, 213-216.

[6] van Der Ploeg, J. R., Iwanicka-Nowicka, R., Bykowski, T., Hryniewicz, M. M., and Leisinger, T. (1999) The Escherichia coli ssuEADCB gene cluster is required for the utilization of sulfur from aliphatic sulfonates and is regulated by the transcriptional activator Cbl, *J Biol Chem 274*, 29358-29365.

[7] Eichhorn, E. (2000) Sulfonate-sulfur assimilation in *Escherichia coli*. , Swiss Federal Institute of Technology Zurich.

[8] Eichhorn, E., van der Ploeg, J. R., Kertesz, M. A., and Leisinger, T. (1997) Characterization of alpha-ketoglutarate-dependent taurine dioxygenase from Escherichia coli, *J Biol Chem 272*, 23031-23036.

[9] Eichhorn, E., van der Ploeg, J. R., and Leisinger, T. (1999) Characterization of a two-component alkanesulfonate monooxygenase from Escherichia coli, *J Biol Chem 274*, 26639-26646.

[10] Gao, B., and Ellis, H. R. (2005) Altered mechanism of the alkanesulfonate FMN reductase with the monooxygenase enzyme, *Biochem Biophys Res Commun 331*, 1137-1145.

[11] Gao, B., and Ellis, H. R. (2007) Mechanism of flavin reduction in the alkanesulfonate monooxygenase system, *Biochim Biophys Acta 1774*, 359-367.

[12] Driggers, C. M., Dayal, P. V., Ellis, H. R., and Karplus, P. A. (2014) Crystal structure of Escherichia coli SsuE: defining a general catalytic cycle for FMN reductases of the flavodoxin-like superfamily, *Biochemistry 53*, 3509-3519.

[13] Cooley, R. B., Arp, D. J., and Karplus, P. A. (2010) Evolutionary origin of a secondary structure: pi-helices as cryptic but widespread insertional variations of alpha-helices that enhance protein functionality, *J Mol Biol 404*, 232-246.

[14] Fodje, M. N., and Al-Karadaghi, S. (2002) Occurrence, conformational features and amino acid propensities for the pi-helix, *Protein Eng 15*, 353-358.

[15] Musila, J. M., Forbes, D. L., and Ellis, H. R. (2018) Functional Evaluation of the π–helix in the NAD(P)H:FMN Reductase of the Alkanesulfonate Monooxygenase System, *Biochemistry*.

[16] Musila, J. M., and Ellis, H. R. (2016) Transformation of a Flavin-Free FMN Reductase to a Canonical Flavoprotein through Modification of the pi-Helix, *Biochemistry 55*, 6389-6394.

[17] Musila, J. M. (2017) Exploring the Functional Roles of p-helices and Flavin-Induced Oligomeric State Changes in Flavin Reduction of Two-Component Monooxygenase Systems, In *Chemistry and Biochemistry*, Auburn University, Auburn, AL.

[18] Zhan, X., Carpenter, R. A., and Ellis, H. R. (2008) Catalytic importance of the substrate binding order for the FMNH2-dependent alkanesulfonate monooxygenase enzyme, *Biochemistry 47*, 2221-2230.

[19] Massey, V. (1994) Activation of molecular oxygen by flavins and flavoproteins, *J Biol Chem 269*, 22459-22462.

[20] Hastings, J. W., Balny, C., Peuch, C. L., and Douzou, P. (1973) Spectral properties of an oxygenated luciferase-flavin intermediate isolated by low-temperature chromatography, *Proc Natl Acad Sci U S A 70*, 3468-3472.

[21] Yeh, E., Cole, L. J., Barr, E. W., Bollinger, J. M., Jr., Ballou, D. P., and Walsh, C. T. (2006) Flavin redox chemistry precedes substrate chlorination during the reaction of the flavin-dependent halogenase RebH, *Biochemistry 45*, 7904-7912.

[22] Eichhorn, E., Davey, C. A., Sargent, D. F., Leisinger, T., and Richmond, T. J. (2002) Crystal structure of Escherichia coli alkanesulfonate monooxygenase SsuD, *J Mol Biol 324*, 457-468.

[23] Farber, G. K., and Petsko, G. A. (1990) The evolution of alpha/beta barrel enzymes, *Trends Biochem Sci 15*, 228-234.

[24] Wierenga, R. K. (2001) The TIM-barrel fold: a versatile framework for efficient enzymes, *FEBS Lett 492*, 193-198.

[25] Malabanan, M. M., Amyes, T. L., and Richard, J. P. (2010) A role for flexible loops in enzyme catalysis, *Curr Opin Struct Biol 20*, 702-710.

[26] Ou, X., Ji, C., Han, X., Zhao, X., Li, X., Mao, Y., Wong, L. L., Bartlam, M., and Rao, Z. (2006) Crystal structures of human glycerol 3-phosphate dehydrogenase 1 (GPD1), *J Mol Biol 357*, 858-869.

[27] Miller, B. G., Hassell, A. M., Wolfenden, R., Milburn, M. V., and Short, S. A. (2000) Anatomy of a proficient enzyme: the structure of orotidine 5'-monophosphate

decarboxylase in the presence and absence of a potential transition state analog, *Proc Natl Acad Sci U S A 97*, 2011-2016.

[28] Zhang, Z., Sugio, S., Komives, E. A., Liu, K. D., Knowles, J. R., Petsko, G. A., and Ringe, D. (1994) Crystal structure of recombinant chicken triosephosphate isomerase-phosphoglycolohydroxamate complex at 1.8-A resolution, *Biochemistry 33*, 2830-2837.

[29] Noble, A. R., and Richards, H. K. (1991) Plasma active and acid-activatable renin during the development of one-kidney, one-clip and two-kidney, one-clip hypertension in the rabbit, *Can J Physiol Pharmacol 69*, 1375-1380.

[30] Wierenga, R. K., Borchert, T. V., and Noble, M. E. (1992) Crystallographic binding studies with triosephosphate isomerases: conformational changes induced by substrate and substrate-analogues, *FEBS Lett 307*, 34-39.

[31] Davenport, R. C., Bash, P. A., Seaton, B. A., Karplus, M., Petsko, G. A., and Ringe, D. (1991) Structure of the triosephosphate isomerase-phosphoglycolohydroxamate complex: an analogue of the intermediate on the reaction pathway, *Biochemistry 30*, 5821-5826.

[32] Campbell, Z. T., and Baldwin, T. O. (2009) Two lysine residues in the bacterial luciferase mobile loop stabilize reaction intermediates, *J Biol Chem 284*, 32827-32834.

[33] Sparks, J. M., and Baldwin, T. O. (2001) Functional implications of the unstructured loop in the (beta/alpha)(8) barrel structure of the bacterial luciferase alpha subunit, *Biochemistry 40*, 15436-15443.

[34] Low, J. C., and Tu, S. C. (2002) Functional roles of conserved residues in the unstructured loop of Vibrio harveyi bacterial luciferase, *Biochemistry 41*, 1724-1731.

[35] Carpenter, R. A., Xiong, J., Robbins, J. M., and Ellis, H. R. (2011) Functional role of a conserved arginine residue located on a mobile loop of alkanesulfonate monooxygenase, *Biochemistry 50*, 6469-6477.

[36] Xiong, J., and Ellis, H. R. (2012) Deletional studies to investigate the functional role of a dynamic loop region of alkanesulfonate monooxygenase, *Biochim Biophys Acta 1824*, 898-906.

[37] Carpenter, R. A., Zhan, X., and Ellis, H. R. (2010) Catalytic role of a conserved cysteine residue in the desulfonation reaction by the alkanesulfonate monooxygenase enzyme, *Biochim Biophys Acta 1804*, 97-105.

[38] Fisher, A. J., Raushel, F. M., Baldwin, T. O., and Rayment, I. (1995) Three-dimensional structure of bacterial luciferase from Vibrio harveyi at 2.4 A resolution, *Biochemistry 34*, 6581-6586.

[39] Fisher, A. J., Thompson, T. B., Thoden, J. B., Baldwin, T. O., and Rayment, I. (1996) The 1.5-A resolution crystal structure of bacterial luciferase in low salt conditions, *J Biol Chem 271*, 21956-21968.

[40] Campbell, Z. T., Weichsel, A., Montfort, W. R., and Baldwin, T. O. (2009) Crystal structure of the bacterial luciferase/flavin complex provides insight into the function of the beta subunit, *Biochemistry 48*, 6085-6094.

[41] Li, L., Liu, X., Yang, W., Xu, F., Wang, W., Feng, L., Bartlam, M., Wang, L., and Rao, Z. (2008) Crystal structure of long-chain alkane monooxygenase (LadA) in complex with coenzyme FMN: unveiling the long-chain alkane hydroxylase, *J Mol Biol 376*, 453-465.

[42] Bruice, T. C. (1982) A progress report on studies of the activation of molecular oxygen by dihydroflavins, *Developments in Biochemistry 21*, 265-277.

[43] Imlay, J. A. (2003) Pathways of oxidative damage, *Annu Rev Microbiol 57*, 395-418.

[44] Walsh, C. (1978) Chemical approaches to the study of enzymes catalyzing redox transformations, *Annu Rev Biochem 47*, 881-931.

[45] Abdurachim, K., and Ellis, H. R. (2006) Detection of protein-protein interactions in the alkanesulfonate monooxygenase system from Escherichia coli, *J Bacteriol 188*, 8153-8159.

[46] Jeffers, C. E., and Tu, S. C. (2001) Differential transfers of reduced flavin cofactor and product by bacterial flavin reductase to luciferase, *Biochemistry 40*, 1749-1754.

[47] Jeffers, C. E., Nichols, J. C., and Tu, S. C. (2003) Complex formation between Vibrio harveyi luciferase and monomeric NADPH:FMN oxidoreductase, *Biochemistry 42*, 529-534.

[48] Kantz, A., Chin, F., Nallamothu, N., Nguyen, T., and Gassner, G. T. (2005) Mechanism of flavin transfer and oxygen activation by the two-component flavoenzyme styrene monooxygenase, *Arch Biochem Biophys 442*, 102-116.

[49] Lei, B., and Tu, S. C. (1998) Mechanism of reduced flavin transfer from Vibrio harveyi NADPH-FMN oxidoreductase to luciferase, *Biochemistry 37*, 14623-14629.

[50] Louie, T. M., Xie, X. S., and Xun, L. (2003) Coordinated production and utilization of FADH2 by NAD(P)H-flavin oxidoreductase and 4-hydroxyphenylacetate 3-monooxygenase, *Biochemistry 42*, 7509-7517.

[51] Dayal, P. V., Singh, H., Busenlehner, L. S., and Ellis, H. R. (2015) Exposing the Alkanesulfonate Monooxygenase Protein-Protein Interaction Sites, *Biochemistry 54*, 7531-7538.

[52] Kertesz, M. A., Schmidt-Larbig, K., and Wuest, T. (1999) A novel reduced flavin mononucleotide-dependent methanesulfonate sulfonatase encoded by the sulfur-regulated msu operon of Pseudomonas aeruginosa, *J Bacteriol 181*, 1464-1473.

[53] Endoh, T., Habe, H., Yoshida, T., Nojiri, H., and Omori, T. (2003) A CysB-regulated and sigma54-dependent regulator, SfnR, is essential for dimethyl sulfone metabolism of Pseudomonas putida strain DS1, *Microbiology 149*, 991-1000.

[54] Endoh, T., Kasuga, K., Horinouchi, M., Yoshida, T., Habe, H., Nojiri, H., and Omori, T. (2003) Characterization and identification of genes essential for dimethyl sulfide utilization in Pseudomonas putida strain DS1, *Appl Microbiol Biotechnol 62*, 83-91.

[55] Mopper, K., and Taylor, B. F. (1986) Biogeochemical Cycling of Sulfur, In *Organic Marine Geochemistry*, pp 324-339, American Chemical Society.

[56] Moran, M. A., Reisch, C. R., Kiene, R. P., and Whitman, W. B. (2012) Genomic insights into bacterial DMSP transformations, *Ann Rev Mar Sci 4*, 523-542.

[57] Charlson, R. J., Lovelock, J. E., Andreae, M. O., and Warren, S. G. (1987) Oceanic phytoplankton, atmospheric sulphur, cloud albedo and climate, *Nature 326*, 655.

[58] de Souza, M. P., and Yoch, D. C. (1995) Purification and characterization of dimethylsulfoniopropionate lyase from an alcaligenes-like dimethyl sulfide-producing marine isolate, *Appl Environ Microbiol 61*, 21-26.

[59] Ledyard, K. M., DeLong, E. F., and Dacey, J. W. H. (1993) Characterization of a DMSP-degrading bacterial isolate from the Sargasso Sea, *Archives of Microbiology 160*, 312-318.

[60] Welsh, D. T. (2000) Ecological significance of compatible solute accumulation by micro-organisms: from single cells to global climate, *FEMS Microbiol Rev 24*, 263-290.

[61] Bentley, R., and Chasteen, T. G. (2004) Environmental VOSCs--formation and degradation of dimethyl sulfide, methanethiol and related materials, *Chemosphere 55*, 291-317.

[62] Schafer, H., Myronova, N., and Boden, R. (2010) Microbial degradation of dimethylsulphide and related C1-sulphur compounds: organisms and pathways controlling fluxes of sulphur in the biosphere, *J Exp Bot 61*, 315-334.

[63] Barnes, I., Hjorth, J., and Mihalopoulos, N. (2006) Dimethyl sulfide and dimethyl sulfoxide and their oxidation in the atmosphere, *Chem Rev 106*, 940-975.

[64] Wicht, D. K. (2016) The reduced flavin-dependent monooxygenase SfnG converts dimethylsulfone to methanesulfinate, *Arch Biochem Biophys 604*, 159-166.

[65] Kahnert, A., Vermeij, P., Wietek, C., James, P., Leisinger, T., and Kertesz, M. A. (2000) The ssu locus plays a key role in organosulfur metabolism in Pseudomonas putida S-313, *J Bacteriol 182*, 2869-2878.

[66] Quadroni, M., James, P., Dainese-Hatt, P., and Kertesz, M. A. (1999) Proteome mapping, mass spectrometric sequencing and reverse transcription-PCR for characterization of the sulfate starvation-induced response in Pseudomonas aeruginosa PAO1, *Eur J Biochem 266*, 986-996.

[67] Gray, K. A., Pogrebinsky, O. S., Mrachko, G. T., Xi, L., Monticello, D. J., and Squires, C. H. (1996) Molecular mechanisms of biocatalytic desulfurization of fossil fuels, *Nat Biotechnol 14*, 1705-1709.

[68] Endoh, T., Habe, H., Nojiri, H., Yamane, H., and Omori, T. (2005) The sigma54-dependent transcriptional activator SfnR regulates the expression of the Pseudomonas putida sfnFG operon responsible for dimethyl sulphone utilization, *Mol Microbiol 55*, 897-911.

[69] Denome, S. A., Oldfield, C., Nash, L. J., and Young, K. D. (1994) Characterization of the desulfurization genes from Rhodococcus sp. strain IGTS8, *J Bacteriol 176*, 6707-6716.

[70] Winsor, G. L., Griffiths, E. J., Lo, R., Dhillon, B. K., Shay, J. A., and Brinkman, F. S. (2016) Enhanced annotations and features for comparing thousands of Pseudomonas genomes in the Pseudomonas genome database, *Nucleic Acids Res 44*, D646-653.

CHAPTER SIX

SUMMARY

Sulfur-containing molecules are essential for mammalian and bacterial organisms. The mechanisms for incorporation of sulfur into metabolically relevant molecules vary depending on the organism. Mammals depend on the availability of the amino acids methionine and cysteine, whereas bacterial organisms rely on sulfite and cysteine. This research is focused on enzymes found within the sulfur metabolic pathway. These enzymes play a role in the oxidation of cysteine or the desulfonation of small chain carbon-sulfur molecules.

Cysteine Dioxygenase (CDO) is an iron containing enzyme belonging to the cupin superfamily. CDO catalyzes the conversion of L-cysteine to cysteine sulfinic acid in the presence of dioxygen. A common structural feature of the cupin superfamily is the double stranded β-helix, more commonly known as the cupin "jelly roll". Several cupin enzymes contain two partially conserved motifs representing the 3-His/1-Glu coordination of the iron center. Unlike many cupin enzymes the mononuclear iron center of CDO is weakly coordinated by a 3-His motif. This traditional glutamate residue is replaced by a cysteine (Cys93) in mammalian CDO.

In order to investigate this evolutionary divergence of mammalian CDO, Cys93 was substituted with a glutamate residue to generate the C93E CDO variant. Three dimensional structural analyses showed that the substituted glutamate residue coordinates the iron center similar to the metal center geometry observed for a traditional 3-His/1-Glu cupin. However in

CDO, coordination by glutamate occupies a ligand coordination site essential for catalysis. Kinetic and spectroscopical evaluation of C93E CDO concluded that the glutamate residue supports L-cysteine binding, but is unable to bind dioxygen due to the absence of a coordination site. Therefore, the replacement of glutamate with cysteine allows for three unoccupied ligand sites for bidentate coordination of L-cysteine and monodentate coordination of dioxygen.

Additionally, the replacement of glutamate with cysteine allows for the formation of a unique thioether crosslink with a nearby tyrosine residue (Tyr157). In wild-type CDO the crosslink exists as a heterogeneous mixture of both non crosslinked and crosslinked isoforms. Previous studies have shown that crosslink formation is dependent on iron, L-cysteine, and dioxygen. Once present, the crosslink increases the catalytic efficiency of cysteine oxidation. Cys-Tyr crosslink formation in other thioether-containing enzymes is not dependent on the substrate. Therefore, it is unusual that crosslink formation in CDO is dependent on L-cysteine.

To understand the role of L-cysteine in crosslink formation, CDO was incubated with L-cysteine structural analogs D-cysteine, cysteamine, and 3-mercaptopropionic acid. In addition to forming the crosslink with L-cysteine, wild-type CDO can also form the crosslink with D-cysteine, but does not form the crosslink with cysteamine or 3-mercaptoproprionic acid. However, a previous study showed that R60A CDO was able to form the crosslink with cysteamine. The conserved Arg60 residue has been previously linked to play a role in substrate coordination. Purification and evaluation of non crosslinked R60A CDO suggests that Arg60 also plays a role in substrate specificity for cysteine oxidation and crosslink formation. Mutation of the charged arginine residue to an alanine allowed for coordination of cysteamine, which in the end promoted dioxygen binding and subsequent crosslink formation. Moreover, wild-type CDO was able to form the crosslink with the stereoisomer D-cysteine. This evidence suggest that crosslink formation in

cysteine dioxygenase is not specific to L-cysteine, but can occur with any small thiol analog capable of priming the iron for dioxygen activation.

Several crosslink mechanisms have been proposed. In all mechanism, formation of the Cys-Tyr crosslink proceeds via a hydroxy radical, with a proton-coupled electron transfer occurring between the hydroxyl group of Tyr157 and the thiol of Cys93. But recent three dimensional crystal structure analyses and pH studies of non crosslinked wild-type CDO showed the thiol of the non crosslinked Cys93 lies closer to the site where oxygen binds suggesting that crosslink formation via a thiol radical is equally as probable. Although essential, crosslink formation in CDO is not required for the production of cysteine sulfinic acid. CSA serves as an important branch point in the cysteine metabolism. CSA is further metabolized into the physiologically significant molecules taurine and sulfite.

Due to the lack of sulfur in the environment, many bacterial organisms possess sets of genes that allow bacteria to acquire inorganic sulfate from various organosulfate molecules. In *E. coli* two of the expressed proteins, SsuD and SsuE, comprise the alkanesulfonate monooxygenase system. The alkanesulfonate system is a FMN-dependent two-component enzyme system comprised of a FMN-reductase (SsuE) and a monooxygenase (SsuD) capable of cleaving the carbon-sulfur bond in C2 – C10 alkanesulfonates into sulfite and the corresponding aldehyde. Monooxygenase enzymes acquire flavin from FMN-reductases through free diffusion or through a channeling mechanism which promotes protein-protein interactions. Protein-protein interaction sites have been identified in SsuE and SsuD. However, flavin transfer by free diffusion would allow monooxygenase enzymes to acquire reduced flavin from FMN reductases that are not dedicated to their respective system. It is possible that the observed ability of FMN reductases to

supply reduce flavin to alternate monooxygenase partners maybe due to structural similarities within these two-component systems.

The alkanesulfonate monooxygenase system is one of several identified two-component systems activated during sulfur starvation in bacteria. Additional *ssi* genes, *msu* and *sfn*, have been identified in *Pseudomonas sp*. These enzymes encompass a series of enzymatic reactions that converts dimethylsulfone ($DMSO_2$) to inorganic sulfite. FMN reductases $SsuE_{Pp}$, $MsuE_{Pa}$, and $SfnE_{PpG}$ were all capable of flavin reduction and transfer to a monooxygenase enzyme. Conversely, $SsuD_{Pp}$ and $MsuD_{Pa}$ were capable of accepting reduced flavin to cleave the carbon-sulfur bond within octanesulfonate and methanesulfonate, respectively. A high amino acid sequence identity (> 57%) exists between SsuE and SsuD enzymes from *E. coli* and *P. putida*, suggesting that protein-protein interactions could play a role in flavin transfer in $SsuE_{Pp}$/$SsuD_{Pp}$. There is currently no spectroscopic evidence to support this theory. However, there are many other chemical methods to identify protein-protein interactions that have not been investigated in this study. There are also numerous other *ssi* genes that encode FMN-dependent two-component systems that could provide evidence to support the link between common structural features and enzyme function.

CHAPTER SEVEN

Changing the Perceptions of Chemistry through Laboratories

Highlighting the Traditional Divisions

7.1 INTRODUCTION

Laboratory experiences are often some of the most memorable to scientists. A laboratory class can be an avenue to explore new concepts while tying them to problem solving skills [1]. Understanding the practical nature of chemistry and difficult scientific concepts are examples of goals highlighted by Hofstein and Lunetta [2, 3] These ideas have been discussed and studied widely in recent years. The necessity of chemistry lab has often been stated, but the outcomes of laboratory learning has never been fully described [4]. A recent study investigated the desired and actual outcomes from the perspectives of the students and the instructor [1, 5, 6]. This study resulted in four laboratory outcomes, as put forth by Reid and Shah, which are general skills, practical skills, scientific skills, and skills related to learning chemistry [4].

The ability of students to learn these four skills have also been shown to influence the student's motivation, interest, and overall attitudes toward science [1]. Furthermore, practical knowledge and application of content often increases student interest and persistence within a subject [7]. Persistence of students is even more important when trying to increase diversity and inclusivity from underrepresented populations [8]. Reinforcing content with practical applications,

even from a single laboratory experiment, has been shown to improve student performance [9].

General chemistry, as its name suggests, is general in nature and covers large amounts of content in a short semester or two. Although important, the content presented typically remains at the microlevel and lacks application [10]. All too often students struggle to find meaning and experience a disconnect between the content and application [11]. The chemistry laboratory is a great place to expose students to the application of chemistry and bridge the gap between the micro and macro worlds. However, lab content covered in first year chemistry is often lacking and primarily focuses on topics in physical chemistry. Two of the fundamental pillars of chemistry, analytical and biochemistry are rarely discussed in the general chemistry lecture or lab, and these two topics comprise a large amount of real world applications and techniques.

Introducing labs focused on the individual divisions of chemistry (analytical, biochemistry, inorganic, and organic) and their applications could promote higher student interest and increase their positive perceptions of chemistry. Students could also develop a firmer understanding of chemistry as an applicable science. This could also spark curiosity that could have otherwise been missed without exposure to upper level classes. Laboratories highlighting a single division of chemistry for undergraduate or high-school students are not uncommon [12, 13]; however, we sought to introduce students to multiple divisions of chemistry while focusing on the practical and scientific skills normally presented in a first-year laboratory class. Through the use of pre- and post-lab surveys we were able to identify the student's initial perception, self-reported knowledge and interest of each division of chemistry and how that perception, knowledge and interest changed once each division was introduced.

7.2 METHODS

7.2.1 Study Setting

This study was conducted at a large, rural research university located in the southern United States during the Fall 2016 and Spring 2017 semesters. The university has approximately 20,000 undergraduates and over 25,000 total students enrolled with an equal ratio of male (50.5%) to female (49.5%). The students have over 140 majors to choose from at their institution.

For this study, the courses of interest were Honors General Chemistry Laboratory I (HCL1; Fall 2016) and Honors General Chemistry Laboratory II (HCL2; Spring 2017). Eligibility for enrollment in honors classes requires prior acceptance into the honors college. The honors college requires a minimum high school grade point average of 3.85 and a minimum ACT score of 29. Additionally, only students that successfully completed HCL1 are eligible to enroll in HCL2 the following semester. A total of 66 students were enrolled in HCL1 and 49 students in HCL2 with equal ratio of male and female students for both semesters. All students were first-time college students in Fall 2016. However due to credits acquired in high school, 65% of students were classified as either sophomores (60%) or juniors (5%). A breakdown of majors, as declared by the students in Fall 2016, are listed in **Table 7.1**.

Table 7.1. Percent of students committed to each major as of Fall 2016.

	% students
Pre-chemical engineering	61
Pre-med	24
Biochemistry	8
Undeclared science	6

Content delivered in HCL1 and HCL2 are consistent with traditional chemistry laboratory classes. Students are required to read background and procedural information prior to lab with most experiments requiring a graded pre-lab quiz. The first 10 -15 minutes of lab cover safety, use of equipment, and any additional chemistry content deemed necessary. Over the course of the semester in HCL1, a large portion of time is spent teaching students to write a manuscript-style lab report. At the end of each experiment, lab reports serve as the graded summative assessment. Experiments performed in HCL1 and HCL2 are typical first year chemistry experiments commonly used. Over the last five years, continual student feedback has been solicited to shape the lab and meet the needs of the changing student population. A final survey at the last lab was also conducted.

7.2.2 Survey Instrument

A Likert scale type survey was employed to assess a wide range of attitudes. Likert scales are used to measure specific attitudes towards survey items and produce a high degree of reliability [14, 15]. Each survey question used in this study included at least one positive and one negative selection. In addition, at least one neutral response such as “neutral” or “I don’t know”, was included for students that did not have a strong attitude or understanding of what was being asked of them. Participation in the surveys was anonymous and completely optional, and therefore did not influence the students’ grade in the course. Since the survey was optional, participation varied from experiment to experiment.

7.2.3 Introduction to Traditional Chemistry Divisions

Over the course of two semesters, one lab representing each of the traditional divisions of analytical, biochemistry, inorganic, and organic chemistry was introduced. Physical chemistry was not highlighted in our study as laboratories previously used in these classes fulfilled that purpose.

Each lab experiment introduced was acquired from the upper level chemistry course of the same name and was modified to the appropriate difficulty level. The analytical lab was an introduction to photometers and 3D printed instruments, the biochemistry lab was focused on DNA and enzymes, the inorganic lab was an introduction to the spectrochemical series, and in the organic lab students performed a fisher esterification synthesis. Prior to each lab, students participated in a short online survey to measure perceptions and self-reported knowledge toward that particular division of chemistry. The pre-survey was meant to provide a baseline toward the specific division of chemistry, before any exposure of reading or lab materials. In order to attain the most accurate survey responses, pre-lab reading materials were withheld until after the pre-survey closed.

To introduce each of the traditional divisions of chemistry prior to lab students were assigned pre-lab readings and were required to write the procedure in their notebook. During lab, each experiment was introduced by a fourth-year chemistry graduate student or a tenured research professor who has specialized experience in the specific division of chemistry. Students were given an overview of the content covered in that particular division of chemistry, as well as real world applications and examples of current research being performed within the department. Additionally, the experienced graduate student or professor remained for the duration of lab to answer any questions the students may have about the experiment or that particular division of chemistry. Upon completion of the experiment, a post-lab wrap-up session was conducted to conceptualize and explain the subtleties of the experiment. A few days following the experiment, an online post-lab survey was administered to evaluate any changes in attitudes or understanding of the division. In typical class fashion, students were also required to complete a formal writing assignment such as a lab report or critical thinking questions.

7.3 LIMITATIONS

One limitation of the broad applications of this study is the student population consisting of only honors students during one academic year. These students are within the top students at the university and therefore the scope of this study could be limited to students who are often the most involved and eager to be challenged. The labs introduced did not seek out the effectiveness of each lab in regards to content learning or obtaining measurable knowledge, but more as a way to engage students in chemistry.

The laboratories were presented to introduce students to an entire division of chemistry, but as divisions of chemistry are very broad and have many subdivisions this is another limitation of this study. The perception or interest in an entire division was self-reported from the students based on one exposure. Additionally, perception as well as perceived interest can be easily changed and can be dependent on the personality of the professor and excitement of the experiment.

7.4 RESULTS

7.4.1 Survey Participation

This study was conducted over two semesters in a two-part laboratory sequence with n = 66 students in the fall and n = 49 students in the spring. Due to individual majors and honor college requirements, a decrease in enrollment between HCL1 and HCL2 is normal. Student participation in surveys was anonymous and on a volunteer basis, and therefore it is possible that students could participate in one survey but not the other. However, there was always a larger number of participants in the pre-survey as compared to the post-survey. Student participation in pre- and post-surveys for each division is outlined in **Table 7.2**. The max number of survey participants for the biochemistry survey is n = 66, and n = 49 for analytical, inorganic, and organic surveys. The highest participation in any survey was 65, and the lowest was 43, corresponding to 99% and 88% total participation, respectively.

Table 7.2: Number of participants in pre- and post-surveys for each experiment.

	Pre-survey	Post-survey
Analytical	47	45
Biochemistry	65	62
Inorganic	49	47
Organic	49	43

7.4.2 Survey Results

In order to determine a baseline for student's perceptions and self-reported knowledge in analytical, biochemistry, inorganic and organic chemistry, the following two questions were asked: 1) Which statement best matches your perception of [division] chemistry, 2) Do you have any basic knowledge of [division] chemistry, and 3) Are you interested in [division] chemistry. For the

last question the following clarification statement was given: “We are not asking if you would change your major, but if you have any interest toward [division] chemistry”. These questions were meant to gauge differences in attitudes or perceptions following the lab students participated in a post-survey. The post-survey questions were similar to the pre-survey questions and included: 1) Did the lab change your perception of [division], 2) Do you think you have a better basic knowledge of [division] chemistry than before the lab, and 3) Did the lab/pre-lab lecture change your interest toward [division] chemistry.

Survey responses for pre-perceptions in chemistry are outlined in **Table 7.3**. Prior to the experiment students showed a 55% positive perception toward biochemistry while 23% of the class stated they did not know enough about biochemistry to form an opinion. Analytical, inorganic, and organic chemistry had the lowest positive perceptions at 6, 22, and 18%, respectively. Interestingly, 45% of students reported not knowing enough about analytical chemistry to form an appropriate perception, whereas zero students indicated that response for organic chemistry. Furthermore, 35% of students regarded organic chemistry as hard while 27% remained neutral to the subject.

Table 7.3: Pre-survey perception; numbers in %

	Fun	Neutral	Boring	Hard	Don’t Know
Analytical	6	21	9	19	45
Biochemistry	55	20	2	0	23
Inorganic	22	43	6	10	18
Organic	18	27	2	35	0

The second pre-lab survey question asked the students to self-report their knowledge of each division of chemistry (**Table 7.4**). Over half of students reported they had some knowledge

of organic chemistry, while 33% of students were not sure. Similar uncertainty existed for students self-reported knowledge of biochemistry at 49%, although 32% said they have some biochemistry knowledge. Curiously, 72% of students said they had no knowledge of analytical chemistry while 19% remained unsure.

Table 7.4: Pre-survey self-reported knowledge; numbers in %

	A lot	Some	Nothing	Not Sure
Analytical	0	9	72	19
Biochemistry	3	32	15	49
Inorganic	0	31	29	41
Organic	0	53	14	33

Concluding the lab, students were asked the same three questions. Overall, responses for the post-lab surveys were more one-sided than the pre-lab surveys. For instance, less than 5% of students reported not knowing enough about a particular division of chemistry (**Table 7.5**). Zero students reported they perceived biochemistry or inorganic chemistry as hard. Furthermore, just over 50% of students were neutral to analytical chemistry, while approximately 60% of students now perceive biochemistry, inorganic, and organic as fun.

Table 7.5: Post-survey perception; numbers in %

	Fun	Neutral	Boring	Hard	Don't Know
Analytical	27	51	13	4	4
Biochemistry	63	32	0	0	5
Inorganic	57	40	0	0	2
Organic	58	33	5	2	2

Responses for post self-reported knowledge showed an overall increase in the students understanding for each division of chemistry (**Table 7.6**). Over 80% of students reported having a better understanding of analytical and biochemistry, whereas 68 and 72% of students felt they had a better understanding of inorganic and organic chemistry following the lab. Less than 2% of students reported having a worse knowledge of inorganic, and zero students reported having a worse knowledge of analytical and biochemistry after the lab.

Table 7.6: Post-survey self-reported knowledge; numbers in %

	Yes	Same	Worse	Don't Know
Analytical	87	13	0	0
Biochemistry	81	19	0	0
Inorganic	68	30	2	0
Organic	72	12	14	2

Student responses for their pre- and post- self-reported interest in the divisions is reported in **Table 7.7** and **Table 7.8**. The questions asked were: 1) Are you interested in [division] chemistry and 2) Did the lab/prelab lecture change your interest or curiosity toward [division] chemistry. As high as 55% of students answered that they did not know enough about the subject to gauge if they were interested, but after the lab exposure these numbers decreased drastically. Positive gains, although slight in some cases, were seen for each division.

Table 7.7: Pre-survey interest; numbers in % of students

	Interested	Somewhat	Not Interested	Don't Know
Analytical	9	23	13	55
Biochemistry	57	31	5	8
Inorganic	18	53	12	16
Organic	49	37	12	2

Table 7.8: Post-survey interest; numbers in % of students					
	More	Same	Less	No	Don't Know
Analytical	40	29	13	13	4
Biochemistry	40	56	2	2	0
Inorganic	36	51	2	9	2
Organic	37	49	7	7	0

At the conclusion of HCL2, a final end of the year survey was given asking for students feedback on the labs, assignments, and performance of their graduate teaching assistant throughout the semester. Since analytical, biochemistry, inorganic, and organic specific labs were introduced, this survey provided the students an opportunity to give feedback on those as well. Students were asked the following questions: 1) Did you like that we introduced upper level chemistry into your lab, 2) Do you have a better understanding of the different division of chemistry than you did prior to this class, and 3) Since taking this lab, are you more/same/less interested in chemistry, pertaining to the labs introduced. The students were also given the option to leave any comments or feedback about the labs introduced.

Introduction of the labs highlighting each division of chemistry was very well received with 86% student satisfaction (**Figure 7.1 A**). When asked if students had a better understanding of chemistry prior to this laboratory class 93% of students responded affirmatively (**Figure 7.1 B**). In addition, 70% of students reported that they were more interested in chemistry since taking HCL1 and HCL2 (**Figure 7.1 C**).

A. Did you like that we introduced upper level chemistry into your lab?

	% students
Yes	86
Neutral	7
No	7

B. Do you have a better understanding of the different division of chemistry than you did prior to this class?

	% students
Yes	93
Same	7
No	0

C. Since taking this lab, are you more/same/less interested in chemistry?

	% students
More	70
Same	28
Less	2

Figure 7.1. Summary of three survey questions and responses from the survey given at the end of the semester for HCL2.

7.5 DISCUSSION

Students enrolled in large schools in the southeastern United States, especially those from rural areas, may first be introduced to chemistry in a college lecture and laboratory setting. Often these introductory classes are the only required course for many majors and therefore the exposure of chemistry in these classes may be the only view of chemistry students receive. Additionally, students are generally unsure of their majors and of the vast possibilities offered by specializing in chemistry. The "upper level" chemistry topics, more appropriately described as the traditional divisions of chemistry, are often approached during lecture but less often in "cookie-cutter" laboratory experiments.

This lack of knowledge of the types of chemistry and applications of each division of chemistry is highlighted in the pre- and post- survey data of the student's self-reported knowledge **(Figure 7.2)**. The introduction of these labs "highlighting" the traditional divisions showed a great increase in the students' perceived knowledge about the divisions. This self-reported knowledge does not necessarily reflect the students measured "knowledge", however the stark increase in the student's perceived knowledge is promising, especially for students to understand the vast nature of chemistry and future job opportunities as well as a variety of applications that chemistry offers.

A key highlight from the reported data is the pre- and post-reported perception of each division of chemistry discussed. **Figure 7.3** is a comparison the students reported pre- and post-positive responses about their perception of each division. Overall there was an increase in the positive perception for each division. The analytical response is especially interesting because the students were using 3D printed photometers made by senior undergraduate students who are majoring in chemistry. This greatly affected the students involvement in the lab, as they could see the kinds of projects they would be able to complete if they were to major in chemistry. The 50%

increase in positive perceptions of organic chemistry partially came from the 33% decrease in students identifying organic chemistry as “hard”. Organic chemistry is a notorious difficult class that causes many students to struggle, which can cause freshman students to have anxiety about the subject. The pre-lab lecture for the organic chemistry lab offered clarity for students on what exactly organic chemistry is and why so many people struggle with it. Therefore the overall increase of positive perceptions most likely came from the students actual understanding of topics covered in organic chemistry, which is evident from the increase in self-reported knowledge of organic chemistry (**Figure 7.2**).

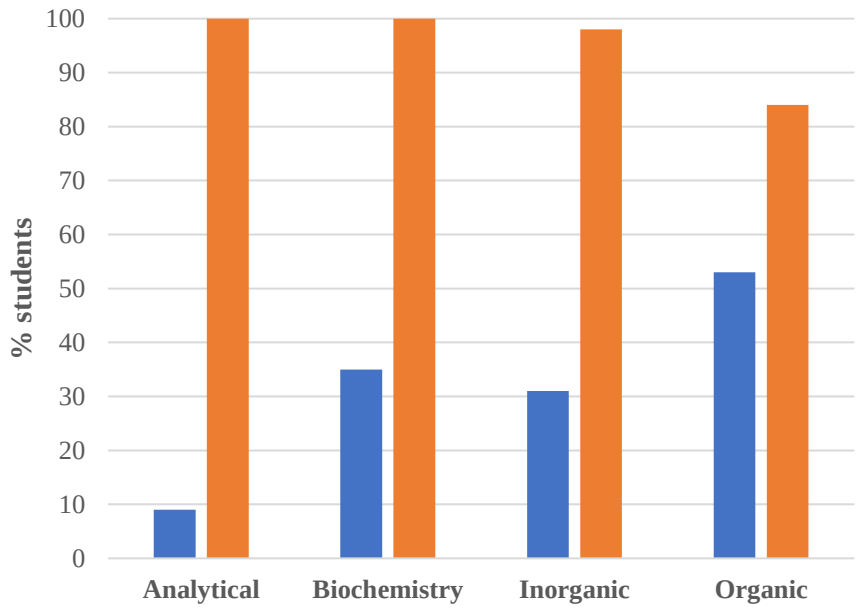

Figure 7.2. Comparison of students self-reported pre-knowledge (blue) and post-knowledge (orange) for each division of chemistry. Self-reported data listed is the combined responses of “a lot” and “some” from **Table 7.4**, and “yes” and “same” from **Table 7.6**.

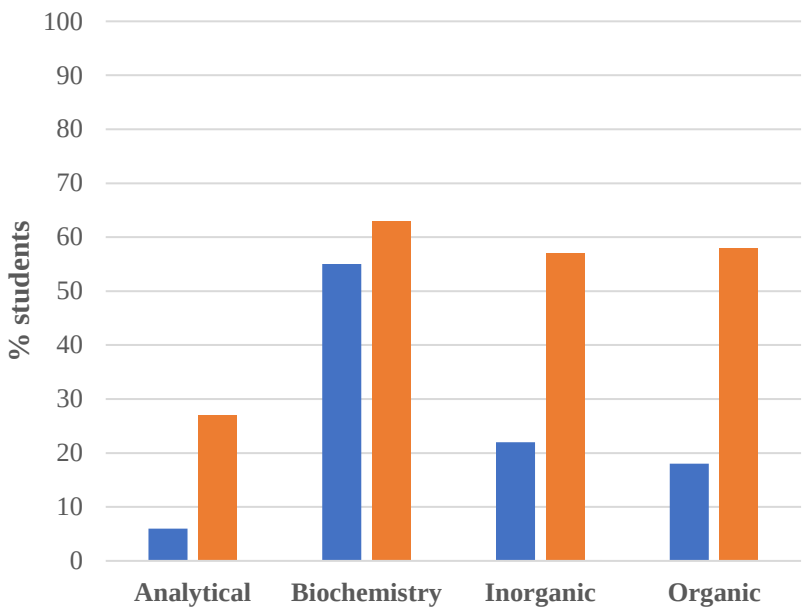

Figure 7.3. Comparison of students positive pre-perception (blue) and post-perceptions (orange) for each division of chemistry. Perception data listed is gathered response of "fun" from **Table 7.3** and **Table 7.5**.

The students self-reported pre- and post-interest was designated as positive, neutral, or negative interest and combined as shown in **Figure 7.4**. Positive interest includes responses of "interest" or "somewhat interested". Overall there was a general increase in interest, albeit only slight for most divisions. It is also important to note that the content presented in the lab did not have a negative impact on the students interest. The high initial interest reported does not come as a surprise, as all of the students in HCL1 and HCL2 have declared a science or engineering major. However, it is interesting that analytical chemistry fell so far behind at 32% interest. This is most likely due to a lack of knowledge on the subject as students indicated very low self-reported knowledge (9%). Over half of students in HCL have declared pre-engineering as their major, with pre-chemical engineering as the most selected subset. Out of all the divisions of chemistry,

analytical chemistry is arguably the closest related field to engineering and this may explain the over 50% increase in interest once the lab was introduced.

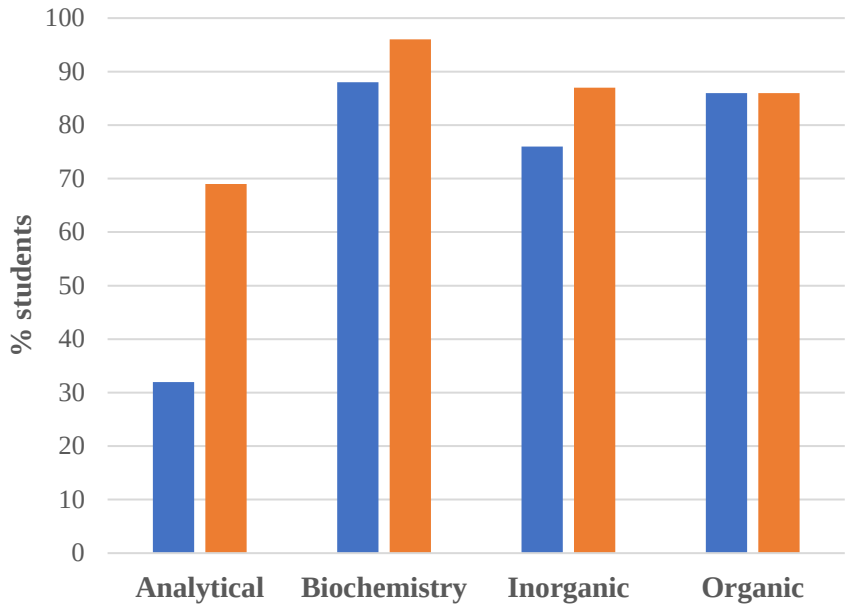

Figure 7.4. Comparison of students pre- and post- positive interest. Pre-interest (blue) data is listed is the combined responses of "interested" and "somewhat interested" from **Table 7.7**, and post-interest (orange) is the combined responses of "more interested" and "same" from **Table 7.8**.

Furthermore, the overall comparison between the students pre-interest and pre-knowledge revealed something very intriguing (**Figure 7.5**). Students reported a greater than 20% difference in interest compared to self-reported knowledge for all the division of chemistry. The largest pre-interest/pre-knowledge gap was 53% for the division of biochemistry. Overall, the students perception of biochemistry was widely positive with 55% of students viewing biochemistry as "fun". It is fascinating that students are reporting a positive perception and interest in a division

that they self-reportingly do not understand. However, this interest could be due to the fact that they seek more information about biochemistry.

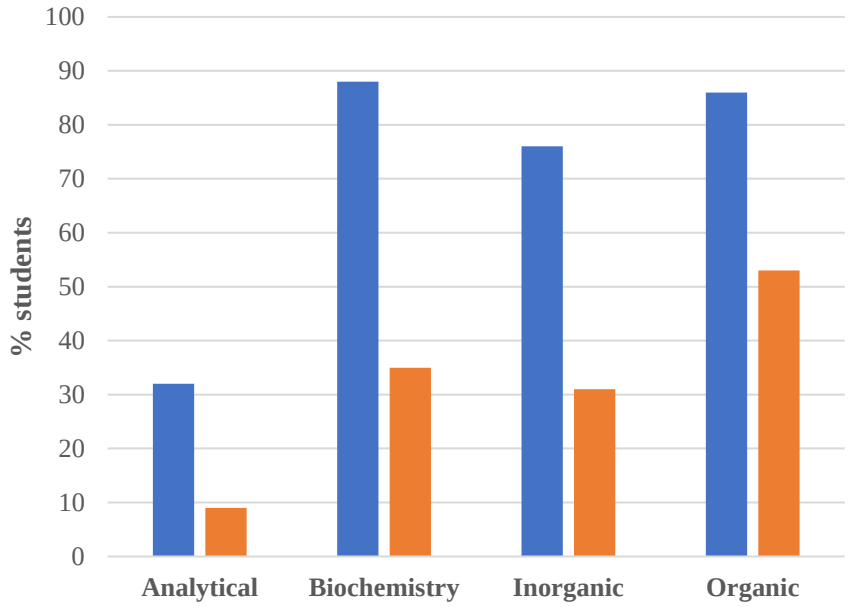

Figure 7.5. Comparison of students pre-interest (blue) and pre-knowledge (orange) for each division of chemistry. Pre-interest data listed is the combined responses of "interested" and "somewhat interested" from **Table 7.7**, and pre-knowledge data is the combined responses of "yes" and "same" from **Table 7.4**.

Overall, the introduction of the "upper level" divisions of chemistry was positively received by the students during the academic year. A sampling of positive and constructive feedback from the students at the end of HCL2 is shown below in **Table 7.9**. These responses highlight the potential benefits of introducing students to a broad range of topics.

Table 7.9: End of the year student feedback about the incorporation of the new labs.

"The upper level chemistry topics were very beneficial because the assignments for each lab required us to critically think about everything that was going on at the molecular level."
"Overall, I really enjoyed this lab. It is great to be exposed to different areas of chemistry that I had not really thought of that much before."
"The analytical lab was really cool because we got to work with something that other students had built."
"Because the material was new, and stuff we did not cover in class, I did not feel like I had a very good grasp of the science behind what I was doing."
"I think it helps freshman start to consider what parts of chemistry they might want to study in the future."

7.6 CONCLUSION

Introducing students to a single laboratory experiment highlighting the traditional divisions of chemistry was found to increase the students self-reported knowledge and positive perceptions of each respective division. While the students did not all decide to become chemistry majors, that is an unrealistic expectation from a single experiment and was not the intended goal for this exercise. Students did report an increase in perception, interest, and knowledge of the traditional divisions, which may lead to the students increased ability to consider chemistry as a viable major. Far from comprehensive, this investigation can serve as a platform for a more in-depth chemical education research study on how students perceive chemistry.

7.7 IRB APPROVAL

This study received an "exempt" status as determined by the Institutional Review Board at Auburn University. IRB 17-292 EX 1708 (08/03/2017 – 08/02/2020)

REFERENCES: CHAPTER 7

[1] Bretz, S. L., Fay, M., Bruck, L. B., and Towns, M. H. (2013) What Faculty Interviews Reveal about Meaningful Learning in the Undergraduate Chemistry Laboratory, *Journal of Chemical Education 90*, 281-288.

[2] Hofstein, A., and Lunetta, V. N. (1982) The Role of the Laboratory in Science Teaching: Neglected Aspects of Research, *Review of Educational Research 52*, 201-217.

[3] Avi, H., and N., L. V. (2004) The laboratory in science education: Foundations for the twenty-first century, *Science Education 88*, 28-54.

[4] Reid, N., and Shah, I. (2007) The role of laboratory work in university chemistry, *Chemistry Education Research and Practice 8*, 172-185.

[5] Galloway, K. R., and Bretz, S. L. (2015) Measuring Meaningful Learning in the Undergraduate General Chemistry and Organic Chemistry Laboratories: A Longitudinal Study, *Journal of Chemical Education 92*, 2019-2030.

[6] DeKorver, B. K., and Towns, M. H. (2016) Upper-level undergraduate chemistry students' goals for their laboratory coursework, *Journal of Research in Science Teaching 53*, 1198-1215.

[7] Richter-Egger, D. L., Hagen, J. P., Laquer, F. C., Grandgenett, N. F., and Shuster, R. D. (2010) Improving Student Attitudes about Science by Integrating Research into the Introductory

Chemistry Laboratory: Interdisciplinary Drinking Water Analysis, *Journal of Chemical Education 87*, 862-868.

[8] Anderson, R. D. (2002) Reforming Sciene Teaching: What Research says about Inquiry, *Journal of Science Teacher Education 13*, 1-12.

[9] Cacciatore, K. L., and Sevian, H. (2009) Incrementally Approaching an Inquiry Lab Curriculum: Can Changing a Single Laboratory Experiment Improve Student Performance in General Chemistry?, *Journal of Chemical Education 86*, 498.

[10] van Berkel, B., Pilot, A., and Bulte, A. M. W. (2009) Micro–Macro Thinking in Chemical Education: Why and How to Escape, In *Multiple Representations in Chemical Education* (Gilbert, J. K., and Treagust, D., Eds.), pp 31-54, Springer Netherlands, Dordrecht.

[11] Tsaparlis, G. (1997) Atomic and Molecular Structure in Chemical Education: A Critical Analysis from Various Perspectives of Science Education, *Journal of Chemical Education 74*, 922.

[12] Johnson, S. M., Javner, C., and Hackel, B. J. (2017) Development and Implementation of a Protein–Protein Binding Experiment To Teach Intermolecular Interactions in High School or Undergraduate Classrooms, *Journal of Chemical Education 94*, 367-374.

[13] Sneha, M., Dulay, M. T., and Zare, R. N. (2017) Introducing mass spectrometry to first-year undergraduates: Analysis of caffeine and other components in energy drinks using paper-spray mass spectrometry, *International Journal of Mass Spectrometry 418*, 156-161.

[14] Schibeci, R. A. (1982) Measuring student attitudes: Semantic differential or likert instruments?, *Science Education 66*, 565-570.

[15] Simpson, R. D., and Oliver, J. S. (1990) A summary of major influences on attitude toward and achievement in science among adolescent students, *Science Education 74*, 1-18.